Universitat Jaume I
Escuela de Doctorado de la Universitat Jaume I
Programa Tecnologías Industriales y Materiales

On the use of nanofluids to enhance the direct absorption of solar radiation

A dissertation presented by Alexandra Gimeno Furió for the Degree of Doctor from the Universitat Jaume I

AUTHOR
Alexandra Gimeno Furió

ADVISOR
Dra. Leonor Hernández López

Castellón de la Plana, 2019

Universitat Jaume I
Escuela de Doctorado de la Universitat Jaume I
Programa Tecnologías Industriales y Materiales

Uso de nanofluidos para la mejora de la absorción de la radiación solar

Memoria presentada por Alexandra Gimeno Furió para optar al grado de doctora por la Universitat Jaume I

AUTORA
Alexandra Gimeno Furió

DIRECTORA
Dra. Leonor Hernández López

Castellón de la Plana, 2019

Financiación

Contrato predoctoral

- Contrato personal investigador en el proyecto: Fabrication of BIOcompatible "green" colloidal NANOparticles by spatial and temporal focusing of femtosecond pulses (Generalitat Valenciana)
- Contrato personal técnico superior de apoyo-Prometeo en el proyecto: Digital control of light beams (Generalitat Valenciana)
- Contrato personal técnico superior de apoyo a la investigación en el proyecto: Utilització de materials de canvi de fase nanoencapsulats per a la millora de les propietats tèrmiques de sales foses en aplicacions d'alta temperatura (Ministerio de Economía y Competitividad)
- Contrato personal técnico superior de apoyo a la investigación en el proyecto: Utilització de materials de canvi de fase nanoencapsulats per a la millora de les propietats tèrmiques de sales foses en aplicacions d'alta temperatura (Ministerio de Economía y Competitividad)

Estancias internacionales

- Leeds, Reino Unido. COST Action CA15119 NANOUPTAKE (European Cooperation in Science and Technology) de la Unión Europea (3 semanas)
- Dresden, Alemania. COST Action CA15119 NANOUPTAKE (European Cooperation in Science and Technology) de la Unión Europea (3 semanas)
- Padova, Italia. COST Action CA15119 NANOUPTAKE (European Cooperation in Science and Technology) de la Unión Europea (6 semanas)

En memoria de Quique

Además de ser un ejemplo a seguir profesionalmente también lo fue personalmente

Gracias por haber sido un padre además de un jefe.

Abstract

This thesis is intended to evaluate the solar nanofluids (liquids with dispersed nanoparticles) potential to directly absorb the sun radiation and to generate steam. Nowadays, as energy consumption continues to rise while conventional energy supplies are close to begin exhausted, there is an increasing demand for renewable energy technologies, especially solar thermal. Solar thermal energy consists of harnessing the power of the sun to produce thermal energy, applicable to different uses, as mechanical to generate electricity. Currently, solar thermal energy systems include numerous losses due to the heat transfer processes, thus, nanofluids have been proposed to enhance the solar collectors efficiency through the direct sunlight absorption. In this way, the overall efficiency of the process is enhanced considerably, saving costs and promoting the replacement of fossil fuels by the renewable energy sources. In order to optimise the use of solar nanofluids systems, it is needed to do a characterisation of them and to study, which is the optimum. In this thesis four different nanofluids have been synthesized, characterised and evaluated. Two of them were water based-nanofluids and the other two were thermal oil-based nanofluids.

On the one hand, the optical properties of the nanofluids have been measured at room temperature with a spectrophotometer, comparing them with that of the base fluid in order to stablish and quantify the improvements produced by the nanoparticles themselves. Generally, the nanofluid's potential to work as a solar absorber is determined by the absorbance without taking into account the scattering. Therefore, the scattering of all nanofluids has been characterised and thus, it has been possible to obtain the net absorbance and to evaluate them based on it. The optical properties, aside of being measured at room temperature have been also evaluated after a thermal treatment carried out on the nanofluids at high temperature. This temperature increment aims to recreate operation conditions to those closer to real applications.

On the other hand, the stability of the nanofluids has been studied as it is a very important property and one of the most complicated aspects to achieve. These measurements have been acquired at room temperature as well as at high temperature and, then again, to bring the test scenario closer to the reality. It is important that the nanofluids were stable to avoid settle and fouling, that is why, even if the nanofluid is stable at room temperature, it is advisable to ensure this also at high temperature to determine the suitability of the nanofluid.

Finally, the sun radiation to thermal energy conversion has been evaluated to ensure the maximum efficiency of the nanofluid under study. For this, a solar simulator has been employed

to move a step forward on the nanofluids characterisation. Therefore, the main objective of this thesis is to contribute to the solar nanofluids characterisation from an optical and stability point of view under different thermal conditions, always in comparison with the base fluid, for the improvement of the absorption of solar radiation.

Resumen

La presente tesis trata de evaluar el potencial de los nanofluidos solares (líquidos con nanopartículas dispersas) para absorber directamente la radiación solar e intentar generar vapor. Hoy en día el consumo de energía continúa aumentando y las fuentes de energía convencionales están cada vez más cerca de agotarse y, en consecuencia, la demanda de las tecnologías de energías renovables está incrementando, especialmente la energía solar térmica. La energía solar térmica consiste fundamentalmente en aprovechar la energía solar para producir energía térmica, aplicable a diferentes usos, por ejemplo mecánica y, a partir de ella generar energía eléctrica. Actualmente, los sistemas de energía solar térmica incluyen numerosas pérdidas debido a los procesos de transferencia de calor, por ello, los nanofluidos han sido propuestos para mejorar la eficiencia de los colectores solares a través de la absorción directa de la radiación solar. De este modo, se consigue aumentar considerablemente la eficiencia global del proceso, ahorrando costes y favoreciendo además la sustitución de fuentes fósiles por fuentes de energía renovables. Para optimizar el sistema de uso de nanofluidos solares, se debe hacer una caracterización de éstos y estudiar cuál es el idóneo. En esta tesis se han sintetizado, caracterizado y evaluado cuatro tipos diferentes de nanofluidos. Dos de ellos se han sintetizado utilizando agua como fluido base y otros dos se han sintetizado en aceites térmicos.

Por un lado, se han medido las propiedades ópticas de los nanofluidos a temperatura ambiente mediante el uso de espectrofotómetros, comparándolas con las del fluido base para poder determinar y cuantificar las mejoras aportadas por las nanopartículas. Generalmente se suele determinar el potencial de un nanofluido como absorbedor solar sin tener en cuenta el scattering de las nanopartículas en las medidas de absorción. Sin embargo, en este trabajo, se ha caracterizado el scattering de todos los nanofluidos y de este modo ha sido posible obtener la absorción neta y evaluarlos sólo con base en ésta. Las propiedades ópticas, a parte de haber sido medidas a temperatura ambiente, también se han caracterizado después de haber tratado los nanofluidos térmicamente a alta temperatura. Con este aumento de temperatura se pretende crear unas condiciones de operación similares a las que se producirían en una aplicación real.

Por otro lado, se ha estudiado la estabilidad de los nanofluidos, propiedad altamente importante y uno de los aspectos más complejos de conseguir. Estas medidas se han llevado a cabo tanto a temperatura ambiente como a alta temperatura, para así acercar el escenario de ensayo a la realidad. Es importante que los nanofluidos sean estables para evitar sedimentaciones y el deterioro de las instalaciones, por ello, aunque el nanofluido sea estable a temperatura

ambiente es conveniente cerciorarse de ello también a alta temperatura para determinar la idoneidad del nanofluido.

Finalmente, se ha realizado también una evaluación de conversión de radiación solar en energía térmica para conocer la eficiencia del nanofluido bajo estudio. Para ello, se ha empleado un simulador solar llevando la caracterización de los nanofluidos un paso más adelante. Es por eso que, el objetivo de la tesis es contribuir a la caracterización de los nanofluidos solares desde un punto de vista óptico y de estabilidad bajo diferentes condiciones térmicas, siempre en comparación con el fluido base, para la mejora de la absorción de la radiación solar.

Resum

Aquesta tesi tracta d'avaluar el potencial dels nanofluids solars (líquids amb nanopartícules disperses) per absorbir directament la radiació solar i intentar generar vapor. Hui dia el consum d'energia continua augmentant i les fonts d'energia convencionals estan cada vegada més a prop d'esgotar-se, en conseqüència, la demanda de les tecnologies d'energies renovables està incrementant, especialment l'energia solar tèrmica. L'energia solar tèrmica consisteix fonamentalment en aprofitar l'energia solar per produir energia tèrmica, aplicable a diferents usos, o mecànica i, a partir d'ella generar energia elèctrica. Actualment, els sistemes d'energia solar tèrmica inclouen nombroses pèrdues a causa dels processos de transferència de calor, per això, els nanofluids han estat proposats per millorar l'eficiència dels col·lectors solars a través de l'absorció directa de la radiació solar. D'aquesta manera, s'aconsegueix augmentar considerablement l'eficiència global del procés, estalviant costos i afavorint a més la substitució de fonts fòssils per fonts d'energia renovables. Per optimitzar el sistema d'ús de nanofluids solars, s'ha de fer una caracterització d'aquests i estudiar quin és l'idoni. En aquesta tesi s'han sintetitzat, caracteritzat i avaluat quatre tipus diferents de nanofluids. Dos d'ells s'han sintetitzat utilitzant aigua com a fluid base i altres dos s'han sintetitzat en olis tèrmics.

D'una banda, s'han mesurat les propietats òptiques dels nanofluids a temperatura ambient mitjançant l'ús de espectrofotòmetres, comparant-les amb les del fluid base per poder determinar i quantificar les millores aportades per les nanopartícules. Generalment se sol determinar el potencial d'un nanofluid com absorbidor solar sense tenir en compte el scattering de les nanopartícules en les mesures d'absorció. Bé doncs, en aquest treball, s'ha caracteritzat el scattering de tots els nanofluids i d'aquesta manera ha estat possible obtenir l'absorció neta i avaluar-los només en base a aquesta. Les propietats òptiques, a part d'haver estat mesurades a temperatura ambient, també s'han caracteritzat després d'haver tractat els nanofluids tèrmicament a alta temperatura. Amb aquest augment de temperatura es pretén crear unes condicions d'operació similars a les que es produirien en una aplicació real.

D'altra banda, s'ha estudiat l'estabilitat dels nanofluids, propietat importantíssima i un dels aspectes més complexos d'aconseguir. Aquestes mesures s'han dut a terme tant a temperatura ambient com a alta temperatura, i així, de nou, apropar l'escenari de l'experiment a la realitat. És important que els nanofluids siguen estables per evitar sedimentacions i el deteriorament de les instal·lacions, per això, tot i que el nanofluid sigua estable a temperatura ambient és convenient assegurar-se'n també a alta temperatura per determinar la idoneïtat del nanofluid.

Finalment, s'ha realitzat també una avaluació de conversió de radiació solar en energia tèrmica per conèixer l'eficiència del nanofluid en estudi. Per a això, s'ha fet ús d'un simulador solar portant la caracterització dels nanofluidos un pas més endavant. És per això que, l'objectiu de la tesi és contribuir a la caracterització dels nanofluids solars des d'un punt de vista òptic i d'estabilitat sota diferents condicions tèrmiques, sempre en comparació amb el fluid base, per a la millora de l'absorció de la radiació solar.

Acknowledgements

Please, I apologise but let me explain the acknowledgements in my mother tongue.

En primer lugar, me gustaría dar las gracias a mi directora de tesis Leonor Hernández por la confianza, por el apoyo ofrecido desde el primer momento, por los consejos que me ha dado a lo largo de estos 4 años juntas, por el tiempo dedicado, por su preocupación, por ser un referente para mí y por permitirme desarrollarme profesional y personalmente a su lado. También me gustaría agradecer a todos los miembros tanto del Grupo de Fluidos Multifásicos con los que he podido colaborar durante estos años. Además, quiero agradecer a diferentes instituciones por concedernos los siguientes proyectos, sin los cuales no hubiese sido posible la realización de la tesis: a la Generalitat Valenciana (proyecto: PROMETEU/2016/079) y al Ministerio de Economía y Competitividad (proyecto: ENE2016-77694-R), a la Universitat Jaume I por el Pla de Promoció de la Investigació a l'UJI (proyectos: P1-1B2013-43 y UJI-B2016-47). También me gustaría mencionar mi gratitud a la Unión Europea por facilitar mis estancias internacionales gracias al proyecto COST Action CA15119 NANOUPTAKE (European Cooperation in Science and Technology).

En segundo lugar, me gustaría agradecer a D. Dongsheng Wen, D. Matthias H. Buschman y D. Simone Mancin por la hospitalidad y el apoyo durante mi estancia en sus instituciones (University of Leeds, Institüt für Lüft- und KältetechnikGmbH y University of Padova, respectivamente), así como a los miembros de sus equipos que me ofrecieron su ayuda en todo momento.

En tercer lugar, quiero darles las gracias a mis amigos por su gran apoyo. En especial a Nuria y Fani por nuestras interminables charlas y risas, que hicieron que pasaran de ser compañeras de trabajo a amigas. A Ester, Pablo y Pepe por nuestros imperdonables descansos de las 12h todos los días, en los que a veces intentamos solucionar el mundo y en otros simplemente desconectar. Los echaré mucho de menos.

En cuarto lugar, quiero agradecer el apoyo de mis padres, pues ellos han hecho posible que llegue a ser doctora. Me han dado cariño, me han transmitido unos valores y educación de los cuales estoy inmensamente agradecida y, además, me han dado los mejores consejos siempre que los he necesitado. También quiero agradecer a mi hermano, porque para mí es un placer seguir creciendo juntos.

Finalmente, quiero mencionar a Carles. La persona que ha estado siempre presente en mi vida como amigo y que, en los últimos años, he tenido la suerte de contar con su apoyo y admiración además como pareja. Gracias por tu confianza, gracias por estar.

Contents

List of Figures

List of Tables

Acronyms list

AH: After Heating
ASTM: American Society for Testing and Materials
BAC: Benzalkonium chloride
BH: Before Heating
BS: Butyl Sulfone
CB: Carbon Black
CSP: Concentrating Solar Power
CNH: Carbon anohorns
CNT: Carbon nanotubes
CTAB: Cetyltrimethylammoniumbromide
DASC: Direct Absorption Solar Collectors
DI-water: deionised water
DLS: Dynamic Light Scattering
DS: Diphenyl Sulfone
FESEM: Field Emission Scanning Electron Microscopy
HTF: Heat Transfer Fluid
NF: Nanofluid
NHSDS: Carbon Nanohorns with Sodiumdodecylsulphate
NHSDSPVP: Carbon Nanohorns with Sodiumdodecylsulphate and Polyvinylpyrrolidone
Ox_CNH: Oxidised Carbon Nanohorns
PV: Photovoltaic
PVP: Polyvinylpyrrolidone
SDS: Sodiumdodecylsulphate
SEM: Scanning Electron Micrscopy
SO: Silicone Oil
SPR: Surface Plasmon resonance
SWCNHs: Single Wall Carbon Nanohorns
TEM: Transmission Electron Microscopy
TH66: Therminol 66

Chapter 1

Introduction

Nowadays, the consumption of energy worldwide has increased, which causes increments in the energy market, decreases in availability and energy security and a growing environmental concern, which is rapidly changing the global energy scenario. At present, world oil consumption is 98 million barrels a day and it is estimated that by 2025 it will be 106 million [6]. If the exponential growth of the population is added, currently the world population is 7 billion [7] and an average annual growth of 1.18% is estimated, is projected a global energy demand more than double during the first half of the 21st century and more than three times by the end of it [8]. Energy and water are basic and indispensable resources for the current lifestyle, as well as for sustainable economic development. Modern industrialized societies depend mainly on fossil fuels, for this reason, securing and developing renewable sources of energy are some of the greatest challenges that humanity is facing nowadays.

The use of traditional fossil fuels, industrialization and current societies have led to serious environmental consequences: CO2 emissions, global warming, air, soil and water pollution, deforestation and a gradual degradation of the environment [9, 10]. In the last century, the Earth's surface temperature has increased 0.6°C, which could cause an increment of the sea level of 20 cm [11]. In addition, if it is taken into account the finite and non-renewable nature of fossil fuels, there is no doubt that significant changes will have to be made in the world's energy infrastructure, where renewable energy sources will play a major role in world prosperity. Renewable energy sources are solar, wind, geothermal, biomass, tidal power which will be the main sources in the global energy economy. The most abundant resource on Earth is solar energy, which radiation per year reaching the Earth is around 3,400,000 EJ; almost 10000 times higher than the sum of world's primary energy consumption per year 450 EJ [12].

Renewables energies represented 7% of electricity consumption in 2017, with solar energy contributing only 1% of the energy consumed from renewables. Presently there exist two principal types of solar energy collection systems: photovoltaic (PV) and solar thermal. Photovoltaic systems work by converting directly the sun's radiation into electrical energy. This electricity is then possible to use it in anything that actively needs electricity. According to the International Renewable Energy Agency, PV systems installed capacity had achieved 385 GW in 2017, approximately [13].

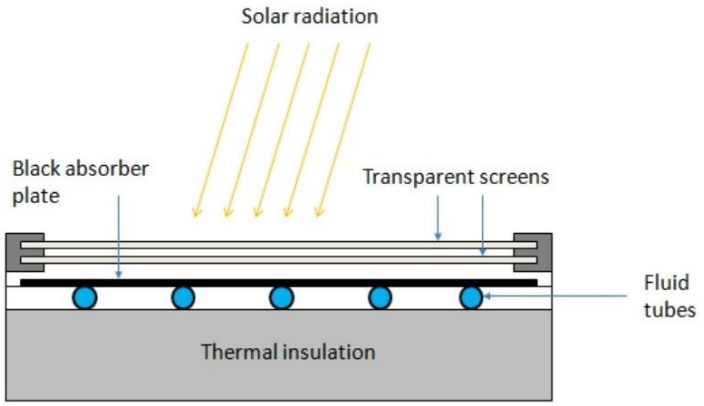

Figure 1.1. Schematic of a typical flat plate solar collector [1]

The other way of producing electricity, solar thermal, consists in the use of energy from the Sun to transfer it to a medium that transports heat and creates thermal energy. This thermal energy can be stored for later use and solve the mismatch between the energy production and demand or can be used to create steam for production of electricity. The growth in solar thermal industry has been much slower than that in PV industry, due to the difficulties in both operation and implementation. Usually, the most typical solar collector devices are flat plate collectors and concentrating collectors. Concentrating collectors use mirrors to concentrate the solar energy incident on the medium to be heated and result in high temperatures in the collector whereas flat plate collectors heat the fluid inside using the sunlight and an appropriated insolation system.

1.1 Solar thermal collectors

The typical solar flat plate collectors work by heating a dark flat surface with the incoming solar radiation and then the energy is transferred to a fluid that then can be used for most residential and small commercial hot water applications. Usually, the main components of a typical flat plate solar collector are: black surface, glazing cover, fluid tubes, absorber plate and insulation cover shown in Fig.1.1 [1].

The glazing cover is a transparent layer that transmits radiation to the absorber, prevents radiative and convective heat loss from the surface, and provide protection of the absorber plate from inclement weather. The absorber plate is a black surface that absorb the maximum of the incident solar energy and then transfers the heat to the fluid in the tubes. The fluid in the tubes traps the heat from the black absorber plate. The thermal insulation prevents heat loss during the fluid transfer. The flat plate solar collector normally operates within the temperature range from 30 to 80°C [14]. However, some new types of collectors using vacuum insulation can reach higher temperatures (up to 100°C). Because of that, the flat plate solar collector is aimed at domestic use.

On the other hand, concentrating solar thermal collectors are usually present in CSP. In 2017, only 5 GW of the total 389 GW were Concentrated Solar Power (CSP) systems installed

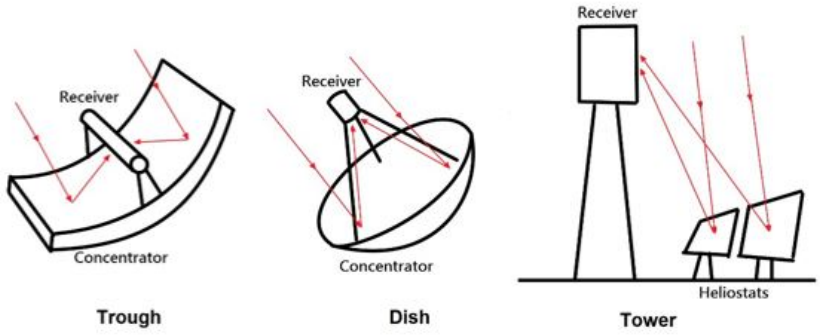

Figure 1.2. The trough, dish and central receiver (tower) concentrating solar panel systems

capacity [13]. Solar thermal collectors are the responsible of capture the thermal energy from the solar radiation. One of the major technologies that transform the Sun radiation into useful energy is the CSP plants. These collectors can achieve higher temperatures and then can be used for industrial processes where the requirement of electricity is higher than that for residential uses. Both systems, flat plate and concentrating collectors are highly similar, but concentrating system uses mirrors to concentrate the sunlight. The most common configurations in the solar concentrating systems are: parabolic trough systems, dish systems and central receiver systems, as can be observed in Fig.1.2.

The parabolic trough systems are 2D tracking concentrators that focus the incident radiation on a solar receiver placed along the axis where the mirrors are focused. The temperature of the thermal fluid inside the tubes is 500°C and the thermal output power ranges from 30 to 700 MW. On the other hand, the parabolic dish are 3D tracking concentrators where, through the axis, it is possible to focus the incident solar radiation on a Stirling engine or a mini Brayton turbine mounted at the focal point obtaining powers of 5-25 kW output . On a larger scale, there are the tower systems with a central receiver, which are 3D concentrators that focus incident solar radiation through a large number of heliostats in a receiver located at the top of a tower. A wide variety of thermal fluids can be used to obtain a temperature range of 500-2000°C [15, 16]. The efficiency of these systems relies on the fact that the amount of the thermal energy incident on the collector is transferred to the working fluid. Due to the losses produced in the heat transference processes, the efficiency does not reach its full potential. Improving the incoming solar radiation to thermal energy conversion is essential to enhance the overall efficiency of energy process. In the last years, the solar thermal collectors have gained an important role in the investigation area. In this context, considering a deeper look on parabolic trough systems, conventional solar collectors (Fig.1.1) are based on absorption by a dark, tube-like surface (usually, a surface black painted or oxidized in thermal contact with the tubes) [17, 18]. Although these collectors have a high photothermal conversion efficiency, the absorbent surfaces are inadequate because they entail uneven heating of the fluid. High concentrations of solar radiation cause great differences in temperature between the absorbent and the fluid, reaching high temperatures on the surface of the latter and large radiative losses. In order to overcome the losses present in conventional solar thermal collectors, an alternative

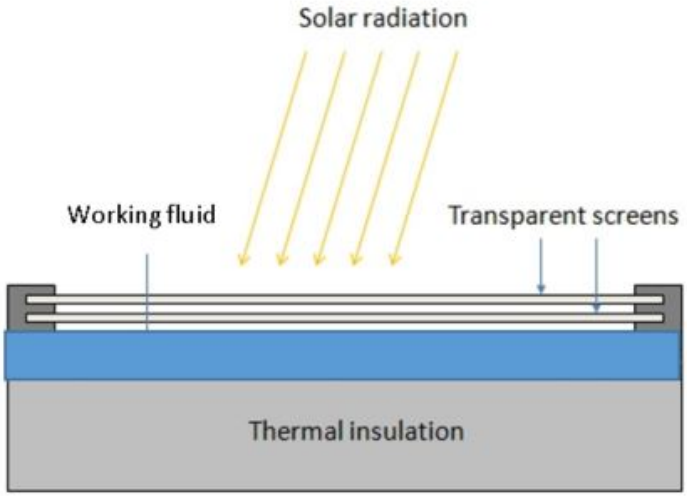

Figure 1.3. New design of thermal solar collector [1]

idea is proposed in which the working fluid is directly exposed to the incident radiation and the heat is volumetrically absorbed within the transport medium instead within a black surface [19]. In this type of collectors, known as volumetric collectors [20, 21], solar energy is absorbed and transported directly by the working fluid [20] A more detailed scheme is depicted in Fig.1.3.

1.2 Direct absorption solar collectors (DASC) using nanofluids

Due to the new proposal of solar collectors, new types of solar receivers have been suggested. Among others, there is the idea of using fluids that directly absorb incident radiation, including the use of dark liquids [20] formed by organic inks or Indian ink or dark particles suspended in gases [22, 23]. However, dark liquids show serious drawbacks due to the thermal degradation at the working temperatures, the instability of the solutions over time and the fouling of the inner part of the tubes' surface. Consequently, nanofluids have been proposed as solar receiver elements for the direct absorption of solar radiation. Nanofluids, which were firstly postulated by Choi [24]. Nanofluids are suspensions of nanoparticles with sizes ranging from 10 nm to 100 nm homogeneously dispersed in the base fluid. It has been observed that optical and thermo-physical properties exhibit improvements in comparison with the base fluids, even though with a low particle loading [25]. Specifically, among the different types of nanofluids, solar nanofluids have been the principal candidates as potential direct absorbers of solar radiation [19]. Considering the limitation of traditional solar receivers, volumetric absorption within the fluid itself is the approach proposed to minimize the difference in temperature between the surface and the fluid. This will lead to an increase in the photothermal efficiency of 5-10%, due to the volumetric absorption. Fig. 1.4 shows a simplified schematic outlining model for the concepts defined above.

To determine the efficiency of solar thermal receivers in solar applications it must be known the ability to convert solar radiation into thermal energy. Thus, the ideal solar thermal receiver must:

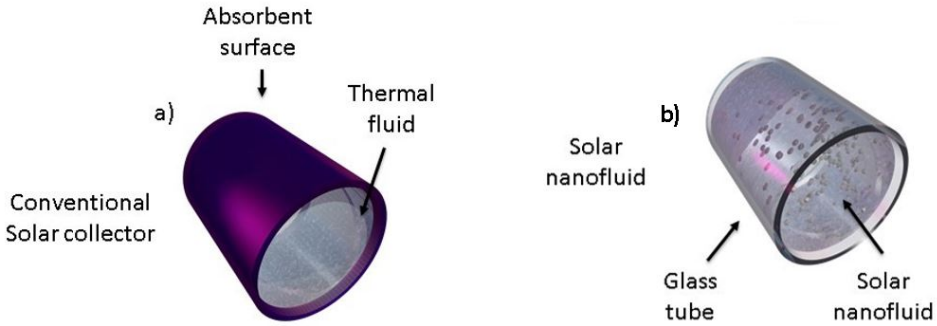

Figure 1.4. Solar thermal collectors formed by: a) absorbent surface, b)thermal fluid (conventional solar collector) with a higher absorption near the surface [2]

1) Efficiently absorb solar radiation (in the 0.25-2.5 μm wavelength range) and connect it to energy in the form of heat within the working fluid

2) Minimize the losses of heat by convection and radiation

3) Keep the system away of fouling / clogging and pump costs to a minimum

Below in Fig.1.5 the solar spectral irradiance is shown.

Throughout this work, the efficiency of the synthesized nanofluids will be studied when absorbing solar radiation. As for point 2), if water is used as base fluid, it absorbs for long wavelengths, but it can also emit at the same wavelengths. There are two possible solutions: a) find a base fluid that has a low emission for long wavelengths or b) install a cover/glazing over the collector that captures the emitted radiation. Solution b) is usually used since there are many systems that solve the problem commercially. As for condition 3), one of the main promising factors of nanoparticles is that they can be added in conventional pumping fluids with few adverse effects, such as obstruction. It has been demonstrated that the material, shape, size and volume fraction of the nanoparticles and the properties of the base fluid play an important role for their potential use in direct absorption collectors, because of that they can be adjusted to achieve that a working fluid absorbs most of the part of the incident radiation. The most common nanoparticle materials are metals, metal oxides and carbon allotropes due to their surface plasmon resonance (SPR). The SPR consists of a collective oscillation of the conduction electrons when they are illuminated with light of the appropriate wavelength, which contributes to maximise the absorption within determined wavelength ranges [26]. Thus, the SPR provides the nanoparticles some optical properties difficult to obtain with traditional optical materials such as semiconductors, fluorescent molecules or pigments. Among others, water, glycols, and oils are quite often employed as base fluids. These fluids are weak absorbers over the ultra-violet and visible ranges of the solar spectrum- absorbing around 13% of the incoming solar energy [19]. The nanoparticle load of these fluids is rather low. However, the dispersed nanoparticles exhibit high absorption capabilities tuned to solar radiation. The expectation is that the nanoparticles added to the base fluid improve its absorption abilities and its thermal conductivity and

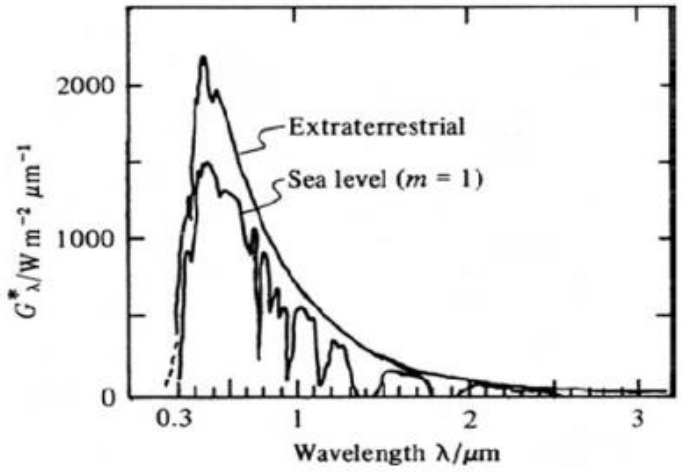

Figure 1.5. Spectral distribution of solar irradiance [3]

therewith the whole heat transfer process [27–29]. In addition to the phenomenon of SPR, it must be borne in mind that the visible spectrum (from 400 to 700 nm) accounts for around 47% of the total energy that reaches the Earth from the Sun and the highest level of solar radiation is found within it, approximately at 500 nm. Therefore, it is important to choose the nanoparticles whose SPR is within the visible range of the solar spectrum, in order to absorb the greatest amount of solar energy.

The light coming from the Sun consists of about 3% UV, 44% visible and 53% infrared radiation or heat. The study of the optical properties of nanofluids enables us not only to use the thermal energy available in the infrared region but also makes possible to employ the energy in the visible region [30]. In this way, by choosing an appropriate fluid to absorb the energy in the infrared as well as in the visible region, not only the most of the solar spectrum could be harvested but can also enhance the solar absorption efficiency.

1.3 Optical properties of nanofluids

Light is defined as electromagnetic radiation in the wavelength range from 3 nm to 30,000 nm [31]. When a surface, whose material has a dielectric constant other than the unity is illuminated, the light that passes through will suffer some variations comparing to the incident light. According to the wavelength of the light and the properties of the materials, optical properties observed in materials can be classified by reflexion, dispersion and transmission. Thus, when light interacts with a material, part of it is reflected in the first surface found, while the other goes into the medium and it is propagated through it. From the light that passes through the medium, part of it reflects again on the back surface of the material and part passes through the system obtaining the transmitted light. Therefore, the transmitted light is related to the reflectivity of the faces with which the light interacts and to the optical properties of the medium that passes through the light. The variations of light when propagating

in the medium are due to the following phenomena: reflection, absorption and scattering. The reflection of light is the change of direction that light undergoes when hitting a different surface to which it is spreading. Part of this light returns to the medium with an angle. Two types of reflection can be found depending on the angle the light is reflected: specular or diffuse. Absorption occurs during the propagation of light in the medium. In this case, the beam will be attenuated as it advances in the medium, affecting the transmission. Absorption is responsible for the colours of many materials; the objects look the colour they do not absorb. Scattering is the phenomenon by which the light is dispersed in all directions when it hits very small particles such as nanoparticles. The amount of scattered light depends on the comparison between the particle size with that of the wavelength. The smaller the wavelengths the higher the scattered light. A schematic is presented in Fig.1.6 for a better understanding of the phenomena.

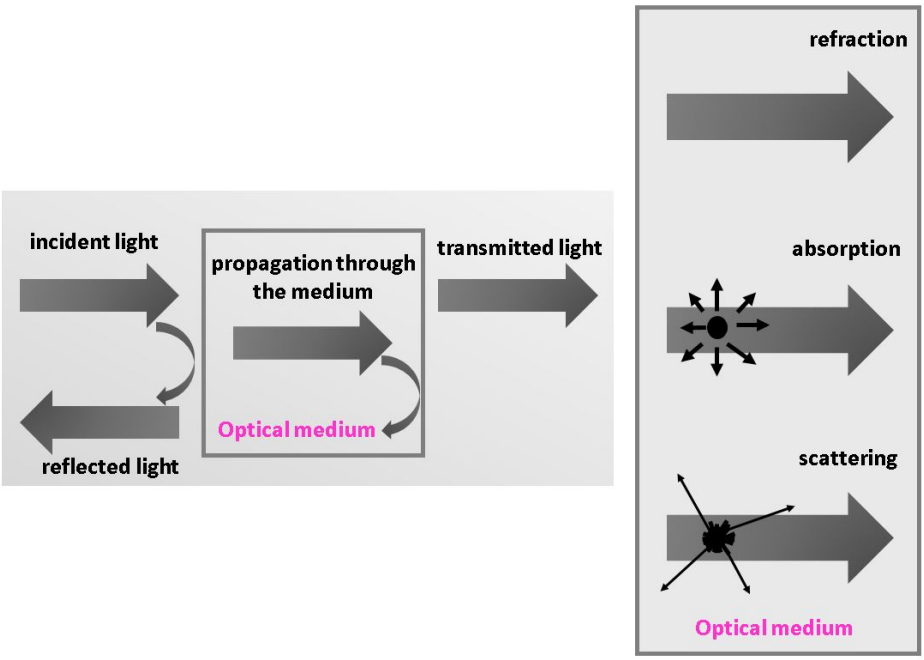

Figure 1.6. Classification of optical phenomena: reflection, transmission and propagation of an incident light. Within the propagation, refraction, absorption and scattering phenomena can take place

It is shown that part of the incident light is reflected when hitting the first surface, then the part that goes into the optical medium can be either refracted, absorbed or scattered by the particles present in the medium. Finally, the light that passes through the sample is the transmitted one.

All the phenomena described above can be quantified by parameters as shown in the equations described below.

$$I_0 = I_T + I_R + I_A + I_S \tag{1.1}$$

The above equation can be normalised by the reference signal (I_0) obtaining the following expression:

$$\frac{I_0}{I_0} = \frac{I_T}{I_0} + \frac{I_R}{I_0} + \frac{I_A}{I_0} + \frac{I_S}{I_0} \tag{1.2}$$

Finally, the global formula that establish the relationship between the optical parameters is as follows:

$$1 = T + R + A + S \tag{1.3}$$

where T is the ballistic transmittance defined as the ratio between the intensity of light passing through the sample and the intensity of light that hits the sample in a small aperture around the forward direction, therefore, no scattered light is taken into account. R is the reflectance, A is the absorbance and S is the scattering. Moreover, it is worth mentioning that the sum of A and S is the extinction (E), but sometimes it is called absorption since the scattering can be negligible.

Optical phenomena in nanofluids occurs by the two media, the base fluid and the nanoparticles. Due to the strange behaviour of the nanoparticles observed in some cases, the optical properties cannot be described as in the case of a macroscopic system. Because of that, scattering and absorption must be included when working with nanofluids for an appropriate study of the optical properties of nanofluids. Therefore, the corresponding linear response of a system formed by nanoparticles is the result of many factors that must be taken into account: the size of the particles, the shape, the material, the base fluid and the distance between different particles in the medium [32–34]. Once the theoretical concepts are defined, the equations that regulate them are described below. First of all, the transmittance is defined as the ratio between the transmitted intensity (I_T) and the incident intensity (I_0) of the system, $T(\lambda)$:

$$T(\lambda) = \frac{I_T(\lambda)}{I_0(\lambda)} \tag{1.4}$$

The transmittance is directly related to the extinction through the following equation:

$$E(\lambda) = -\log_{10}(T(\lambda)) \tag{1.5}$$

Transmittance and extinction defined in the previous equations 1.4 and 1.5 are suitable for every system including particles, even if the scattering process is high in comparison to the absorption. When nanoparticles suspended in a fluid are illuminated according to the preliminary considerations, as it is observed in Fig.1.7 the incident light beam is scattered and absorbed by each nanoparticle or cluster.

Therefore, a part of the light intensity ($dI(x)$) is propagated in the direction of the incident beams ($x - axis$), the ballistic component, become extinct in an infinitesimal distance between x and $x + dx$, as follows:

$$dI(x) = -\mu_{ext} I(x) dz \tag{1.6}$$

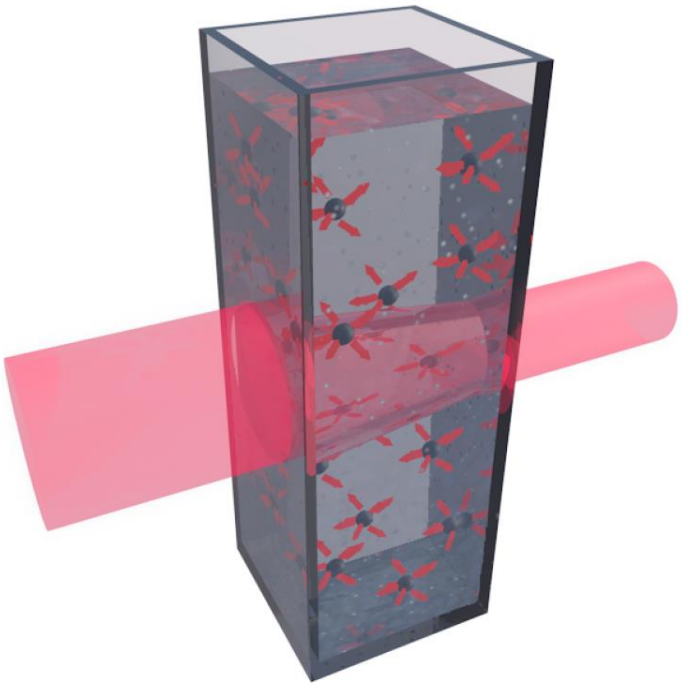

Figure 1.7. Absorption and scattering phenomena in a nanofluid

where $I(x)$ is the intensity of the light in the x position and μ_{ext} is the extinction coefficient. Scattered light, as opposed to the absorbed light, changes the direction and the beam becomes extinct in the propagating direction. However, it is possible that scattered light returns to the ballistic component because of multiple scattering; that is, light scattered by other particles can contribute to the ballistic component at the x position. Now, if the distribution of the particles is random, the multiple scattering can be ignored, then integrating equation 1.6, the Beer-Lambert's law is obtained. Combining it with equation 1.4, a relationship between transmittance or extinction and the optical properties of the nanoparticles is obtained:

$$T(\lambda) = \mathrm{e}^{-\mu_{ext}(\lambda)x} \tag{1.7}$$

$$E(\lambda) = \log_{10}(\mu_{ext}(\lambda)x) \tag{1.8}$$

Therefore, extinction can be defined as the attenuation of an electromagnetic wave because of the phenomena of absorption and scattering when passing through a certain medium [34, 35]. As can be deduced, extinction information is obtained from the measurement of ballistic transmittance. However, there are systems in which both processes, absorption and scattering can occur simultaneously, while in others one of them prevail over the other. Then, it is not possible to differentiate between absorption and scattering just based on the ballistic transmitted light. Therefore, the extinction coefficient is defined as the sum of the absorption plus scattering.

Moreover, absorption coefficient is defined as a percentage of the extinction coefficient varying depending on the type of nanoparticles.

$$\mu_{ext}(\lambda) = \mu_{abs}(\lambda) + \mu_{sca}(\lambda) \tag{1.9}$$

where $\mu_{abs}(\lambda)$ is the absorption coefficient and $\mu_{sca}(\lambda)$ is the scattering coefficient.

It can be observed that only with the transmittance measurement and the equations mentioned above, absorption and scattering coefficients cannot be obtained. Therefore, Kubelka-Munk theory [36] is used to obtain them. This theory is one of the most adequate theories in optical calculations; it relates the scattering and absorption coefficients directly with the measured reflectance (R) and transmittance (T) by means of the following equations:

$$\frac{\mu_{abs}(\lambda)}{\mu_{sca}(\lambda)} = \frac{R(\lambda)^2 - T(\lambda)^2 + 1}{2R(\lambda)} \tag{1.10}$$

$$\mu_{sca}(\lambda) = \frac{1}{C(\lambda)d}\coth^{-1}\frac{T(\lambda)^2 - R(\lambda)^2 + 1}{2R(\lambda)C(\lambda)} \tag{1.11}$$

$$C(\lambda) = \sqrt{\frac{\mu_{abs}(\lambda)}{\mu_{sca}(\lambda)}\left(\frac{\mu_{abs}(\lambda)}{\mu_{sca}(\lambda)} + 2\right)} \tag{1.12}$$

where d is the sample thickness. The experimental measurements of the reflectance and transmittance needed to obtain the parameters mentioned above will be explained deeper in section 2.2

Additionally, scattering albedo that relates the ratio of the scattered light above the extincted light, is calculated by the following equation:

$$\omega(\lambda) = \frac{\mu_{sca}(\lambda)}{\mu_{ext}(\lambda)} \tag{1.13}$$

Finally, to complement the optical analysis of the nanofluids, two key parameters to study the suitability of solar nanofluids as direct solar absorbers, as well as to optimize the design of the installation are calculated. On the one hand, the fraction of the incident power absorbed ($F(x)$) along the path length is important in volumetric solar collectors, and is evaluated by $F(x)$. This parameter calculates the sunlight absorbed fraction of the incident sunlight $I(\lambda)$ which is absorbed in the fluid after a propagation length x and is given by equation 1.14 [18,37]. On the other hand, the spatial distribution of the energy absorbed ($S(x)$) indicates the stored energy inside the nanofluid volume. This distribution, for a cold fluid in absence of convective mixing, is calculated by equation 1.15 [18,37]. The equations that determine these parameters are shown below:

$$F(x) = 1 - \frac{\int_{\lambda_{min}}^{\lambda_{max}} I(\lambda)\cdot \mathrm{e}^{-\mu_{abs}x}d\lambda}{\int_{\lambda_{min}}^{\lambda_{max}} I(\lambda)d\lambda} \tag{1.14}$$

$$S(x) = \frac{\int_{\lambda_{min}}^{\lambda_{max}} I(\lambda) \cdot \mu_{abs} \cdot \mathrm{e}^{-\mu_{abs} x} d\lambda}{\int_{\lambda_{min}}^{\lambda_{max}} I(\lambda) d\lambda} \tag{1.15}$$

where $I(\lambda)$ denotes the spectral distribution of the incident light, obtained from ASTM solar radiation on a surface [38], and λ_{min} and λ_{max} are the limits of the working wavelength range. Approximated spectral absorption coefficients μ_{abs} are given by Kubelka-Munk theory.

1.4 Theoretical background

Absorption is the parameter of main interest when adding nanoparticles to the base fluid since the nanofluids are proposed as direct solar absorbers. In any case, the information available in the literature about the stability, absorption, transmittance, scattering and extinction coefficient of different nanofluids have been compiled to have an overview on this topic.

1.4.1 Stability

One of the most demanding aspects when working with nanofluids is the stability of the nanoparticles in suspension and, therefore, the method of preparation is a challenge. It is interesting to achieve a good stability of the nanofluids because the thermos-physical and optical properties of the base fluid are improved when nanoparticles are added; but if they agglomerate, the clusters formed are no longer on the nanometer scale. Theoretically, if the particles remain sufficiently small (<100nm) the random movement of the nanoparticles in suspension, called "Brownian motion", overcomes the forces of gravity and attraction between the particles, thus avoiding sedimentation and agglomeration. However, in the reality, due to van der Waals forces, nanoparticles tend to aggregate and form clusters that eventually settle. Therefore, two main methods for the stabilization of nanofluids have been developed: the use of dispersants and the chemical functionalization of the surface of the nanoparticles. Surfactants are organic compounds formed by a hydrophobic and hydrophilic group. These are favourable since, the hydrophobic surface of the nanoparticles becomes hydrophilic and consequently, the repulsive forces between the nanoparticles become larger and exceed the attractive forces of Van der Waals. However, it must be taken into account that solar nanofluids will work at high temperatures, which can deteriorate surfactants and, therefore, the stability is lost [39]. On the other hand, the chemical functionalization of nanoparticles consists of modifying the surface of these, anchoring functional groups, which make them dispersible in the liquid medium. This method is a promising approach to achieve long-term and high temperature stability of nanofluids [40].

1.4.2 Optical features

Several studies have been developed testing different types of base fluids, particle sizes and concentrations, as well as different nanoparticles in order to study the relationship with the optical parameters.

The starting point of this research line, using nanofluids for direct absorption solar collector as well as the deep study of nanofluids' optical properties, was established by Taylor et al. [41–43]. For the case of metallic nanoparticles, Saidur et al. [44] have studied Al nanoparticles in water changing the size and concentration. They have verified that the size of the nanoparticles practically does not affect the absorption; however, the concentration shows a direct relationship with the absorption. Moreover, Rativa et al. [45] studied Au and Ag nanoellipsoids observing that, in both types of nanoparticles, the higher the size the lower absorption, and for smaller volume fractions the absorption is higher. Kameya and Hanamura [46] have investigated Ni nanoparticles of 5 nm and a concentration of 0.001%v, obtaining that the highest absorption values were obtained in UV region, becoming lower in visible region. Nevertheless, in the infrared region, the absorption remained the same as the one of the base fluid due to the thermal radiation emitted from the nanofluid. Jana et al. [47] innovated with hybrid nanoparticles. On the one hand, they combined Cu nanoparticles with CNT. Previously, it has been observed that CNT showed a linear relationship between concentration and absorption, whereas those of Cu did not have a linear dependence. Furthermore, it was observed that a lower concentration of CNT greater absorption than with a higher concentration of Cu. Subsequently, once both nanoparticles are combined, it is observed that the absorption of the mixture is greater than only with the Cu nanoparticles. He at al. [48] investigated the optical properties of Cu nanofluids based in water for different sizes and volume fractions and it was found a decrease in transmittance when increasing the nanofluid concentration and nanoparticle size. Zhang et al. [49] compared Ni an ionic liquid to Cu nanofluids and reported higher extinction coefficients for the Ni samples at the same volume fraction (10 ppm) and nanoparticle size (40 nm). Regarding the studies of metal oxide nanoparticles, Said et al. [50] studied Al_2O_3 and TiO_2 in water and it was observed that the higher the concentration, the greater the absorption in both nanofluids. However, both nanofluids also have a zero absorption region between 450 and 550 nm. Karami et al. [51] analysed the optical properties of CuO nanoparticles suspended in a blend of water and ethylene glycol. It was observed a considerable absorption increment with very low volume fraction. Xuan et al. [52] innovated with a mixture of Ag nanoparticles with TiO_2 nanoparticles, obtaining excellent results and a greatly enhanced absorption. The compounds of the CNT have been a crucial issue and of great interest in recent years due to their excellent optical and thermal properties. Natarajan and Sathish [53] studied the behavior of water-based molten wall carbon nanotubes (MWCNT) nanofluids with and without surfactant, obtaining an inverse relationship between sedimentation and absorption, the greater the sedimentation, the lower the absorption. Sani et al. [37] studied the optical properties of the CNH suspended in water, observing an important improvement comparing to the base fluid in transmittance, extinction coefficient and the stored energy capability. Mercatelli et al. [17] investigated the same CNH but suspended in ethylene glycol, obtaining a scattering of less than 5%. Sani et al. [18] compared the properties of CNH with amorphous carbon in ethylene glycol, observing considerable higher stability and absorption in CNH nanofluid for the same concentration. Lee et al. [54] analysed the optical properties of water-based MWCNT of 53 nm and very low volume fraction, and it was found an enhancement in the extinction coefficient when increasing concentration.

1.5 Objectives

The present thesis aims to contribute in providing deeper knowledge to the solar nanofluids to be used in DASC. Concretely, this thesis is focused on the study of the needed solar nanofluids properties to determine their suitability as solar absorbers in a new solar thermal collector approach. The new concept of solar collector is based on using a fluid that act both as solar absorber and fluid transport, then, some heat losses are avoided comparing with the conventional ones. In order to know which nanofluids are the optimal for solar applications, some different tests are carried out evaluating the major properties involved. This innovation is a promising one and a great deal of research is focused on it today, despite its high potential, it is still only at a preliminary stage. The main objective of this thesis is to provide a step forward in solar nanofluids characterization, and paying special attention to the optical properties and its behaviour under thermal exposure. Furthermore, the main objective of the solar collectors field is to find the optimum solar nanofluids to overcome the current obstacles in this technology and to contribute in its further development achieving the commercialization of it. The partial objectives of the proposed thesis, which allow to control and evaluate the optical characterization of solar nanofluids for its use in solar thermal collectors, are the following:

- To obtain an experimental database of solar nanofluids, through a homogeneous and systematic method, and to determine the relevant variables in the process of direct solar absorption.
- To provide an overview on experimental solar nanofluids characterization techniques and the available solar thermal collectors.
- To build an experimental set-up at laboratory scale and thus present the possibility of varying the light source, the temperature of the nanofluid and the path length and to observe the relationship of the optical properties of the different solar nanofluids with these parameter's changes.
- To develop different optical methods that, with the help of the database obtained in the previous stages, allow to predict how the different parameters will influence solar absorption.
- To identify the most influencing and suitable solar nanofluids characteristics for the direct solar absorption process as well as to choose the optimum solar nanofluid.
- To study how temperature will influence the optical properties, as solar nanofluids will be under thermal exposure in real applications.
- To provide new knowledge and go a step forward in direct solar absorption process with the use of solar nanofluids.

Chapter 2

Characterization techniques

In order to characterise the samples, different techniques have been used depending on what property is under study. In this work, the techniques can be classified as morphological, optical and thermal. The first one comprises the morphological aspects referred to microscopy as well as the study of the particle size distribution. The second one includes the test carried out with a spectrophotometer to determine its optical parameters. Finally, the third one involves the experiments to analyse the thermo-physical properties of the nanofluids, concretely, the thermal conductivity. In the following sections, those techniques will be explained in detail.

2.1 Morphological techniques

The structural study of the nanofluids performed in this work was carried out using a high-sophisticated instrument to obtain better interpretations and more accurate results. To this end, a scanning electron microscope (FESEM) with a SIGMA Zeiss instrument (Carl Zeiss SMT Ltd, UK) was used for micro structural examination of nanomaterials. SEM technique consists of producing high-resolution images of the sample surface using the electron-matter interactions. That is, the electron microscope scans the surface of the sample with a focused beam of electrons and displays images from the scan. The electrons interact with atoms in the sample, producing signals that contain information about the surface topography and composition of the sample. The electron beam is scanned in a scan pattern, and the composition of the beam is combined with the detected signal to produce an image [55]. Moreover, it is possible to determine the ordination and planes of atoms through the finest resolution [56].

In addition, it possible to evaluate the variation of the morphology through a technique which also allows to determine the particle size distribution. The technique widely used to study this information is Dynamic Light Scattering (DLS). DLS relates the Brownian motion of the particles with the size. Brownian motion is the random movement of the particles. When a sample is irradiated with a laser beam of a specific wavelength, particles' Brownian motion origin temporally fluctuations in the intensity of the light scattered at a given angle. Particles are in constant Brownian motion, what makes them placed different positions. The dispersed

electrical field, which depends on the position, it is changing constantly, and then the light intensity oscillates through the time. Intensity fluctuations are in inverse proportion to the translational diffusion coefficient. That is, the smaller particles the faster the Brownian motion. From the analysis of the intensities fluctuations, it is obtained the speed of the Brownian motion and, therefore, the particle size is defined by using the Stokes-Einstein equation:

$$d(H) = \frac{kT}{3\pi\eta D} \tag{2.1}$$

where d is the hydrodynamic diameter, D the translational diffusion coefficient, k is Boltzmann's constant, T the absolute temperature and η is the viscosity. This equation is valid for spherical particles suspended in a Newtonian fluid, and it establishes that the translational diffusion coefficient of a spherical particle depends on its size, temperature and viscosity. The translational diffusion coefficient is the property that defines the speed of the Brownian motion. Due to this dependence, it is necessary a known temperature for DLS because viscosity and temperature are related. The temperature needs to be stable to avoid convection currents in the sample that will produce a wrong interpretation of the size because of the predicted and non-random movement. DLS measurements were performed using a Zetasizer Nano ZS which is commonly used in literature. The main components of the equipment are a laser source centered at 532 nm, that illuminates the cell containing the sample, functioning performing size measurements in a range from 0.6nm – 6 μm. A detector placed at 173° of the light traveling axis acquires the scattered light to use non-invasive backscatter detection. Several advantages are found when using this detection: multiple scattering is reduced because the laser does not travel through the entire sample. Contaminants detection are greatly reduced because they used to be larger and large particles provides forward scattering. Everything is enclosed in the system, and the diameter of the particle is obtained from the intensity of the backscattered light at 173°. Moreover, the Zetasizer Nano ZS (Malvern Instruments) incorporates a heating system that allows measures at high temperature up to 90°C, which allows evaluating stability and particle size at different temperatures. Note that when measuring at high temperature, the viscosity value of the sample has to be known since it is related to the temperature.

Fig.2.1 illustrates de DLS Zetasizer Nano ZS (Malvern Instruments) system used in this work.

Figure 2.1. Zetasizer Nano ZS (Malvern Instruments) [4]

On the other hand, another new DLS system was employed to measure the stability of a nanofluid. VASCO FLEX particle size analyser is external, and then the laser head is external and contains the light source and the receiver. In this system, the light registered corresponds to backscattering with an angle of 170°. It is also possible to measure at high temperature in this device, but as it is external, the temperature range in which it is possible to measure the particle size of the samples only depends on the cuvette design. The cuvette is made of aluminium with two fused quartz windows on the sides with a 20ml sample volume. A heating ring surround the cuvette and two K-thermocouple are used to control the temperature on the wall of the cuvette and inside the fluid. The maximum working temperature of this system is 300°C. An image of the DLS Vasco system is presented in Fig.2.2 A more detailed scheme of the cuvette and general experimental set-up can be observed in Fig. 2.3.

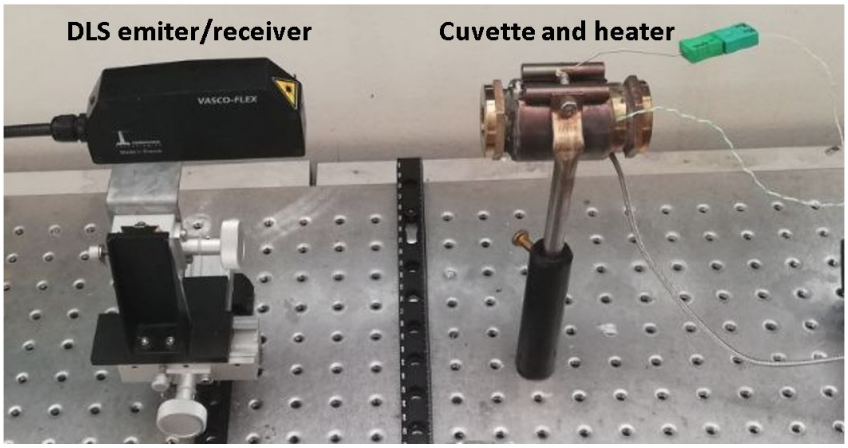

Figure 2.2. Experimental set-up of VASCO FLEX system

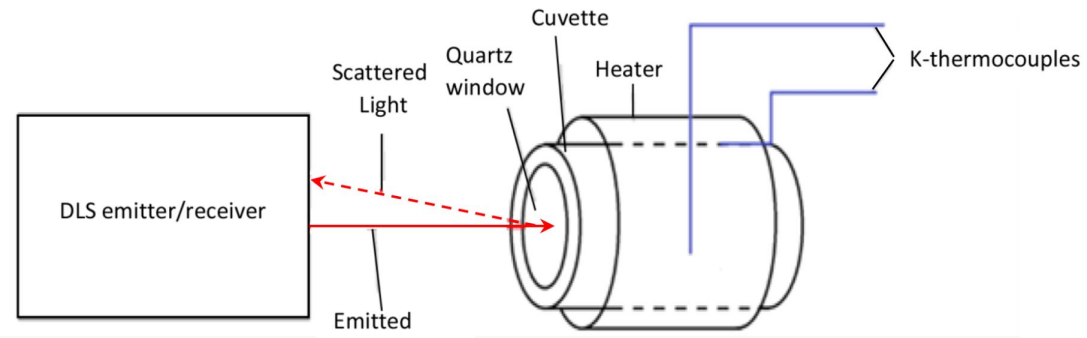

Figure 2.3. Experimental set-up of VASCO FLEX system

2.2 Optical techniques

In this project, nanomaterials with important optical characteristics are under study. Therefore, it must be performed the optical characterization of the samples which consists of analysing the optical response of the nanomaterials. Transmission, absorption and scattering of light are three optical properties of nanofluids which determine the potential of nanofluids for solar thermal applications. They are interconnected as it was mentioned above in section 1.3 and help to make the distinction between different solar nanofluids. Optical features of the solar nanofluids are measured with a spectrophotometer. In this work, a commercial spectrophotometer CARY 500 UV-Vis-NIR (Varian, Devices) was used.

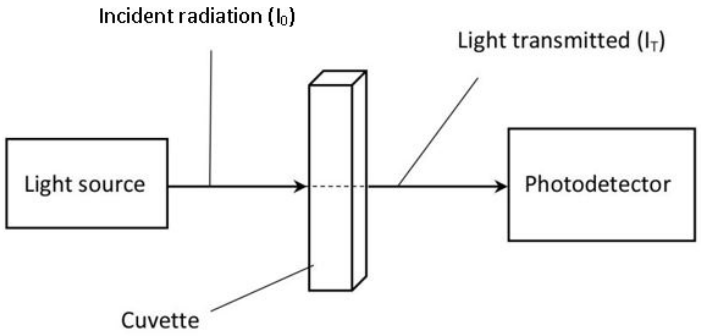

Figure 2.4. A schematic of the spectrophotometer

CARY 500 UV-Vis-NIR is equipped with dual beam, 200-2500 nm wavelength range, approximately 1.5nm fixed spectral bandwith, full spectrum Xenon pulse lamp light source and room light immunity. The operating principle of this system is to select a particular wavelength and the light is directed to the quartz cuvette where the sample is contained. A quartz cuvette is selected because allows 90% of light transmittance at a wide wavelength range from 200 nm to 2500nm. The light passes through the sample and the radiation transmitted in the direction of the original beam is collected by a detector. The ratio between the transmitted light (I_T) and the incident radiation (I_0) represents the transmission spectrum. From it, it is possible to determine the ballistic transmittance $T(\lambda)$ (Fig. 2.4). It includes the absorbance but also the scattering of the sample as in the case of the measurement obtained in the spectrophotometer.

Fig.2.5 presents an image of the CARY 500 UV-Vis-NIR.

To be able to measure the absorbance and scattering of the sample, an integrating sphere is attached to the spectrophotometer CARY 500 UV-Vis-NIR. Fig.2.6 illustrates the detection geometry of the integrating sphere. Two laser beams are directed to the sphere, one directed to the sample itself and a second serving as reference. Once the beams enter the sphere, they impact onto its inner Teflon surface and suffer many internal reflections before being captured by the photodetector (D) at the top of the integrating sphere. Note that the reference beam enters the sphere through a diffusing window (R1) to reduce the losses that would arise from a direct reflection at R2. This beam serves to monitor the laser power changes over the measurement time required for a full wavelength scan. The sample beam enters the integrating sphere through

Figure 2.5. CARY 500 Spectrophotometer [5]

a hole in port S1 and impinges directly onto the port S2 (which can be in a tilted as in Fig. 2.6 or not tilted position). In the practice, the sample can be placed in any of the two ports depending on the desired property to be measured. In order to obtain the scattering spectrum, three measurements are needed.

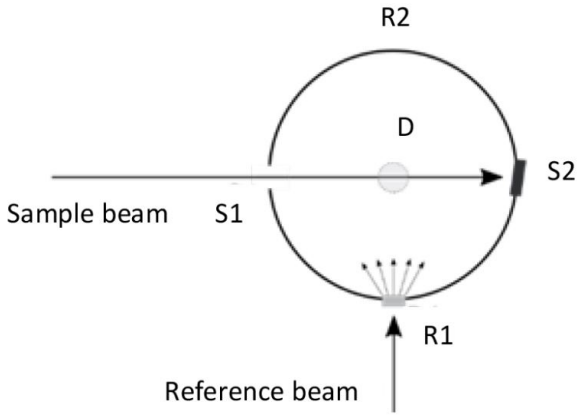

Figure 2.6. A schematic of the integrating sphere, reference and sample beam paths and measuring port locations (S1 and S2)

For the first measurement, named $I_{T+FS}(\lambda)$, the cuvette was placed at port S1 and the tilted Teflon cap at port S2. In this configuration, the sample beam first passes through the cuvette with the sample, and the light that emerges on the other side enters the integrating sphere through S1, hits S2 and undergoes many reflections before being detected. The resulting intensity was proportional to the light power that has been either directly transmitted through the sample or has suffered forward scattering. For the second measurement, port S1 is left opened and the Teflon cap is replaced by the cuvette with the sample at port S2 (the cuvette is also tilted 3° with respect to the normal). The resulting signal, $I_{R+BS}(\lambda)$, is proportional to the sum of reflected and backward scattered light power. For the third, port S1 was left opened and the Teflon cap was replaced by the cuvette with the sample at port S2 (the cuvette was not tilted). The resulting signal, $I_{BS}(\lambda)$, was proportional to the backward scattered light

power. Moreover, all the measurements were normalised by their corresponding reference signal $I_0(\lambda)$, obtained by directly measuring the light from the source with no cuvette in the optical path. Once the measurements mentioned above were acquired, the scattering spectra (including backward and forward scattering)is calculated as:

$$S(\lambda) = \frac{I_S}{I_0} = \frac{I_{T+FS}(\lambda)}{I_0(\lambda)} - \frac{I_T(\lambda)}{I_0(\lambda)} + \frac{I_{BS}(\lambda)}{I_0(\lambda)} \tag{2.2}$$

where $I_T(\lambda)$ is the ballistic transmittance spectrum measured without integrating sphere in CARY 500 UV-Vis-NIR.

These measurements are also needed to obtain the reflectance ($R(\lambda)$) used in Kubelka-Munk theory (3.4),(3.5).

$$R(\lambda) = \frac{I_R}{I_0} = \frac{I_{R+BS}(\lambda)}{I_0(\lambda)} - \frac{I_{BS}(\lambda)}{I_0(\lambda)} \tag{2.3}$$

In order to calculate the absorption spectrum instead of the absorption coefficient of solar nanofluids, the following expression is used:

$$A(\%) = \frac{I_0 - I_{T+FS} - I_{R+BS}}{I_0} \cdot 100 \tag{2.4}$$

where, I_0 is proportional to the total incident light of the beam, I_{T+FS} is the light that has been either directly transmitted through the sample or forwardly scattered, and I_{R+BS} is the light that has been either reflected or backward scattered.

Finally, it is worth mentioning that UV-Vis Spectrometry is an effective tool for determining optical characteristics of nanofluids, such as absorption range and SPR position.

2.3 Thermophysical techniques

In 1993 Masuda et al. [57] proposed the use of nanoparticles to improve the thermal properties of water. One of the key benefits of adding nanoparticles is the increased thermal conductivity of the base fluid. Thermal conductivity measures the convective heat transfer rate. It describes the speed in which the heat transfer process takes place in a material. This heat transfer process occurs by molecules with a high thermal energy. They will move faster than that with less thermal energy, that is, when hotter is a sample the higher is the kinetic energy, and in consequence, atoms and molecules of the sample will move faster. Thermal conductivity is different for each kind of material since they have different atoms and molecules distribution. For example, metals are the highest thermal conducting materials. For this reason, when nanoparticles which present high thermal conductivity are dispersed in a base fluid with low thermal conductivity, then the final suspension presents a higher thermal conductivity [58, 59]. Because of that, in recent years, some researches are focus on the use of nanomaterials to enhance the thermal conductivity of those who present low thermal conductivity [60, 61].

This parameter was measured in this work using a KD2 Pro conductimeter. The KD2 Pro is a commercial device that measures thermal conductivity by means of the transient hot wire technique with an accuracy of ±0.01 W/m°C and maximum deviation of 5%, moreover, it has been previously used in several experimental studies for solar nanofluids (NFs) [62–64]. Fig. 2.7 represents the KD2 Pro conductimeter with the needle sensor.

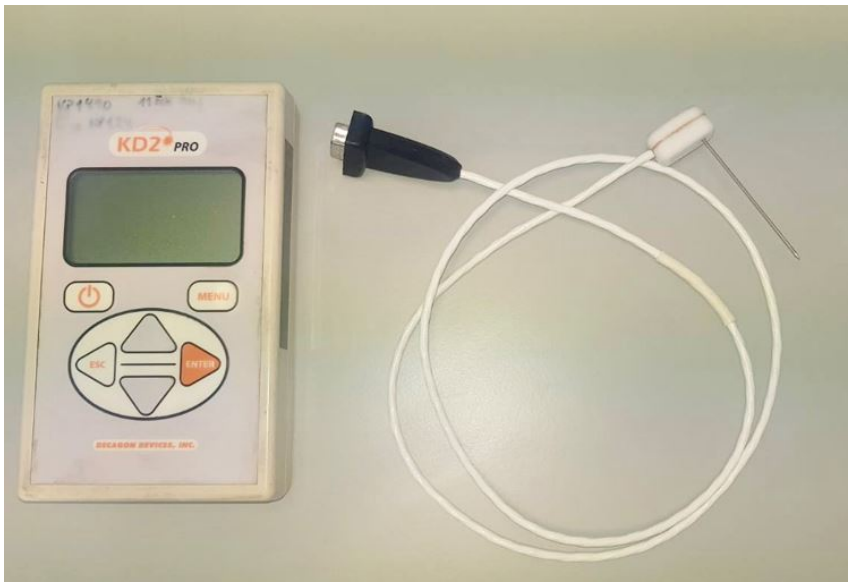

Figure 2.7. KD2 Pro conductimeter with the needle sensor

The thermal conductivity of the tested sample can be derived from the temperature change of the hot wire in response to an abrupt electrical pulse. In this method, a thin metallic wire is embedded into the test liquid, which act as both a heat source and temperature sensor. The transient hot wire technique works by measuring the temperature/time response of the wire within a specific time interval. The sample is placed inside a sealed glass tube (20 ml), into which the sensor is vertically inserted. To carry out the test under high-temperature conditions, the tube is immersed in a thermostatic bath where the temperature is controlled. A 1-hour time period is left for the sample to reach the desired temperature before testing. After this time, five measurements per sample are taken. During the measuring time, the bath is switched off to avoid vibration. Finally, all the equipment used in this research work for characterising the solar nanofluids under study, were selected due to their high accuracy and suitability demonstrated in previous investigations present in the literature [60, 61].

Regarding to the conversion of solar radiation into thermal energy, a new test rig was used which main components are an artificial sun and a sample holder. The experiments are carried out in a separate chamber with an available space of about 250 m^3 (6,500 mm x 5,500 mm x 7,000 mm). A fan with a power of 500 W is located in this measuring chamber to ensure an uniform ambient temperature during the measuring period so that all experiments are carried out under controlled conditions. The artificial sun comprises twelve lamps with a power of 2,000 W each (Fig. 21). The inclination of the structure carrying the lamps is 64.0 ± 0.3° in order

to achieve the optimal radiation exposure with respect to the sample holder (Fig.5.1). Fans provided a line outlet below the lamps with cooling air to prevent the lamps from overheating.

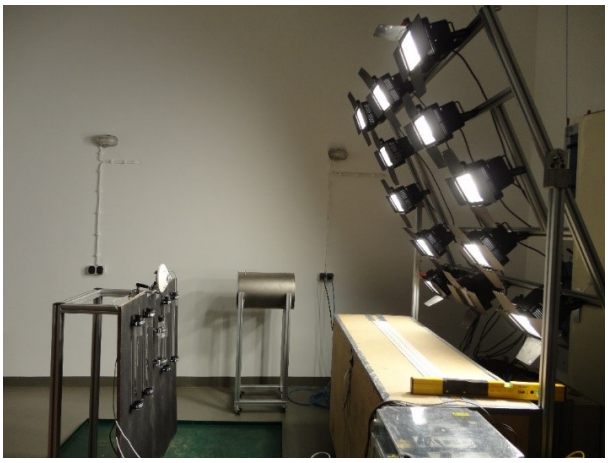

Figure 2.8. Test rig with artificial sun. Lamp array (right) imitating sunlight, with the samples placed opposite. The sample holder consists of a black painted vertical plate (left), on which the pyranometer mounted (white probe) on its upper part

The sample holder consists of a black plate of an area of 1 m^2 (1,000 mm x 1,000 mm) which supports 5 glass tubes. Four of the five tubes (Fig.5.2, all except the middle one) have an inner diameter of 25 mm and a length of 300 mm. All tubes are sealed with a rubber plug. However, the seals are designed in a way the that air can escape when the sample is heated and therewith the fluid inside expands. For the sake of safety, the whole sample holder is placed in a shallow tub to capture any black nanofluid that may escape during the experiments. The irradiation coming from the artificial sun is measured employing a pyranometer (CMP11, KIPP & ZONEN, The Netherlands). The pyranometer is positioned in the upper middle part of the sample holder.

In order to measure the working fluid temperature, a thermocouple Pt100 is positioned centrically in each glass tube. Three thermocouples are used to determine the temperatures at the front and back sides of the sample holder and below the lamps. All thermocouples are calibrated before the measurement campaign. Additionally, all thermocouples are adjusted before each measurement series. The measurement accuracy of all thermocouples is $\pm$ 0.1 K. The measurement value logging of the test rig consists of a message device and the software ProfiSignal (Delphin Technology AG, Germany) working with MS Windows. ProfiSignal compiles all data in tabular and graphical form. Moreover, all data are stored on hard disk.

After filling the glass cylinders, the samples are left without heating to equilibrate to the ambient temperature of the measuring chamber. Each test series starts by switching on the lamps and the fans. The samples are heated for 4 hours and every second a temperature value of all thermocouples is taken. This time is sufficient for all test cases to reach a constant temperature at all measurement positions. The artificial sun and the fans are switched off after this first measurement period and the whole chamber is left without heating the subsequent night for cooling. The sample holder with the NHSDS nanofluids is shown in Fig.5.2. The tubes that are

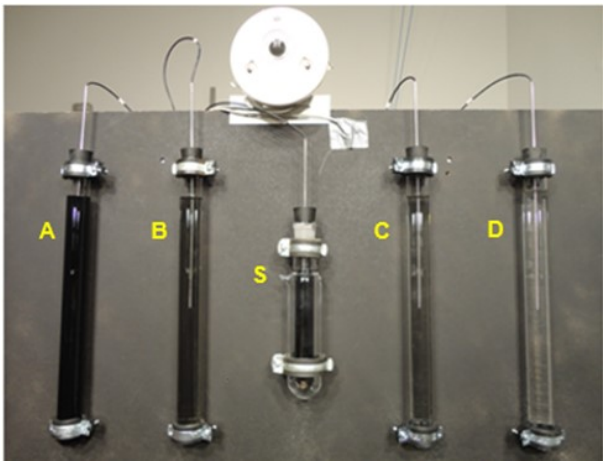

Figure 2.9. Sample holder with the black nanofluid samples of different concentrations. A pyranometer is placed at the upper centre of the holder. Temperature inside each sample is measured with a Pt-100-thermocouple. Surface temperature of the holder measured with the thermocouple visible just to the right of the pyranometer. Letters indicate the names of the tubes

mounted on the plate of the sample holder are labelled A, B, C and D. Tube A contains – if not filled with DI-water – the highest nanoparticle concentration studied. All other tubes are filled with dilutions. These dilutions were 1/10, 1/100, and 1/1000 of the original concentration in tubes B, C, and D, respectively. Tubes A, B, C, and D are geometrically identical. Tube S is a reference tube which is not employed in the analysis because it is double-walled and therewith not comparable with tubes A to D.

It is assumed, that the heat losses are very similar for each of the glass cylinders. Moreover, the study aims to highlight the differences among the black nanofluids with respect to their absorption abilities. Therefore, a detailed modelling of the heat losses is not carried out.

Chapter 3

Optical characterisation of oxidised carbon nanohorn nanofluids

Carbon nanohorns and oxidised carbon nanohorns-based nanofluids were characterised by taking one step forward. The advantage of studying oxidised carbon nanohorns is that they are surfactant-free. The stability of both nanofluids was checked after a 3-month preparation period at high temperature, which comes closer to real applications. Two different dynamic light scattering (DLS) systems were used to measure stability at high temperature before being compared. A deep optical analysis was run. An integrating sphere was attached to the classic spectrophotometer to determine the scattering of nanofluids. After obtaining the experimental values of the optical parameters for both nanofluids, the Kubelka-Munk Theory was applied to obtain optical coefficients. Finally, the scattering albedo was calculated to facilitate comparisons with the literature. Studying both nanofluid types provided us with new knowledge about their potential use as direct solar absorbers in solar thermal collectors.

3.1 Introduction

In recent years, solar thermal energy has attracted a lot of interest due to given its thermal storage possibilities and economic appeal [65]. Conventional solar thermal collectors transform solar radiation energy into thermal energy that is transmitted to the transport medium. Typical solar collectors use a black surface to absorb incoming sunlight. Then this energy is transferred to water to form high quality pressurised steam in a boiler/heat exchanger.

Thus, in general, many transfer steps (via radiation, convection, conduction and boiling) are required to follow this process and convert light energy into thermal energy for a power cycle. In order to minimise limitations, which result from following many energy transfer steps, some alternative concepts have been addressed [19]. Among these, the idea of absorbing light inside the working fluid while generating steam has been well studied [66]. Direct steam generation can make solar plants more economic and more environmentally friendly, and would present

fewer thermal losses than conventional solar plants, which would improve the cost of energy by 11% [67, 68]. Moreover, when only light is absorbed by the working fluid, the efficiency is enhanced by around 10% compared to absorbing light on a black surface, as in typical collectors [16, 41–43, 67–71].

One proposal is to use nanofluids as working fluids to directly absorb light. Nanofluids are defined as engineered colloidal suspensions of nanometric solid particles in a base fluid [72, 73]. The reason for suspending these small particles is to enhance heat transfer capabilities, especially thermal conductivity over the base fluid [39, 74, 75]. Among the particles utilised as part of nanofluids, single-wall carbon nanohorns (SWCNHs) [76] are modest graphene sheets wrapped to form horn-shaped cones with a half-fullerene cap. They are 30-50 nm long, have a variable diameter of 2-5 nm [77], and the tips of nanohorns are cone-shaped with an edge of around 20° [78, 79]. SWCNHs tend to form aggregates that resemble "dahlia" flowers or buds [80]. One major characteristic of SWCNHs is a lack of metal contamination. Consequently, their production does not need to resort to decontamination processes.

Suspensions of SWCNH in water have also been investigated for energy applications to produce black fluids for volumetric solar absorption in solar collectors [17, 18, 81–83]. As SWCNHs are not effortlessly dispersible in water given the hydrophobic nature of their surface, surfactants are normally used to accomplish the proper stability. However, utilising surfactants entails some drawbacks that can make the colloid unstable [84–86]. Thus another method has been used to mostly oxidise SWCNH surfaces as a perfect strategic device to achieve stable suspensions in water without having to resort to surfactants [87].

The aim of this paper is to study and compare the stability and optical properties of SWCNH and oxidised SWCNH suspensions in water to use them as a possible direct sunlight absorbing fluid in a solar thermal collector. Different measurements were obtained to ensure the potential of these nanofluids in real applications. These measurements were taken for two different particle concentrations of each SWCNH sample, and included particle morphology, long-term dispersion stability at room temperature, particle size distribution with two devices, and also for different temperatures, the scattering and the absorbance spectra of four samples.

3.2 Experimental

3.2.1 Synthesis of nanofluids

Four different nanofluids were herein synthesised and studied. The base fluid employed for all of them was water (Millipore, 18 MΩ cm). The difference between them layes on the type of nanoparticles, the stabilisation method and the nanoparticle concentration in nanofluids. One of them consisted of SWCNH suspended in water using sodium dodecyl sulphate (SDS, ∼99%, Sigma) as a surfactant at two different SWCNH concentrations (0.005 and 0.002 %wt). The other nanofluid was also based on an aqueous suspension, but oxidised SWCNH were used to avoid resorting to surfactants, and also at two different concentrations (0.005 and 0.002

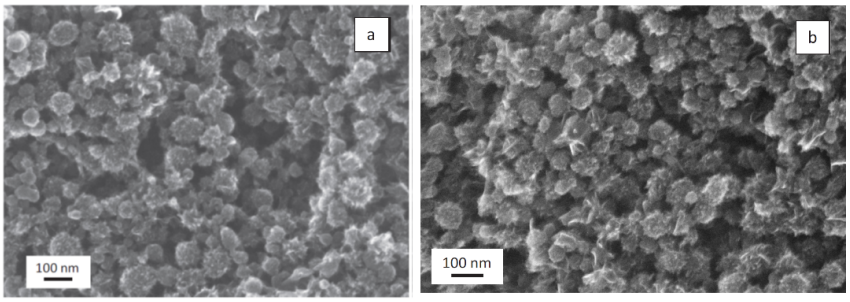

Figure 3.1. SEM images of SWCNH powder (a) and oxidised SWCNH (b)

%wt). These concentrations have been determined in previous works as being suitable for solar nanofluids [63, 88].

SWCNHs were provided by Carbonium S.r.l. and were produced by a process based on the rapid condensation of carbon atoms with no catalyst, but gave considerably reduced production costs [89]. The morphological characterisation of nanoparticles was made by Field Emission Scanning Electron Microscopy (FESEM) with a SIGMA Zeiss instrument (Carl Zeiss SMT Ltd, UK). Two SWCNH suspensions were prepared with concentrations of 0.005 %wt and 0.002 %wt in water according to the following procedure. Firstly, 250 mL of the water solution containing 69±11 mg/l of SDS as the surfactant (10:1 surfactant-to-nanoparticle weight ratio) were taken, after which the appropriate amount of SWCNHs was dispersed in the solution via initial homogenisation in an ultrasonic processor (VCX 130, Sonics & Materials), which operated at 60 kHz and 65 W for 10 min with a 12 mm-diameter Ti_6Al_4V alloy tip. Next the suspension was processed for 20 minutes in a high-pressure homogeniser (Panda, GEA Niro Soavi, Germany) operating at 1,000 bar. By this method, dispersions ensured long-term stability as no particle settling was observed over a 3-month period.

In order to make SWCNH suspensions stable in water without surfactants, surface oxidation was prepared by using concentrated HNO_3 (68-70%, provided by Alfa Aesar) according to a previously described procedure [87]. Firstly, 0.5 g SWCNH were poured into 250 mL HNO_3. This mix was magnetically stirred for 2 h at 80°C, followed by spinning in a centrifuge at room temperature for 10 minutes at 8,000 rpm. Afterwards, the processed powders and acid were divided into two phases to be separated by paper filtering and thoroughly washed with deionised water until the filtrate reached a pH that came close to 6. Finally, the powder was washed with 100 mL of ethanol (absolute anhydrous, provided by Carlo Erba, Italy) and air-dried at 80°C for 2 h. The oxidised SWCNH suspensions were prepared at the 0.005 and 0.002 %wt concentrations by mixing the SWCNH oxidised with deionised water by the same procedure used for the suspensions with the surfactant.

Fig. 3.1 (a) shows the structure of the SWCNH in powder's structure, while Figure 11 (b) illustrates that of the oxidised SWCNH. As the figures clearly denote, the typical morphology was maintained in both cases.

The investigated SWCNH samples are listed in Table 3.1 with their corresponding label.

Table 3.1. The samples investigated in this work

Label	Particle type	Concentration (% wt)
CNH_0.002	SWCNH	0.002
CNH_0.005	SWCNH	0.005
oxCNH_0.002	oxSWCNH	0.002
oxCNH_0.005	oxSWCNH	0.005

3.2.2 Experimental techniques

Two different systems were used to measure and validate the particle size distribution in nanofluids which, if repeated over time, can be related to their stability. Both used dynamic light scattering (DLS) as the measuring technique and were assessed at different temperatures.

One of the devices used for measuring the stability was Zetasizer Nano (Malvern Instruments), which is commonly found in the literature to measure particle size distributions of nanofluids by DLS. Zetasizer Nano also includes a heating system that can measure at high temperature (up to 90°C), which helps to evaluate the stability at different temperatures. The same equipment type is available at the ITC-CNR (Padova, Italy) and the Universitat Jaume I (Castellón, Spain), and was used in different research stages.

The other system was a VASCO FLEX particle size analyser (Cordouan Technologies). This is a new commercial system used to measure a nanofluid's stability. The main difference between both devices is that Vasco FLEX can analyse samples outside the apparatus. As acquisition is external, the temperature range within which it is possible to measure sample's particle size depends only on the cuvette design. In this case, this system's maximum working temperature is 300°C. A spectrophotometer (with an integrating sphere) was employed to measure sample's different optical properties.

The spectrophotometer employed to measure the sample's NIR-Vis spectra was CARY 500 (Varian Devices), which enables the use of an integrating sphere. This system was chosen because different optical parameters, such as ballistic transmittance, reflectance, and forward and backward scattering, can be measured. To measure a sample's scattering, an integrating sphere was attached to the spectrophotometer. Ballistic transmittance is obtained (T) when measuring with no integrating sphere. Fig. 3.2 provides a scheme of the system.

Three measurements were needed to obtain the whole parameters that were involved in this phenomenon. If the cuvette was placed in front of the sphere at port S1, transmittance and forward scattering were obtained (I_{T+FS}). If the cuvette was located at the back of the sphere at port S2, there were two possibilities: not tilted and then backward scattering (I_{BS}) obtained or tilted 3° to obtain reflectance plus backward scattering (I_{R+BS}). Fig.3.3 represents a detailed scheme of the system.

All the measurements were normalised by their corresponding reference signal (I_0), obtained by directly measuring light from the source with no cuvette on the optical path; for example, ballistic transmittance (T) was calculated with no sphere.

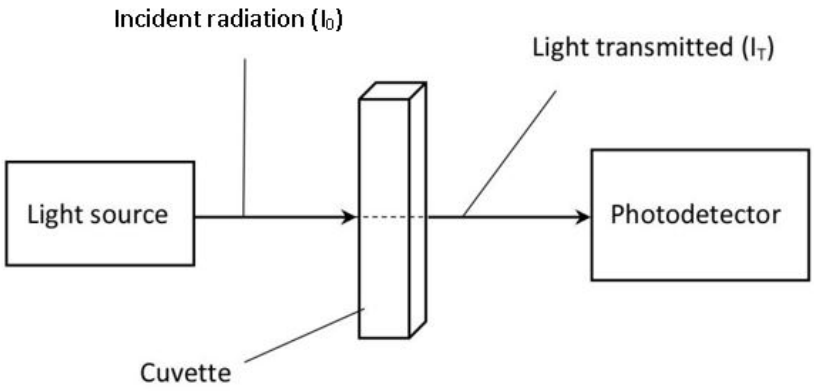

Figure 3.2. A schematic of CARY 500 the spectrophotometer without integrating sphere

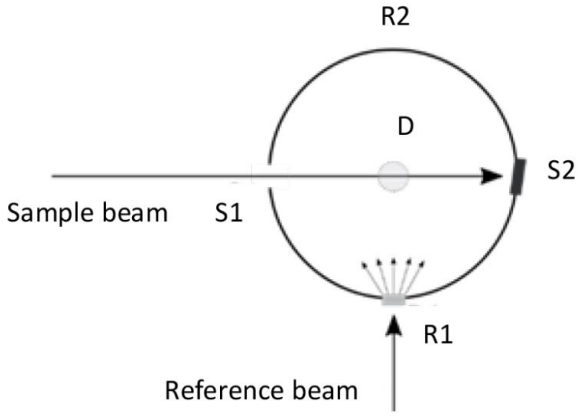

Figure 3.3. A schematic of the spectrophotometer CARY 500 with integrating sphere

$$\mathrm{T} = \frac{I_T}{I_0} \tag{3.1}$$

The extinction spectra can be directly calculated as:

$$\text{Extinction} = -\log_{10}\frac{I_T}{I_0} \tag{3.2}$$

The scattering spectra values were obtained, and normalised by their corresponding reference signal as:

$$S(\lambda) = \frac{I_S}{I_0} = \frac{I_{T+FS}(\lambda)}{I_0(\lambda)} - \frac{I_T(\lambda)}{I_0(\lambda)} + \frac{I_{BS}(\lambda)}{I_0(\lambda)} \tag{3.3}$$

The absorption spectra were calculated by subtracting scattering from the extinction spectra. Finally, the data absorption (μ_{abs}), scattering (μ_{sca}), extinction ($\mu_{ext} = \mu_{abs}+\mu_{sca}$) and scattering albedo ($\omega=\mu_{sca}/\mu_{ext}$) coefficients were calculated by the Kubelka-Munk Theory [36] using the following equations:

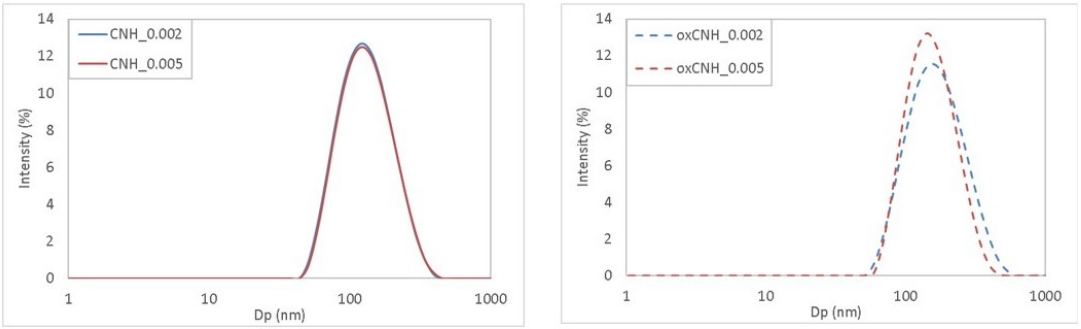

Figure 3.4. The averaged particle size distribution measured over 1 month for the SWCNH (left) and oxidised SWCNH (right) suspensions at two different concentrations

$$\frac{\mu_{abs}(\lambda)}{\mu_{sca}(\lambda)} = \frac{R(\lambda)^2 - T(\lambda)^2 + 1}{2R(\lambda)} \tag{3.4}$$

$$\mu_{sca}(\lambda) = \frac{1}{C(\lambda)d} \coth^{-1} \frac{T(\lambda)^2 - R(\lambda)^2 + 1}{2R(\lambda)C(\lambda)} \tag{3.5}$$

$$C(\lambda) = \sqrt{\frac{\mu_{abs}(\lambda)}{\mu_{sca}(\lambda)} \left(\frac{\mu_{abs}(\lambda)}{\mu_{sca}(\lambda)} + 2 \right)} \tag{3.6}$$

where T is transmittance, d is sample thickness and R is reflectance and it is calculated as:

$$\mathrm{R} = \frac{I_R}{I_0} = \frac{I_{R+BS}}{I_0} - \frac{I_{BS}}{I_0} \tag{3.7}$$

3.3 Particle size characterisation

In order to test the stability of the nanofluids, the particle size distribution of the four samples was measured by DLS at room temperature.

3.3.1 Particle size distribution

The nanofluid's particle size distribution was measured daily for 1 month after it was prepared at room temperature. The averaged results of the measurements taken over the 30-day period are shown in Fig. 3.4.

Similar particle size distributions were obtained for the four nanofluid samples during the 1-month period.

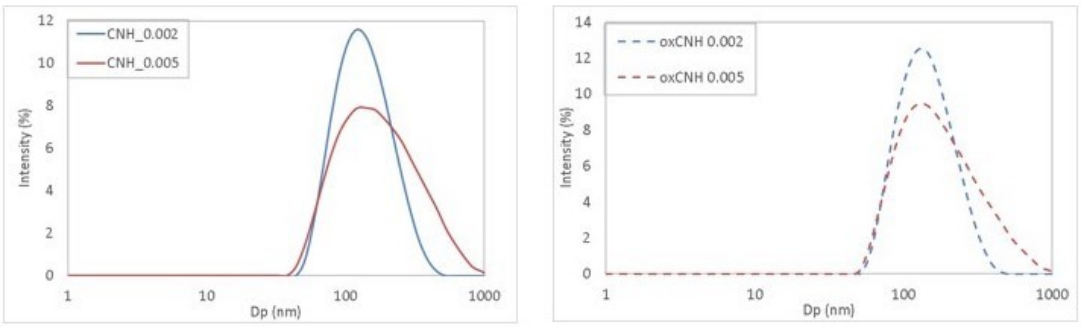

Figure 3.5. The particle size distribution for the SWCNH (left) and oxidised SWCNH (right) suspensions at two different concentrations, measured 3 months after preparation

3.3.2 Long term stability

Three months after preparing the nanofluid, the size distribution of the four samples was measured again. Fig. 3.5 shows the particle size distribution obtained by the Zetasizer Nano system for the SWCNH suspension at two different concentrations, measured 3 months after preparation at room temperature.

The curves in Fig. 3.4 and 3.5 are centred on the same values, which confirms that the agglomeration was almost negligible for a 3-month period. Thus these nanofluids were stable at both concentrations. In addition to particle size distribution, the samples' Z average values over time are presented. This is an intensity-based overall average size based on a specific fit to the raw correlation function data [90].

Table 3.2. A comparison of the Z average results between months 1 and 3 (room temperature)

	CNH_0.002	CNH_0.005	oxCNH_0.002	oxCNH_0.005
1^{st}Month	144	145	163	149
3^{rd}Month	132	156	154	156

When comparing the Z average values in Table 3.2 of the samples measured for 1 month after preparation (in Padova) with those measured 3 months later (in Castellón), no significant differences were observed (including the measurements taken by both devices). This result reveals that the samples remained stable over time.

3.3.3 Particle size distribution

After evaluating the stability of the nanofluid samples at room temperature, it was necessary to check their stability at high temperatures; that is, under conditions that come closer to those in real applications. Therefore, samples were thermally treated to test if this process affected their size distribution and, therefore, their stability at high temperature. The thermal treatment was performed by introducing sealed glass tubes filled with nanofluids inside a stove

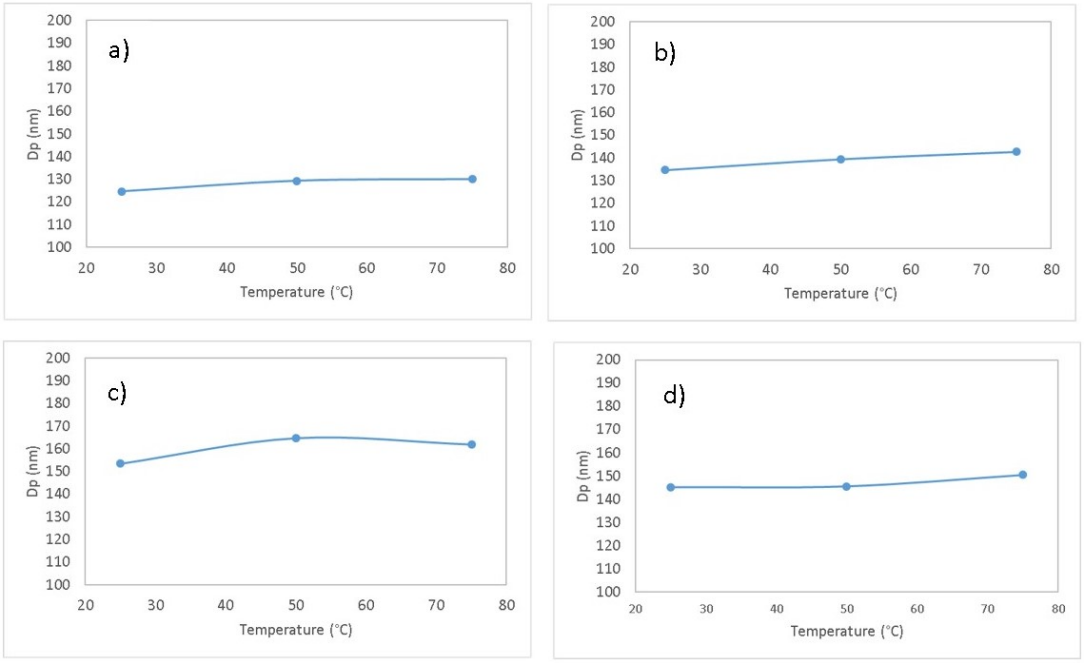

Figure 3.6. Z average variation with the temperatures of the thermally treated samples measured for a) CNH 0.002 b) CNH 0.005 c) oxCNH 0.002 and d) oxCNH 0.005

(Digitronic 2005141, J.P. Selecta, S.A.) for 30 minutes at 75°C. After this thermal treatment, particle size distributions were measured by the Zetasizer Nano system at 20°C, 50°C and 75°C. Fig. 3.6 shows the Z average results of the thermally treated samples at different measuring temperatures. The graphs demonstrate that particle size remained almost constant when temperature varied, and only a slight Z average increasing trend was observed.

The Z average results obtained with the fresh samples and the thermally treated samples at 25°C were compared in Table 3 to observe if any variation occurred after thermal treatment.

Table 3.3. The Z average comparison between the fresh and thermally treated samples at 25°C

	CNH_0.002	CNH_0.005	oxCNH_0.002	oxCNH_0.005
3^{rd}Month fresh	132	155	154	156
3^{rd}Month thermally treated	125	135	154	145

After analysing particle size and the Z average results, it was concluded that samples remained stable within this temperature range.

3.3.4 Particle size distribution with two DLS equipment

The reproducibility of the particle size distributions measured at different temperatures (25°C and 75°C) by two different DLS systems (VASCO FLEX and Zetasizer Nano systems) was analysed in this section. Fig.3.7 shows that the particle size distributions obtained for all the

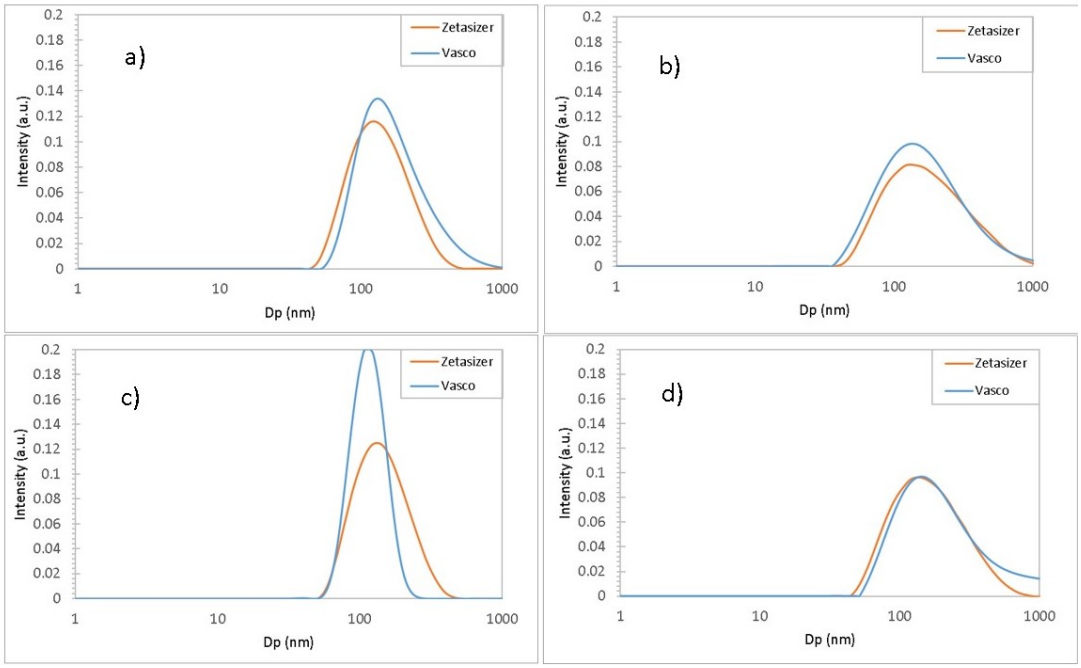

Figure 3.7. Particle size distribution measured in two DLS systems at 25°C of a) CNH 0.002 b) CNH 0.005 c) oxCNH 0.002 and d) oxCNH 0.005

samples were similar for both DLS systems, with only negligible differences especially in mean size terms.

Fig. 3.8 shows a graph for all four samples, where the particle size distributions obtained in each DLS device at 75°C were compared. Similar mean size data were observed for both DLS systems at high temperature, even when the oxidised samples measured by the VASCO system displayed slightly wider distributions.

From the stability characterisation, it was concluded that all the samples proved were stable in the different studied circumstances: for 3 months at room temperature and corroborated by two different systems; after being thermally treated at 75°C for 30 minutes.

3.4 Optical characterization

Considering the importance of the optical properties of the studied nanofluids, the spectra of the SWCNH and oxidised SWCNH samples were measured in a CARY 500 Spectrophotometer (Varian Dev) from 400 to 800 nm. To minimise the effects of undesired reflections and absorptions, samples were placed inside a quartz cuvette with a path length of 1 mm and a planar interface. Fig. 3.9 shows the extinction, scattering and absorption spectra from 400 to 800 nm of the SWCNH nanofluids at different weight nanoparticle concentrations.

In the extinction spectra, a 665% increase within the 400-800 nm range was obtained for the lowest concentrate versus pure water, while the highest concentrate presented an 860% improvement for the same wavelength range. These results imply that the extinction significantly

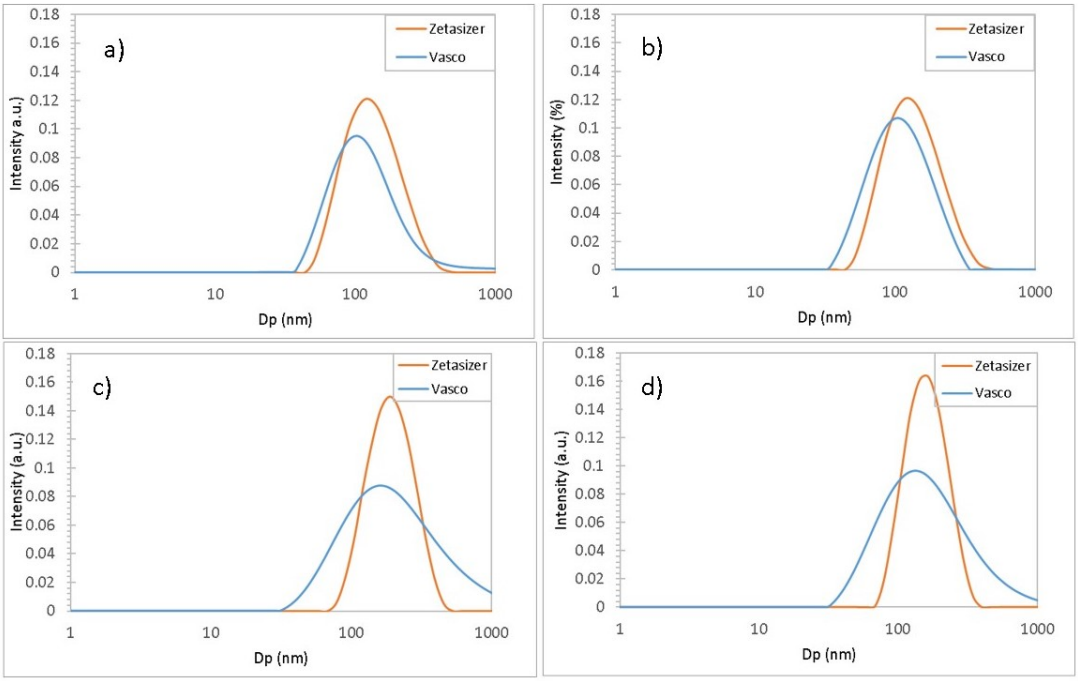

Figure 3.8. Particle size distirbution measured in two DLS systems at 75° of a) CNH 0.002 b) CNH 0.005 c) oxCNH 0.002 and d) oxCNH 0.005

improved with only a small amount of nanoparticles (0.002 %wt). Once again, a substantial enhancement in extinction terms was achieved when the oxidised SWCNH were added to water. By comparing the enhancements accomplished between the oxidised SWCNH and those of the analogous SWCNH concentrations, the results of the oxidised ones were lower, but still considerable. The most remarkable aspect was that the scattering (Fig. 3.9, c and d) contribution remained constant within the whole wavelength range for both nanofluids, at around 0.1 a.u. This value was similar in both cases because the scattering mostly depends on the nanoparticle size and shape.

The averaged values of scattering measurements for each sample over the 400-800 nm range are shown in Table 3.4.

Table 3.4. The averages of the scattering results for the four samples

	0.0002 %wt	0.0005 %wt
CNH	0.11	0.12
oxCNH	0.07	0.09

Table 3.4 and Fig.3.9 reveal that for the SWCNH nanoparticles within the 400-800 nm range, the scattering represented around 30% of the extinction, increased slightly with the nanoparticle concentration and their contribution remained constant within this whole wavelength range. This is in accordance with the literature [17, 18, 78–80], which also indicates that the scattering of the SWCNH and oxidised SWCNH remain constant within a certain wavelength range. The

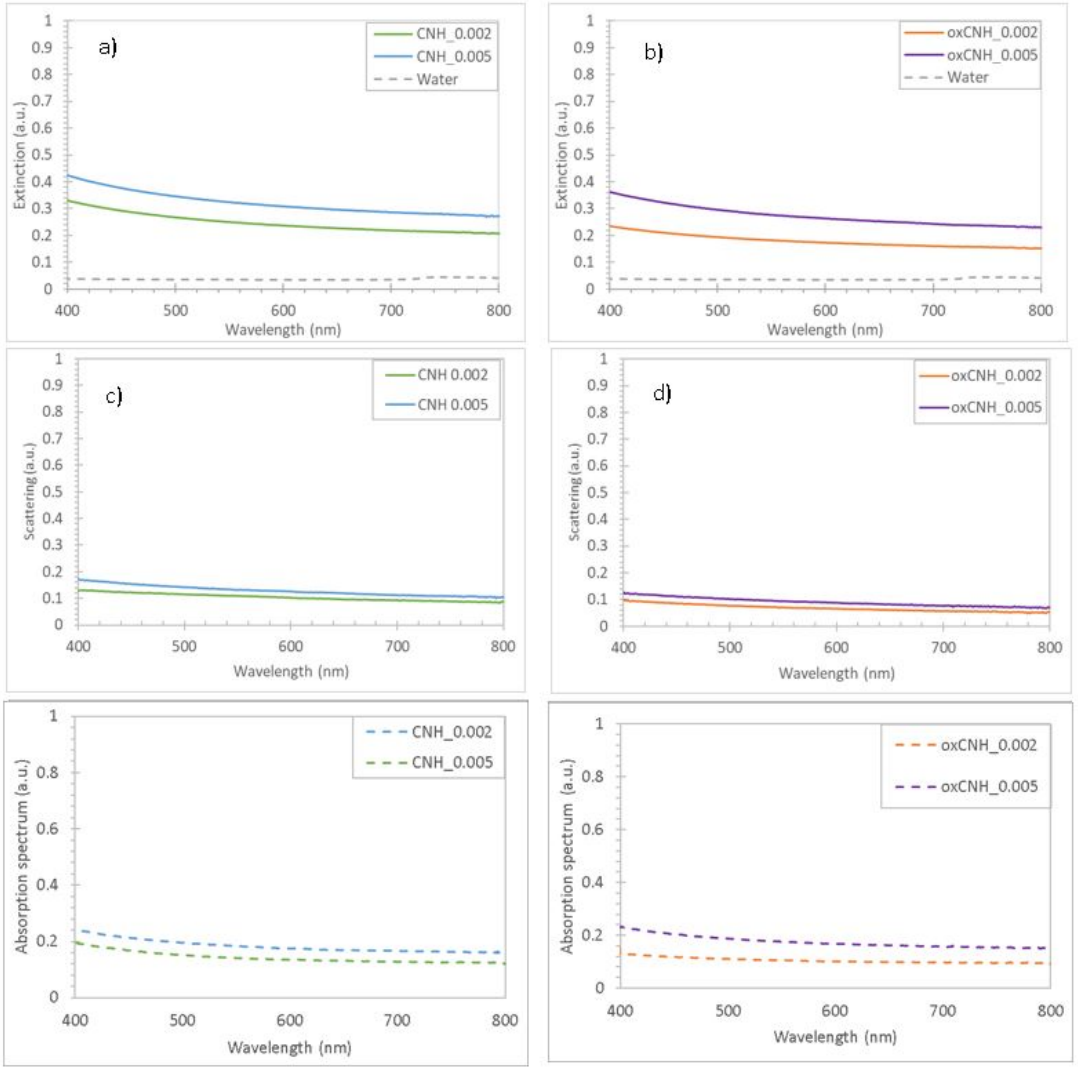

Figure 3.9. a,b) Extinction, c,d) scattering and e,f) absorbance spectra for the SWCNH (left) and oxidised SWCNH (right) water suspensions at different concentrations

absorbance spectra of the four samples are shown in Fig.3.9 (e, f). Higher dependences were obtained in these spectra in relation to nanoparticle concentration, and a constant behaviour was also observed within the measured wavelength range. Apart from the different spectra, the extinction, scattering, absorption and scattering albedo coefficients were also calculated by the Kubelka-Munk Theory. These values are shown in Fig.3.10 according to the wavelength for the different measured nanofluids.

As with the different spectra, nanoparticle load and type (oxidised and non-oxidised) exhibit more strongly influenced absorption than the scattering coefficient. A reduction in relation to wavelength was observed for these two coefficients. The constant scattering albedo coefficient values within this wavelength range are shown in Fig.3.10 d). For the different measured nanofluids, these values varied from 10-15%, which coincides with the bibliography for such nanoparticles [18, 91, 92]. Therefore, it can be concluded that, even at small concentrations, the

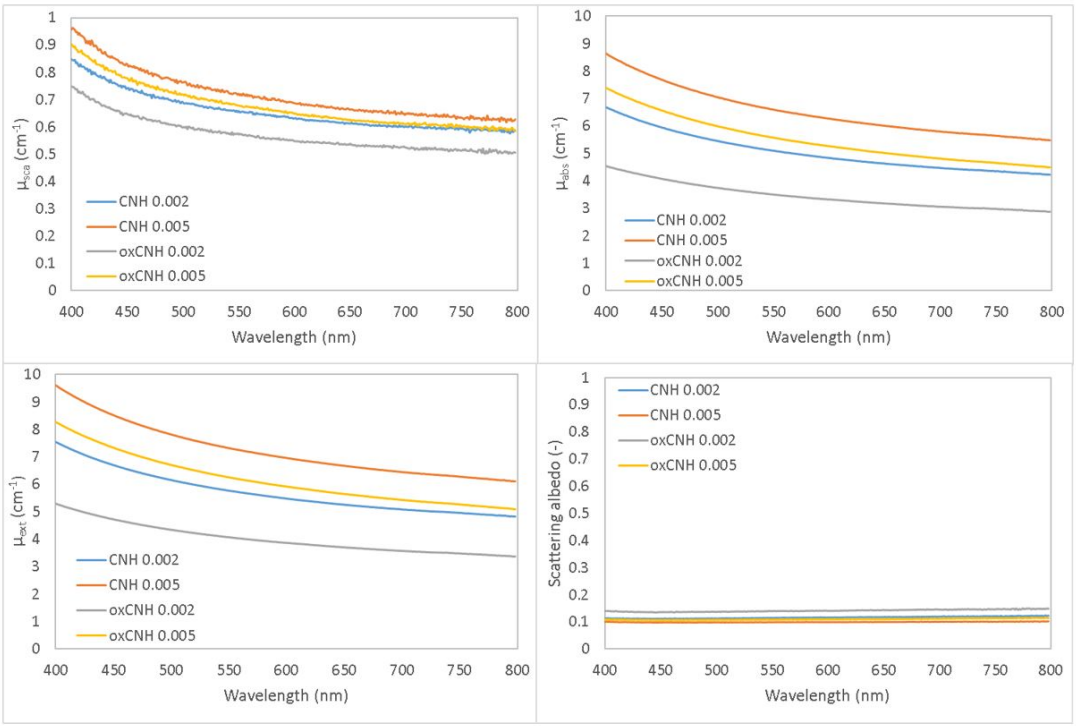

Figure 3.10. a) Scattering coefficient b) Absorption coefficient c) Extinction coefficient and d) Scattering albedo coefficients for the four measured nanofluids

higher the concentration, the greater absorbance and scattering. Finally, these results highlight the major improvement that nanoparticles confer absorption, which make such nanofluids very interesting candidates as direct sunlight absorbers.

3.5 Conclusions

Four water-based nanofluids with two different concentrations of SWCNH and oxidised SWCNH were synthesised and evaluated herein as possible direct sunlight-absorbing fluids by measuring their stability and optical properties.

In order to measure the stability of nanofluids at different temperatures, two DLS systems were used. One of the systems is frequently found in the literature, Zetasizer Nano, while the other one is a new external system that is suitable for high-temperature measurements. Stability over 3 months was evaluated at room temperature with Zetasizer Nano, with good results (between -35 and -55 mV). Afterwards, the samples were thermally treated at 75°C for 30 minutes, and their size distribution was measured again. As the results were similar to those obtained with the fresh samples, it can be concluded that the thermal treatment that goes up to 75°C does not affect their stability.

The particle size distributions were measured from 25°C to 75°C in both DLS devices. The concordance obtained between both systems' results ensures the reproducibility of this

measurement. Moreover, the samples exhibited a good stability with temperature when considering a similar size particle distribution at different temperatures. Regarding optical properties, an integrating sphere was used to measure the scattering phenomena produced by nanoparticles to isolate this effect from absorbance. An increment from 665% to 860% in extinction within the 400-800 nm range was obtained for nanofluids in relation to their base fluid. This significant improvement was obtained even for low nanoparticle concentrations.

For both nanofluid types, the higher the concentration, the greater the absorbance and scattering spectra. Moreover, the same trend was observed for their corresponding Kubelka-Munk coefficients. In accordance with the literature, constant scattering albedo ranging values between 10-15% were found along the whole wavelength range from 400 to 800 nm for all the nanofluids measured herein. Considering their stability and optical properties, the SWCNH and oxidised SWCNH water-based nanofluids can be good candidates as direct sunlight absorber fluids. The highlighted advantages of oxidised nanofluids are that they present higher absorbance values and do not need surfactants to be stable, which provides a more environmentally friendly nanofluid.

Chapter 4

Influence of high temp. exposure on the thermal and optical properties of thermal oil-based solar nanofluids

Concentrated solar power (CSP) plants with parabolic trough technology require a solid absorber and a liquid to transfer heat. In recent years, some research groups have developed new materials that can act as both a solar absorber and heat carrier. Higher efficiencies are achieved with such materials, which are called solar nanofluids. In solar nanofluids, nanoparticles absorb solar radiation. This absorption causes the temperatures of nanoparticles to increase and, therefore, the heat transfer fluid (HTF) temperature rises during an energy transfer process. Accordingly, solar to thermal conversion efficiencies up to 95% can be obtained. In this work, nanofluids based on two different thermal oils were prepared. One is composed by therminol 66 as the base fluid with diphenyl sulfone as the surfactant and carbon black nanoparticles. The second is based on silicone oil with butyl sulfone as the surfactant, and also carbon black nanoparticles. Both nanofluids were evaluated as potential solar nanofluids. For this purpose, they underwent ageing treatment, which consisted in heating up to 200°C at a constant N2 flow rate of 60 l/s for 60 h. The absorption spectrum was calculated by reflection, transmission spectrum and scattering phenomena. A spectrometer was used with an integrating sphere to measure the spectra within the 400-2000 nm range, which included infrared and visible ranges. Thermal conductivity was measured within the whole working temperature range of nanofluids and base fluids. Relevant thermal and optical measurements were taken before and after thermal ageing.

4.1 Introduction

Various synthetic oils are widely employed as heat transfer fluids. Different commercial heat transfer oils exist, such as thermal oil, engine oil and turbine oil, which are all used for medium-

and high-temperature applications. However, these oil types present a disadvantage as they possess low thermal conductivity. If the thermal properties of heat transfer oils were slightly improved, it could lead to higher heat-transfer efficiency processes. Several studies indicate that adding nanoparticles (1-100 nm) to heat transfer fluids enhances their thermal properties [39, 93–97].

Maxwell proposed the concept of adding small solid particles to a base fluid to increase the thermal properties of suspension, which has been practiced since 1881. However, most studies have been performed using suspensions of millimetre- or micrometre-sized particles, which has led to problems like poor suspension stability and channel clogging that limit practical applicability. In 1993 Masuda et al. [57] proposed the use of nanoparticles to improve the thermal properties of water. In 1995 Choi [98] coined the term "nanofluid" (NF) for colloidal suspensions with nano-sized solid particles in thermal applications. NFs present some major advantages over conventional colloidal suspensions, such as high stability, reduced particle clogging and high heat transfer capabilities due to the Brownian motion of nanoparticles. All these potential advantages have boosted research in the NFs field. NFs are advanced materials developed by nanotechnology and constitute an interdisciplinary research field by nature.

Thermal, fluid, material and chemical sciences are needed to characterise and theoretically model a NF behaviour. In the last years, review papers, and several text books, on the thermal applications of NFs have been published [74]. However, NFs dynamic viscosity and stability are the main problems that appear when using NFs. A slight increment in the viscosity of NFs can have an undesired impact on any heat transfer process. The stability of NFs is one of the key problems for any industrial application [99]. The reason for the agglomeration that takes place in nanoparticles is enhanced by Van der Waals' attractive force due to the large surface area caused, in turn, by small-sized nanoparticles. Different techniques, such as transmission electron microscopy (TEM), UV-Vis spectrometry or dynamic light scattering (DLS), are used to determine stability [100–105]. These different techniques have been reviewed in the literature and are applied to stabilise the nanoparticles in base fluids, such as surfactant addition, ultrasonication and surface modification [62, 106].

Solar NFs are transparent fluids within the visible and near infrared ranges with low loads of dispersed nanoparticles and high absorption for solar radiation, which are then transferred to the base fluid. These solar NFs have been proposed as volumetric solar radiation receivers in solar thermal applications [66],to provide high efficiency conversion from solar radiation into thermal energy. Thus, solar NFs for which thermal oils are employed as base fluids are promising materials as they combine solar absorption properties together with heat transfer capabilities [39, 62, 74, 93, 95, 97, 98, 100, 101, 105]. However, the industrial implementation of solar NFs depends on several factors, including NF stability, and good thermal and optical responses at temperatures that come closer to those found in practical applications.

Even if solar NFs are proposed as a promising material for thermal solar energy applications, their optical properties have to be investigated to ensure their potential as direct sunlight absorbers. Carbon black (CB) nanoparticles are widely used in solar thermal collector applications because black fluids can work as both a light absorber and a heat exchanger [19,22,107]. This implies more advantages than the classic operating mode, where a transparent

fluid exchanges heat with a solid, and usually a black absorber. Nevertheless, the use of surfactants is required to avoid CB nanoparticle agglomeration. The challenge posed by high-temperature applications is that the surfactant has to present thermal stability under such high-temperature working conditions. The most common surfactants have been studied only for temperature conditions lower than those used in real-life applications [108]. The most widely used surfactants in synthetic thermal oil-based NFs are sodium dodecyl sulphate (SDS) [16], oleic acid [73, 109, 110], cetyltrimethylammoniumbromide (CTAB) [101, 111, 112] and benzalkonium chloride (BAC) [16, 102, 113].

Solar collector systems utilise a heat transfer fluid that flows to a heat exchanger and transfers thermal energy to storage tanks. The working temperature of these heat transfer fluids normally falls within the 70-150°C range [114]. Usually thermal oils are utilised as heat transfer fluids instead of water because they can reach higher temperatures. When thermal oils are employed as HTFs, their exposure to medium-high temperatures entails the risk of degradation and the formation of new products during use. In the present study this effect was imitated by a thermal ageing process. The effects of the degradation of thermal oils and their optical properties during this process were investigated.

The objective of the present work was to evaluate the thermal degradation of solar oil-based NFs. Additionally, the impact on the optical properties of two thermal oils, therminol 66 (TH66) and silicone oil (SO), was investigated. These thermal oils were selected for their high stability at high temperature, which makes them very interesting for solar applications. Special emphasis was placed on their potential as direct absorbers and heat transfer fluids in sunlight collectors. The developed NFs were based on therminol 66 and silicone oil using carbon black nanoparticles and different surfactants according to the employed base fluid. Black nanoparticles were added to improve the absorption properties of the base fluid and to increase efficiencies in the solar collector. Thermal ageing treatment was carried out for both NFs to analyse how temperature affected them. Moreover, the optical properties of both the base fluid and NF were measured before and after ageing treatment. The thermal conductivity of the same fluids was performed under high-temperature conditions. Finally, the parameters relevant for the design of the collector and absorber devices were calculated.

4.2 Materials and methods

4.2.1 Synthesis

The base fluids used herein were TH66 (Solutia Inc.) and SO (Sigma Aldrich, Ltd). TH66 consists of a hydrogenated terphenyl with high thermal stability, which allows its use for high-temperature working conditions. SO is a polymerised siloxane with organic side chains. The interest of SO as a solar absorber results lies in its high thermal stability due to the presence of polydimethylsiloxane. CB nanoparticles (ELFTEX 570, Cabot Corporation) were selected due to their high solar absorption ability and their stability at high temperature. According to the manufacturer, they consist of spherical amorphous carbon particles with a

primary diameter of 10 nm. Different dispersants were used for each thermal oil: diphenyl sulfone (DS, Sigma Aldrich Co. Ltd) for the TH66-based NFs and butyl sulfone (BS, Sigma Aldrich Co. Ltd.) for the SO-based NFs. The dispersants were selected for their chemical affinity to the thermal oils and their thermal stability at high temperature. The nanofluids were prepared by adding CB nanoparticles to thermal oils at a 0.0016% weight concentration by the two-step method. Firstly, the stabiliser was mixed and dispersed in the base fluid by an ultrasound probe (Sonopuls HD2200, Bandelin) for 1 min. Then the CB nanoparticles were added and dispersed by an ultrasound probe for 1 min. The nanoparticle concentration was selected so that the transmission of the resulting NFs lowered by 20% of the base thermal oil values. The selected surfactant/nanoparticle weight ratio was 1:1.

4.2.2 Thermal ageing

Thermal ageing was performed by introducing the sample into a stove (Digitronic 2005141, J.P. Selecta, s.a.). The air inside the stove was removed by applying a constant N_2 flow before placing the samples inside. The samples were bubbled with N_2 for 10 min to avoid the presence of diluted oxygen before placing them in the stove. Sealed glass tubes filled with the NFs were then placed inside the stove for 60 h at a constant N_2 flow of 60 l/s.

4.2.3 Thermal conductivity

The thermal conductivity (k) of the different samples was measured at several temperatures, which ranged from room temperature to 140°C. A KD2 Pro KS-1 was used to measure the thermal conductivity with an accuracy of ±0.01 W/m°C. This device measures thermal conductivity by the transient hot wire technique and has been previously used in several experimental studies for solar NFs [62]. In this method, a thin metallic wire is embedded into the test liquid, which acts as both a heat source and temperature sensor. The transient hot wire technique works by measuring the temperature/time response of the wire within a specific time interval. The sample is placed inside a sealed glass tube (20 ml), where the sensor is vertically inserted in. To carry out the test under high-temperature conditions, the tube is immersed in a thermostatic bath where the temperature is controlled. A 1-hour time period is left for the sample to reach the desired temperature before testing. After this time, five measurements per sample are taken. During the measuring time, the bath is switched off to avoid further vibrations.

4.2.4 Optical characterisation

Optical characterisation was carried out to evaluate the potential of the studied NFs as solar energy absorbers. To obtain further characterisation, ballistic transmittance, absorption spectra, and the fraction of the absorbed incident power and the spatial distribution of energy were evaluated.

4.2.4.1 Ballistic transmittance

Ballistic transmittance is the ratio between the intensity of light passing through the sample and the intensity of light that hits the sample in a small aperture around the forward direction. Therefore, no scattered light is taken into account. The ballistic transmittance spectra T_b (λ) of the sample with a 1-cm path length (x) was taken in a CARY 500 (Varian, Dev.) spectrophotometer at room temperature from 400 nm to 2,000 nm, with a 1-nm spectral resolution. The extinction coefficient $\mu_{ext}(\lambda)$ was calculated from the ballistic transmittance following the Lambert-Beer law [115]:

$$T(\lambda) = \mathrm{e}^{-\mu_{ext}(\lambda)x} \tag{4.1}$$

The extinction phenomenon is due to the absorption and scattering processes:

$$\mu_{ext}(\lambda) = \mu_{abs}(\lambda) + \mu_{sca}(\lambda) \tag{4.2}$$

On the basis of previous works [18], absorption coefficient $\mu_{abs}(\lambda)$ of the CB NFs are estimated according to extinction coefficient $\mu_{ext}(\lambda)$:

$$\mu_{abs}^{CB}(\lambda) = 0.85\mu_{ext}^{CB}(\lambda) \tag{4.3}$$

4.2.4.2 Fraction of absorbed incident power

The solar absorption ability of NFs is important in volumetric solar collectors. This parameter is evaluated by the measurement of $F(x)$, fraction of absorbed incident power in the fluid along path length x. Using the absorption coefficient of each NF, the absorbed energy fraction was calculated following the expression:

$$F(x) = 1 - \frac{\int_{\lambda_{min}}^{\lambda_{max}} I(\lambda) \cdot \mathrm{e}^{-\mu_{abs}x} d\lambda}{\int_{\lambda_{min}}^{\lambda_{max}} I(\lambda) d\lambda} \tag{4.4}$$

Where $I(\lambda)$ denotes the solar spectral distribution of the incident light, obtained from ASTM solar radiation on a surface [38], and $\lambda_{min} = 400$ nm and λ_{max}= 2,000 nm are used as integration limits. The approximated spectral absorption coefficient μ_{abs} is given by 4.3 after calculating the respective spectral extinction coefficient. The resulting value is, therefore, representative of the fraction of solar radiation absorbed by the sample within the visible and infrared ranges.

4.2.4.3 Spatial distribution of absorbed energy

The spatial distribution of absorbed energy S(x) is an important parameter to determine both the potential of thermal oil-based NFs as direct solar energy absorbers and the optimal system dimensioning. $S(x)$ is calculated with the extinction coefficient from 4.1, following the expression:

$$S(x) = \frac{\int_{\lambda_{min}}^{\lambda_{max}} I(\lambda) \cdot \mu_{abs} \cdot \mathrm{e}^{-\mu_{abs} x} d\lambda}{\int_{\lambda_{min}}^{\lambda_{max}} I(\lambda) d\lambda} \tag{4.5}$$

where λ_{min}, λ_{min} and $I(\lambda)$ values are the same as those used in 4.4. The information provided by this parameter is very important for the solar collector design as it indicates the path length at which energy absorption takes place. It is also an appropriate parameter to optimise the employed NF concentration.

4.2.4.4 Absorption spectrum

The absorption spectra $A(\%)$ of the thermal oil-based samples were obtained by a spectrophotometer (Spectrophotometer CARY 500, Varian Dev) with an integrating sphere. The measured spectrum ranged from 400 nm to 2,000 nm, with a 1-nm spectral resolution. According to the manufacturer, the error in the measurement is less than 0.003% due to the equipment's high accuracy [116]. To reduce the effects of undesired reflections and absorptions, the samples were placed inside a quartz cuvette with a planar interface. The absorption spectra were obtained as:

$$A(\%) = \frac{I_0 - I_{T+FS} - I_{R+BS}}{I_0} \cdot 100 \tag{4.6}$$

where, I_0 is proportional to the total incident light of the beam, I_{T+FS} is the light that has been either directly transmitted through the sample or forwardly scattered, and I_{R+BS} is the light that has been either reflected or backward scattered.

4.3 Results

4.3.1 Thermal ageing

Fig.4.1 shows the samples before and after thermal ageing for both thermal oils and their corresponding NFs.

The difference in colour between TH66 before and after the 60-hour thermal ageing was obvious. However with the SO sample, no change following the thermal ageing was observed. For the thermal oils with nanoparticles (Fig. 4.1c and 1d), similar colours were visually perceived before and after ageing. These changes in the optical properties of samples were further analysed with the measured spectra (see Section 4.3.3). The samples in Fig. 4.1 were kept and examined 1 month after the experiments. A similar visual aspect remained, with not precipitations noted at the bottom of glasses, which thus visually showed the stability of the suspensions through the time.

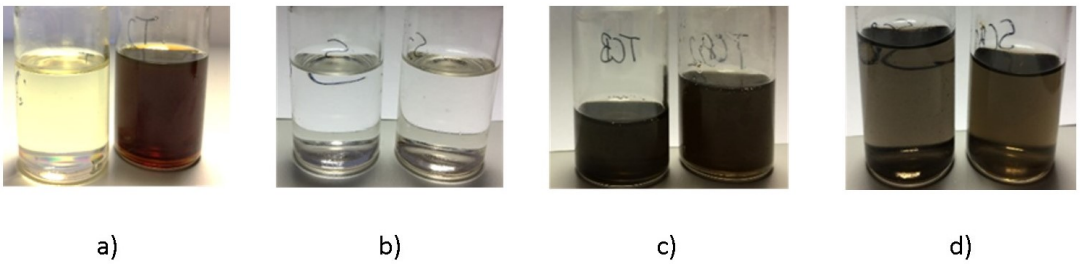

Figure 4.1. The left-hand images are from samples before and the right-hand images are after thermal ageing. Each image represents the following: a) therminol 66 b) silicone oil c) therminol 66 with the CB nanoparticles d) silicone oil with the CB nanoparticles

4.3.2 Thermal conductivity

Fig.4.2 shows the thermal conductivity of TH66 (T), TH66 with the CB nanoparticles (TCB), TH66 after the 60-hour thermal ageing (T_60h) and TH66 NF after thermal ageing (TCB_60h). Measurements were taken at room temperature, 100°C and 140°C. No changes in thermal conductivity were observed in the experimental error with either addition of nanoparticles or thermal ageing.

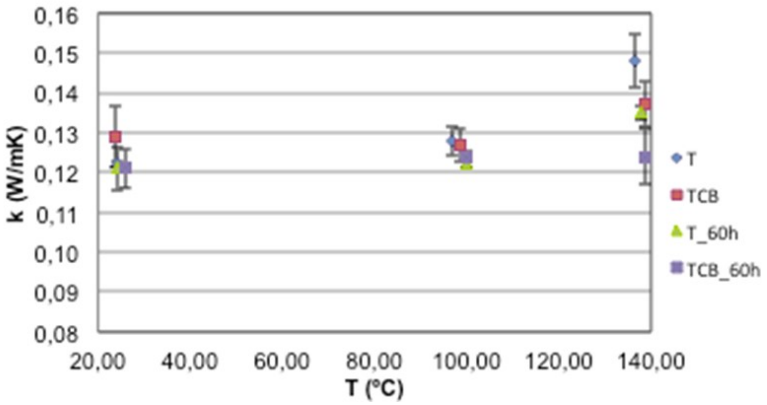

Figure 4.2. Thermal conductivity of the TH66-based samples

Fig.4.3 presents the thermal conductivity of SO (S), SO with nanoparticles (SCB), SO after 60 h of thermal ageing (S_60h) and the SO NF after thermal ageing (SCB_60h). In addition, in this case no change was observed in the thermal conductivity values by either adding CB nanoparticles or thermally ageing.

These results agree with those found in the literature [62, 64, 115, 117–120].

4.3.3 Optical characterisation

4.3.3.1 Ballistic transmittance

The transmittance spectra of all the NFs and base fluids were measured before and after thermal ageing. Fig.4.4 presents the transmittance spectra of both the aged and unaged TH66-based

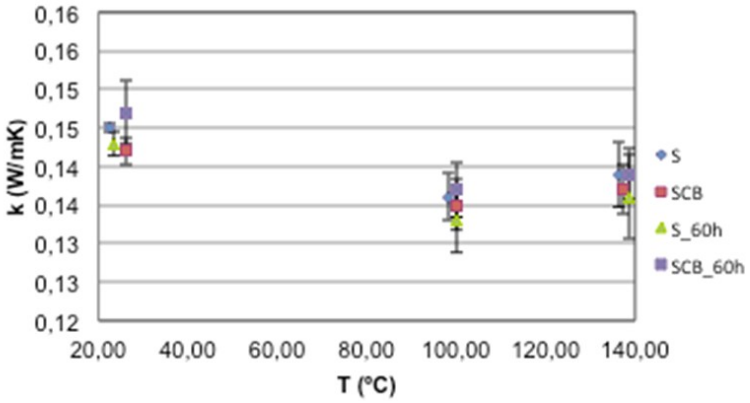

Figure 4.3. Thermal conductivity of the SO-based samples

fluids. The spectra of the SO-based fluids are shown in Fig.4.5.

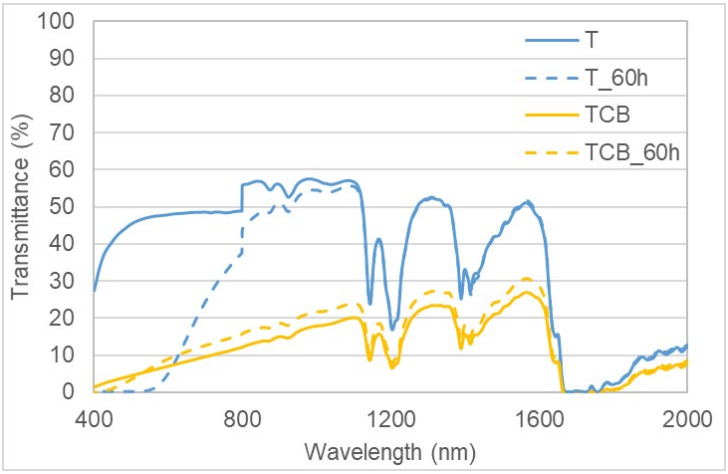

Figure 4.4. Transmittance spectra of TH66 (T), TH66 with the CB nanoparticles (TCB), TH66 after thermal ageing (T_60h) and TH66 NF after thermal ageing (TCB_60h)

The measurements revealed that the transmittance spectra for NFs were much lower than those for their base fluids given the contribution of the black CB nanoparticles. Thermal degradation was observed for TH66 after 60 h of ageing, which especially affected the visible range. However, SO remained unchanged after the same ageing treatment and resulted in a similar spectra, which were obtained for the samples before and after ageing. When comparing Fig. 4.4 and 4.5, we observed that the transmittance values of the TH66-based fluids were lower than those of the SO-based samples. This effect was expected as SO was more transparent than TH66 which, in turn, allowed a higher percentage of light to pass through the sample. The extinction coefficient quantifies the light that does not pass through the sample and is defined as the sum of the absorption and scattering coefficients. The results of the extinction coefficient of TH66 and the SO-based fluids are shown in Fig. 4.6 a) and Fig. 4.6 b), respectively.

Fig.4.7 presents the absorption coefficients of the TH66- and SO-based fluids.

Finally, in order to quantify the scattering phenomenon produced by the CB nanoparticles,

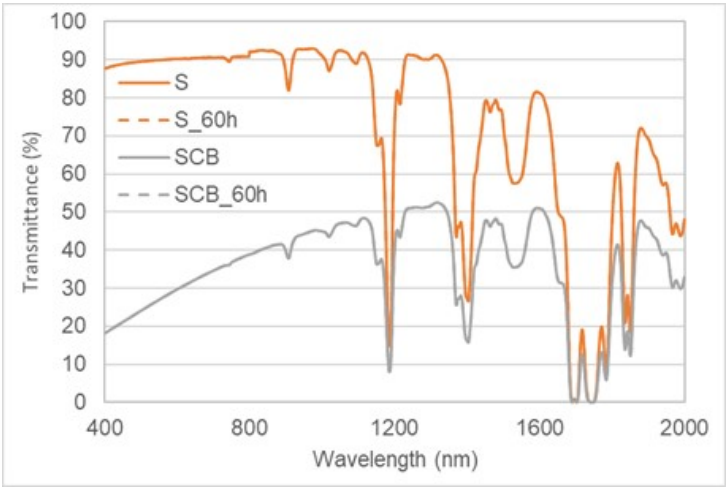

Figure 4.5. Transmittance spectra of SO (S), SO with the CB nanoparticles (SCB), SO after thermal ageing (S_60h) and SO NF after thermal ageing (SCB_60h)

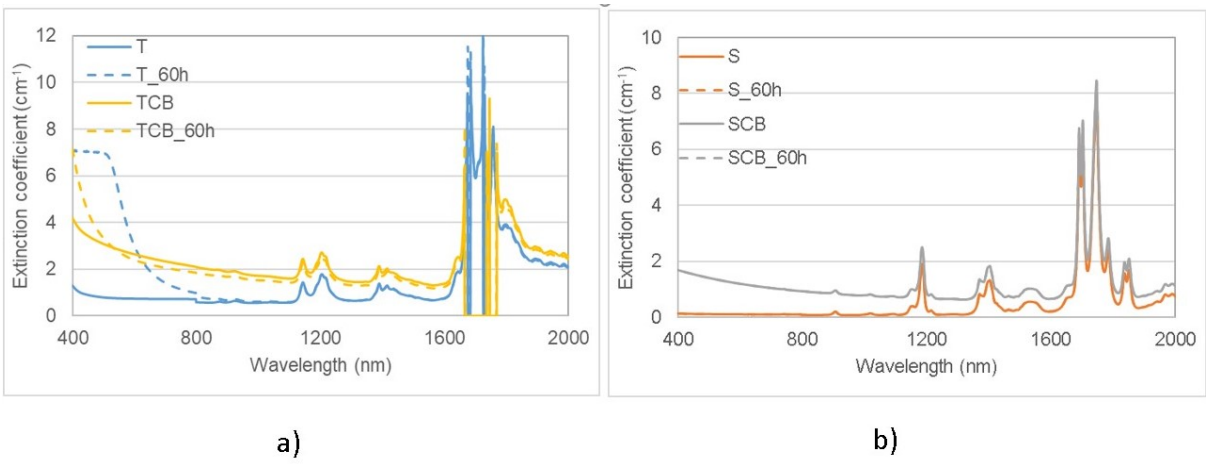

Figure 4.6. The extinction coefficient of: a) the TH66-based fluids before and after thermal ageing; b) the SO-based fluids before and after thermal ageing

the scattering coefficients of the samples are shown in Fig. 4.8a) and Fig. 4.8 b) for the TH66-and SO-based fluids, respectively.

As observed in Fig. 4.7 and 4.8, adding small amounts of CB nanoparticles resulted in the enhancement of the absorption properties of both base fluids (TH66 and SO). The SO base fluid showed lower absorption and extinction coefficients than the TH66 one. SO displayed no degradation with thermal ageing, and its absorption and extinction coefficients remained, while TH66 underwent certain thermal degradation, which increased its absorption and extinction coefficients mainly for low wavelengths. The scattering coefficients for both base fluids (Fig.4.8) had low values. This result was expected as the base fluid contained no nanoparticles, which are responsible for scattering phenomena. Moreover, scattering effects were very weak because the CB nanoparticles were small in size [18, 83, 121].

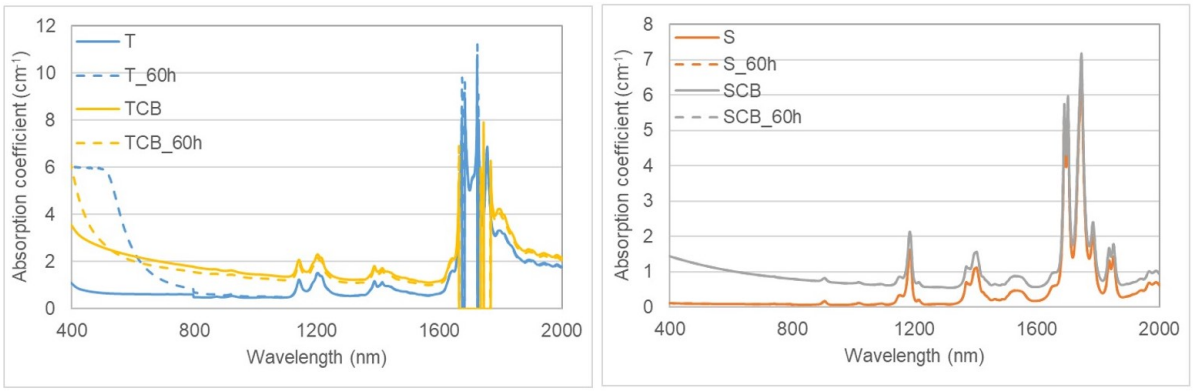

Figure 4.7. The absorption coefficient of: a) the TH66-based fluids before and after thermal ageing; b) the SO-based fluids before and after thermal ageing

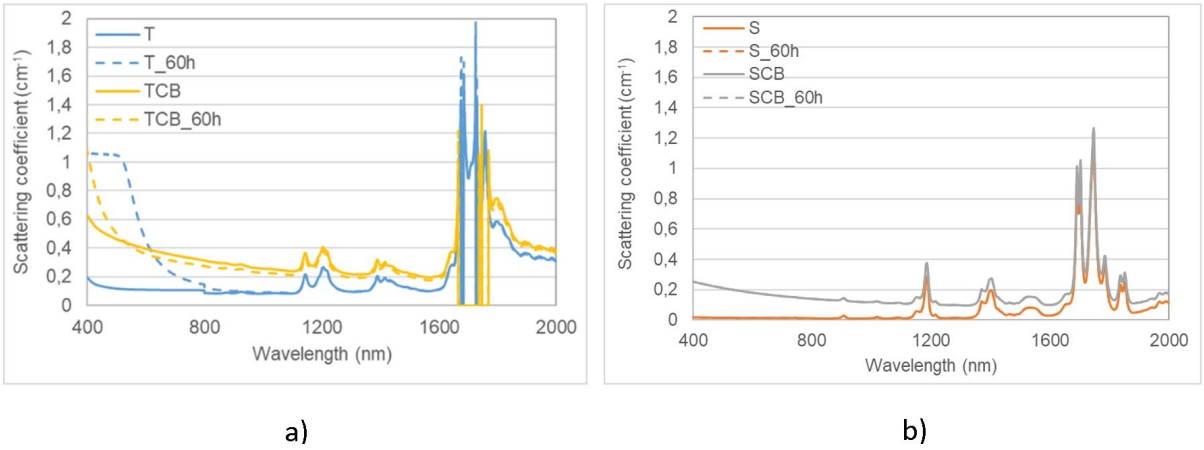

Figure 4.8. The scattering coefficient; a) the TH66-based fluids before and after thermal ageing; b) the SO-based fluids before and after thermal ageing

4.3.3.2 Fraction of absorbed incident power

The absorbed energy fractions obtained from equation 4.4 are represented in Fig.4.9 for a representative fluid length range of the solar thermal collector geometries.

A remarkable difference was found in the fraction of the absorbed incident power values when comparing base fluids with their corresponding NFs. While NFs reached around 95% of absorption at 4 cm of liquid thickness, the base fluids only achieved around 10% of absorption at the same penetration distance. In parallel, the TH66-aged fluid had a maximum absorption values of 80%. The reason for this increment, compared with the unaged TH66, was the colour change after the ageing treatment. Moreover, by following the same trends as the absorption coefficient, the TH66-based NFs gave exhibited F(x) values for the same penetration distance as the SO-based ones.

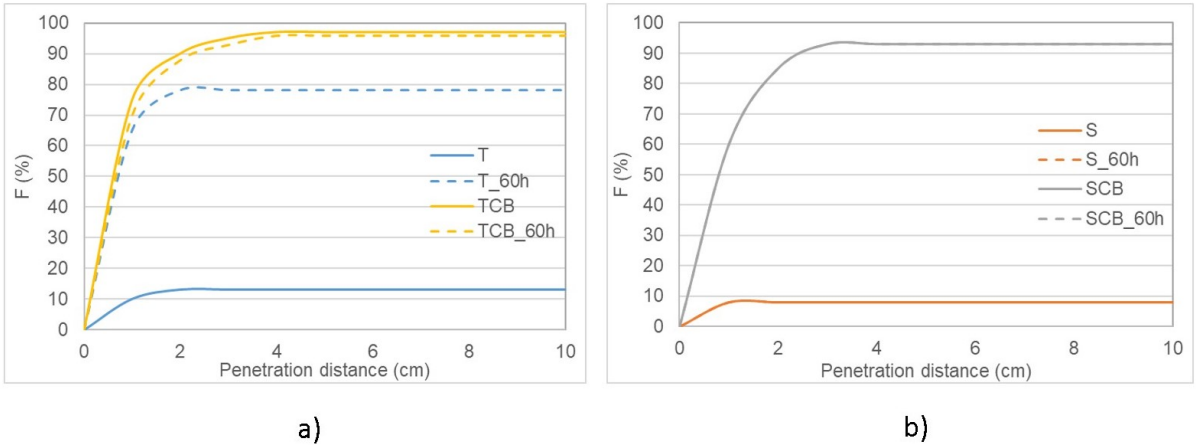

Figure 4.9. Fraction of absorbed incident power of: a) the TH66-based fluids before and after thermal ageing; b) the SO-based fluids before and after thermal ageing

4.3.3.3 Spatial distribution of absorbed energy

From 4.5 it is possible to calculate the spatial distribution of the absorbed energy, as for the previous parameters, before and after thermal ageing. Fig.4.10 presents the obtained results.

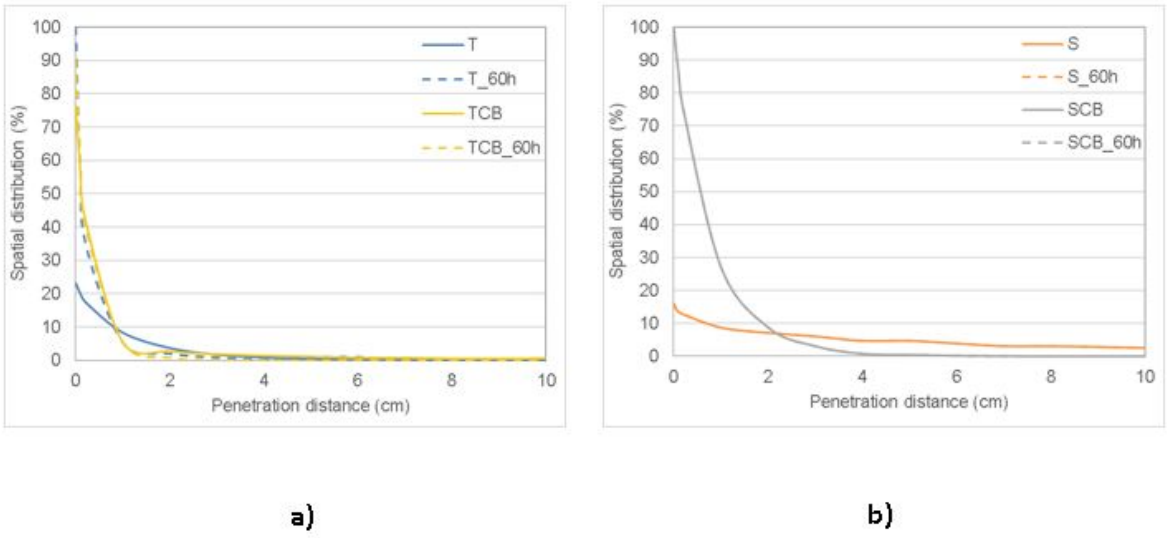

Figure 4.10. Spatial distribution of absorbed energy of: a) the TH66-based fluids before and after thermal ageing; b) the SO-based fluids before and after thermal ageing

Fig.4.10 shows how the energy was absorbed mainly in the first layers of the samples. In both NF cases, about 80% of the energy was already absorbed at a 1-cm sample length. This means that for these CB NFs, the energy was stored near the surface in both the aged and unaged samples. Additionally, deeper layers were heated by thermal conduction [18]. The spatial distribution of energy for the two base fluids was greater than that of their corresponding NFs.

4.3.3.4 Absorption spectrum

In order to study the effect of the thermal treatment on the optical parameters, the absorption spectra were calculated for the eight samples.

Fig.4.11 shows the absorption spectra of the samples based on TH66 and SO before and after thermal ageing, and with and without nanoparticles.

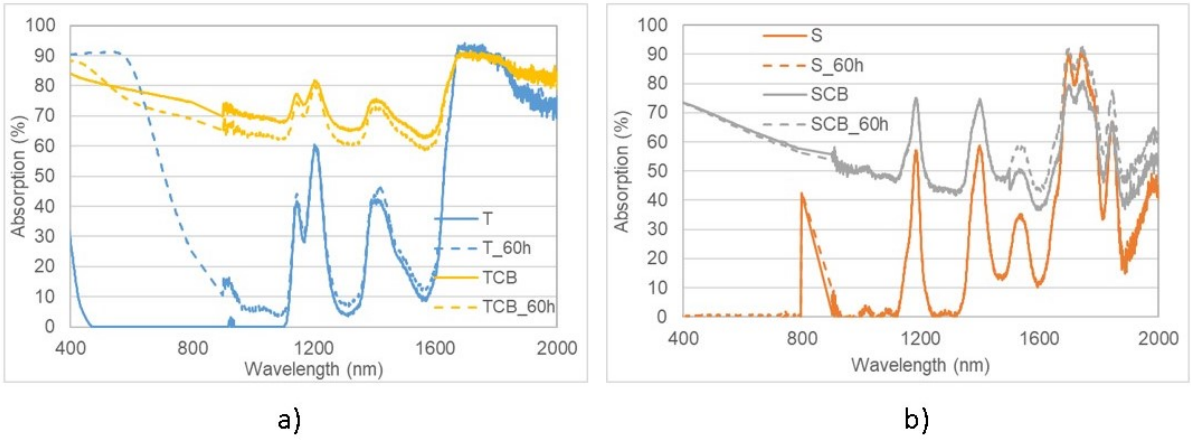

Figure 4.11. Absorption spectra of: a) the TH66-based fluids before and after thermal ageing; b) the SO-based fluids before and after thermal ageing

Large absorption differences were observed in TH66 after the CB nanoparticle addition, especially for small wavelengths (Fig.4.11 a). An appreciable change was also observed between the absorption values of the TH66 samples before and after ageing, especially within the visible spectral range. This agrees with Fig. 4.1 a) and c). Fig.4.11 b) shows the main absorption differences in the SO thermal oil after the CB nanoparticle addition. Fig.4.11 b) also displays similar absorption values for SO before and after the 60-hour thermal ageing. These results agree with that previously observed in Fig.4.1 b) and d). The optical values obtained for these samples match with the results reported in the literature [18, 117].

4.4 Conclusions

In this work, two thermal oil-based NFs were synthesised and analysed as direct solar radiation absorbers and heat transfer fluids. The evaluated base fluids were therminol 66 and silicone oil. In both cases, carbon black nanoparticles was the nanomaterial used to increase the nanofluids' solar absorption properties. Diphenyl sulfone and butyl sulfone were respectively added as stabilisers to improve the stability of the resulting NFs at both room and high temperature (up to 200°C).

The samples underwent thermal ageing for 60 h at 200°C so that the effect of thermal degradation on the optical and thermal properties could be analysed for both base fluids and their corresponding NFs.

No appreciable changes were observed in the thermal conductivity measurements in any of the samples when nanoparticles were added or after thermal ageing. The silicone oil samples (both with and without nanoparticles) did not show appreciable changes before and after ageing. However, a significant change in colour was observed in the TH66 sample after thermal ageing.

The absorption spectrum of both thermal oils notably increased when CB nanoparticles were added. The increment when adding CB nanoparticles to the TH66-based fluid within the 400-2000 nm range was 39.5%, while the increment in the SO-based fluid was 66%. For the thermal oil-based NFs evaluated herein, a large fraction of solar radiation energy was absorbed even at small nanoparticle concentrations (97% for TCB and 93% for SCB after 4 cm of NF). By studying the spatial distribution parameter, this energy was absorbed mainly in the first lengths of the fluids.

The study of the optical and thermal properties is very helpful for optimising the sunlight collector design and for improving its heat transfer efficiency. In conclusion, these first steps revealed that thermal oil-based NFs are promising materials to both absorb solar radiation and transfer collected heat, which lead to higher efficiencies than with classic technologies.

Chapter 5

Nanofluids as direct solar energy absorbers

Carbon nanohorns with a mean dimension of 55 ± 15 nm are suspended in deionised water to obtain black solar nanofluids. In order to achieve long-term stability, these solar nanofluids are stabilised by employing a new strategy; coined double stabilisation method. This approach consists of adding a second surfactant that provides stability to the nanofluids even at medium-high temperatures. The obtained solar nanofluids are exposed to an artificial sun to investigate the double stabilisation. Absorption spectra are measured employing an integrating sphere in the range of 400-2,000 nm. Averaging the data obtained for the different nanofluids, it is found that the absorption values of nanohorn nanofluids stabilised with sodium dodecyl sulphate alone are higher than those of nanohorn nanofluid stabilised with sodium dodecyl sulphate and polyvinylpyrrolidone. However, for both nanofluids it is found that the absorption spectra increase after being exposed to the artificial sun. In the case of nanohorn nanofluid stabilised with sodium dodecyl sulphate, by 5%, and in the case of nanohorn nanofluid stabilised with sodium dodecyl sulphate and polyvinylpyrrolidone, by 28%. These results demonstrate the enhanced performance of double stabilisation over single stabilisation and, also, that double stabilisation is effective at high temperatures. Therefore, while the sample is singly stabilised the suspension presents higher absorption values, doubly stabilised samples represent a better option due to its high absorption combined with its high stability.

5.1 Introduction

Climate change is the consequence of the use of technologies that emit CO_2 to the atmosphere. These technologies burn fossil fuels mainly for energy production. Therefore, renewable energies are playing a growing role in the world economy because they are less harmful, more environmentally friendly, and, at the same time, take advantage of natural resources like wind,

sun, and geothermal reservoirs [122]. Among the different types of renewable energies, solar energy and, more specifically, solar thermal energy are of great importance [123]. The solar thermal process consists of two components, namely collecting solar radiation and transforming this energy into sensible and/or latent heat of a heat carrier. Usual solar thermal technologies employ black surfaces as an absorber, which transfer the heat to a heat transfer fluid (HTF). This strategy is connected with some drawbacks and new alternatives to reach higher efficiencies are currently under study [19]. One alternative that is becoming increasingly important is the application of solar nanofluids.

Nanofluids are suspensions in which nanoparticles with sizes ranging from 1 nm to 100 nm are dispersed. The most common nanoparticle materials are metals, metal oxides, and carbon allotropes. Among others, water is quite often employed as base fluid. One group within the nanofluid family are solar nanofluids. These special liquids absorb sun light in the visible and near infrared range. The nanoparticle load of these special suspensions is rather low. However, the dispersed nanoparticles exhibit high absorption capabilities with respect to solar radiation. The expectation is that the nanoparticles added to the base fluid improve its absorption abilities and its thermal conductivity and therewith the whole heat transfer process [27–29]. Thus, as solar nanofluids are proposed as direct sunlight absorbers, the study of their optical properties to ensure its suitability is of high importance. Moreover, it has to be mentioned that the addition of nanoparticles to water cause turbidity, which is an optical property of a suspension that causes light to be scattered and absorbed rather than transmitted through the suspension [124]. The turbidity is related with the concentration of solid particles suspended in the water.

First preliminary studies investigating black fluids working both as heat exchanger and solar thermal collector have already been carried out and indicate promising results [19, 22, 43, 107, 125]. The term black nanofluid is a commonly employed in the nanofluid community to characterise suspensions with mostly carbon based (except diamond) but in any case black nanoparticles to distinguish these specific suspensions from others. Solar thermal collectors are devices that harvest solar radiation energy by employing black nanofluids as direct solar energy absorbers. The fact that these fluids are used in solar thermal collectors both as highly efficient light absorbers and as heat transfer fluids indicates an important advantage over the current systems employing a transparent liquid exchanging heat with a solid absorber. Black nanofluids might be based on organic Indian ink [83] or synthetic carbon nanohorns (CNH). However, these liquids are known to degrade to various extents through exposure to solar light. Even if this drawback is present in almost every material studied so far, suspensions with CNH still seem to be very promising candidates for solar absorbers [24, 37, 126].

In this work, black nanofluids are investigated with respect to their capabilities to be used as such direct sunlight absorbers. Heat absorption capacities of the black nanofluids are studied by exposing the samples to an artificial sun and measuring the temperature developments of each sample. Optical property measurements are carried out, enabling the determination of the fraction of energy absorbed and their spatial distribution. The results of the study will allow an optimised design of solar collector and absorption systems.

5.2 Materials and methods

In the following sections the test rig employed for the thermal investigation of the black nanofluids and the synthesis of these suspensions are described.

5.2.1 Test rig for thermal investigations

Besides the apparatus employed for optical characterisation of black nanofluids (see Sec. 5.3), a special test rig is designed and built for the thermal testing of these fluids. The two main components of this test rig are an artificial sun and a sample holder. The experiments are carried out in a separate chamber with an available space of about 250 m^3 (6,500 mm x 5,500 mm x 7,000 mm). A fan with a power of 500 W is located in this measuring chamber to ensure an uniform ambient temperature during the measuring period so that all experiments are carried out under controlled conditions. The artificial sun comprises twelve lamps with a power of 2,000 W each (Fig. 21). The inclination of the structure carrying the lamps is 64.0 $\pm$ 0.3° in order to achieve the optimal radiation exposure with respect to the sample holder (Fig.5.1). Fans provided a line outlet below the lamps with cooling air to prevent the lamps from overheating.

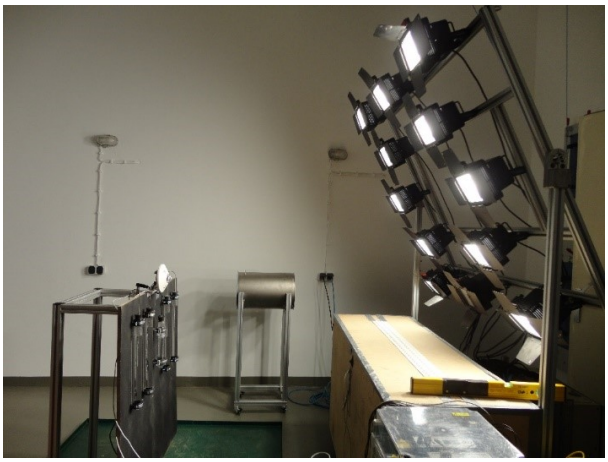

Figure 5.1. Test rig with artificial sun. Lamp array (right) imitating sunlight, with the samples placed opposite. The sample holder consists of a black painted vertical plate (left), on which the pyranometer mounted (white probe) on its upper part

The sample holder consists of a black plate of an area of 1 m^2 (1,000 mm x 1,000 mm) which supports 5 glass tubes. Four of the five tubes (Fig.5.2, all except the middle one) have an inner diameter of 25 mm and a length of 300 mm. All tubes are sealed with a rubber plug. However, the seals are designed in a way the that air can escape when the sample is heated and therewith the fluid inside expands. For the sake of safety, the whole sample holder is placed in a shallow tub to capture any black nanofluid that may escape during the experiments. The irradiation coming from the artificial sun is measured employing a pyranometer (CMP11, KIPP & ZONEN, The Netherlands). The pyranometer is positioned in the upper middle part of the sample holder.

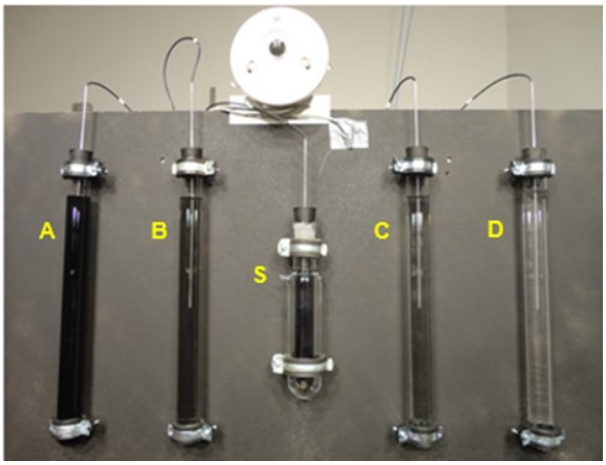

Figure 5.2. Sample holder with the black nanofluid samples of different concentrations. A pyranometer is placed at the upper centre of the holder. Temperature inside each sample is measured with a Pt-100-thermocouple. Surface temperature of the holder measured with the thermocouple visible just to the right of the pyranometer. Letters indicate the names of the tubes

In order to measure the working fluid temperature, a thermocouple Pt100 is positioned centrically in each glass tube. Three thermocouples are used to determine the temperatures at the front and back sides of the sample holder and below the lamps. All thermocouples are calibrated before the measurement campaign. Additionally, all thermocouples are adjusted before each measurement series. The measurement accuracy of all thermocouples is $\pm$ 0.1 K. The measurement value logging of the test rig consists of a message device and the software ProfiSignal (Delphin Technology AG, Germany) working with MS Windows. ProfiSignal compiles all data in tabular and graphical form. Moreover, all data are stored on hard disk.

After filling the glass cylinders, the samples are left without heating to equilibrate to the ambient temperature of the measuring chamber. Each test series starts by switching on the lamps and the fans. The samples are heated for 4 hours and every second a temperature value of all thermocouples is taken. This time is sufficient for all test cases to reach a constant temperature at all measurement positions. The artificial sun and the fans are switched off after this first measurement period and the whole chamber is left without heating the subsequent night for cooling.

The sample holder with the NHSDS nanofluids is shown in Fig.5.2. The tubes that are mounted on the plate of the sample holder are labelled A, B, C and D. Tube A contains the highest nanoparticle concentration studied. All other tubes are filled with dilutions. These dilutions were 1/10, 1/100, and 1/1000 of the original concentration in tubes B, C, and D, respectively. Tubes A, B, C, and D are geometrically identical. Tube S is a reference tube which is not employed in the analysis because it is double-walled and therewith not comparable with tubes A to D.

It is assumed, that the heat losses are very similar for each of the glass cylinders. Moreover, the study aims to highlight the differences among the black nanofluids with respect to their absorption abilities. Therefore, a detailed modelling of the heat losses is not carried out.

5.2.2 Synthesis of the nanofluids

SWCNHs were provided by Carbonium S.r.l. and were produced by a process based on rapid condensation of carbon atoms without any catalyst and with highly reduced production costs [89]. The morphological characterisation of the nanoparticles was performed by Field Emission Scanning Electron Microscopy (FESEM) with a SIGMA Zeiss instrument (Carl Zeiss SMT Ltd, UK). Two suspensions containing 0.02 g/l of SWCNHs in a water solution containing surfactants were prepared. In the first sample, sodium dodecyl sulphate was used as a surfactant with a concentration of $5{\cdot}10^{-3}$ g/l, while in the second sample a mixture of SDS and PVP, with concentrations of $5{\cdot}10^{-3}$ g/l and $5{\cdot}10^{-2}$ g/l respectively, was used. The two suspensions were prepared according to the following procedure. Firstly, 250 mL of the surfactant solution in water was prepared, after which 0.02 g/l of SWCNHs were dispersed in the solution through an initial homogenisation with an ultrasonic processor (VCX 130, Sonics & Materials) operated at 20 kHz and 65 W for 10 min. Thereafter, the suspension was processed for 15 minutes in a high-pressure homogeniser (Panda, GEA Niro Soavi, Germany) operated at 1,000 bar.

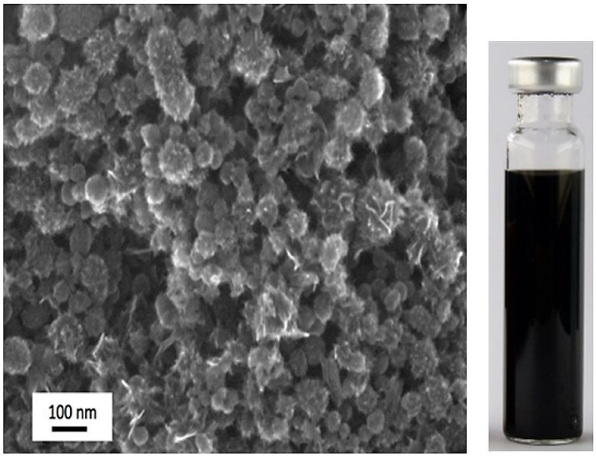

Figure 5.3. FE-SEM micrograph of carbon nanohorns powder and black nanofluids. The right sample shows NHSDS before use

A Malvern Zetasizer Nano ZS exploiting the Dynamic Light Scattering (DLS) technique was used for the evaluation of aggregate size distribution within the colloids and of the ζ-potential. Fig.5.3 shows an example of FESEM micrograph of carbon nanohorn powder. The mean dimension of the carbon nanohorns, evaluated by means of the software ImageJ IJ 1.46r, is 55 ± 15 nm. The aggregation is due to the drying process while preparing the specimen to perform the FESEM observation. The ζ-potentials of the sample containing only SDS and of that containing SDS and PVP are - 43 mV and - 35 mV, respectively. The presence of PVP, being a non-ionic surfactant, leads to a slight reduction of the zeta potential, but its steric action still lead to an improved colloidal stability. In fact, DLS measurements show a similar average hydrodynamic size of 138 nm for the sample containing SDS and 135 nm for the sample containing SDS and PVP, but with a much sharper size distribution for the latter, as reported in Fig.5.4.

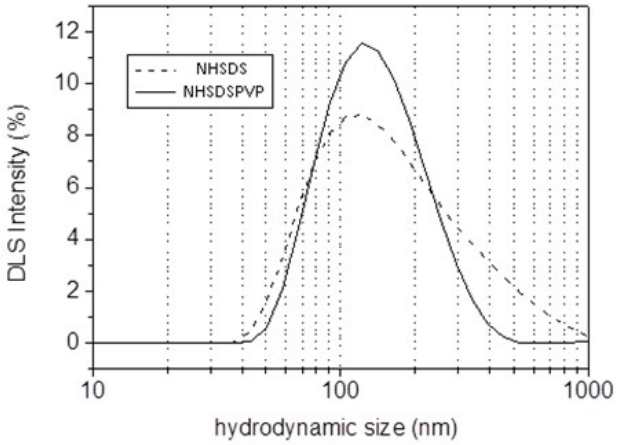

Figure 5.4. DLS measurements of black nanofluids

5.3 Characterisation of black nanofluids

Thermophysical properties as thermal conductivity, density and viscosity are not the central parameters with respect to the absorption behaviour of the black nanofluids investigated in this study. Therefore, the characterisation of the suspensions is focused on their optical qualities. Optical characterisation is carried out in order to evaluate the potential of the studied black nanofluids as direct solar energy absorbers. To get a deeper optical characterisation, ballistic transmittance, absorption spectra, and fraction of the incident power absorbed are investigated.

5.3.1 Ballistic transmittance

Ballistic transmittance is the ratio of transmitted to incident intensity in a small aperture facing the forward direction, thereby ensuring the scattered light is not taken into account. The transmittance spectra T_b (λ) for a 1 cm path length x, is assessed by employing a CARY 500 spectrophotometer (Spectrophotometer Varian, Dev.). Experiments are carried out at room temperature from 400 nm to 2,000 nm with a spectral resolution of 1 nm. The extinction coefficient $\mu_{ext}(\lambda)$ is calculated from the ballistic transmittance following the Lambert-Beer law [115]

$$T(\lambda) = \mathrm{e}^{-\mu_{ext}(\lambda)x} \tag{5.1}$$

When measuring the ballistic transmittance, the scattered light is not measured, but care must be taken in splitting absorbed and scattered light. Following equation 5.2 based on previous works [18], the absorption coefficient $\mu_{abs}(\lambda)$ for the nanofluid used in this work is approximated as a function of the extinction coefficient $\mu_{ext}(\lambda)$

$$\mu_{abs}^{CNH}(\lambda) = 0.95\mu_{ext}^{CNH}(\lambda) \tag{5.2}$$

This assumption is valid for a constant scattering along the wavelength range. Then, after calculating the extinction coefficient by using the equation 5.1 and the absorption coefficient calculated according to equation 5.2, the scattering coefficient is obtained as follows since the extinction phenomena is the sum of the absorption and scattering coefficients:

$$\mu_{ext}(\lambda) = \mu_{abs}(\lambda) + \mu_{sca}(\lambda) \tag{5.3}$$

The ballistic transmittance of all black nanofluids and of the base fluid as reference are performed before and after being exposed to the artificial sun. Indeed, samples of the two black nanofluids employed in the experiments are taken out of the glass cylinders and analysed with respect to their transmittance spectra.

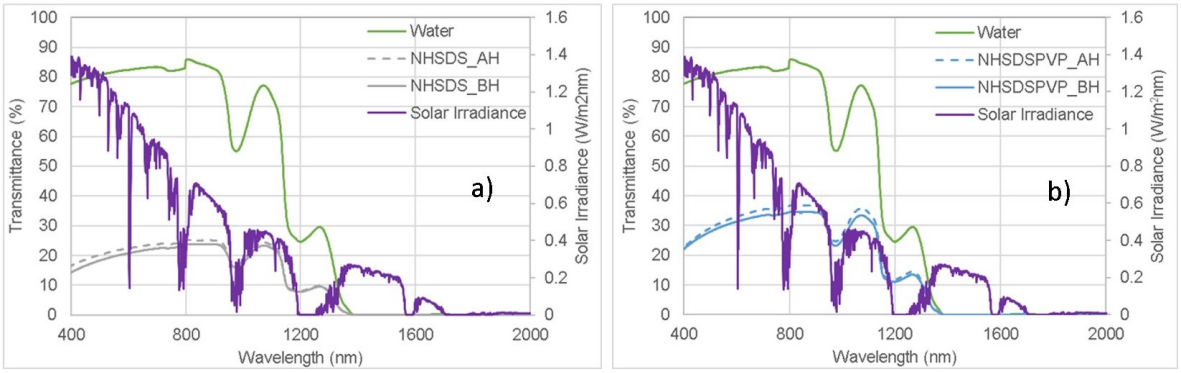

Figure 5.5. Transmittance spectra for suspensions of CNH in DI-water. Left plot (a) shows NHSDS before heating (NHSDS_BH) and NHSDS after heating (NHSDS_AH) and right plot (b) NHSDSPVP before heating (NHSDSPVP_BH) and NHSDSPVP after heating (NHSDSPVP_AH) samples. The behaviour of the base fluid is also shown for comparison (green curve)

The left plot of Fig.5.5 presents the transmittance spectra of the ordinarily stabilised black nanofluids (NHSDS). The spectra of the doubly stabilised black nanofluids (NHSDSPVP) are presented in the right plot of Fig.5.5. In both cases, the transmission of CNH nanofluids is lower than that of pure DI-water. Moreover, it is clearly observable that in the range between 1,500 nm and 2,000 nm the transmission becomes zero for all the liquids, including DI-water. Moreover, the transmittance values of the doubly stabilised nanofluid are on average about 32% higher than that of the singularly stabilised nanofluid. This effect is an indicator that double stabilisation works properly in the sense that it avoids agglomeration, which in turn leads to a higher percentage of the light passing through the sample. Note that it has to be distinguished between sufficient and necessary experimental results to claim, that a certain suspension shows less agglomeration compared to a reference liquid. The changes of the absorption spectra found indicate a necessary condition that doubly stabilised nanofluids show less agglomeration than the singly stabilised once. Sufficient certainty would be obtained by direct measurement of the agglomeration grade during heating. Extinction, absorption, and scattering coefficients are calculated employing the above discussed transmittance spectra. The results are shown in Fig.5.6 a), Fig.5.6 b), and Fig.5.6 c), respectively. While the extinction coefficient designates the amount of light that does not pass through the sample, and is generally defined as the sum of the

absorption and scattering coefficient, the absorption coefficient indicates the amount of energy absorbed by the sample. Both parameters clearly indicate that adding a small amount of CNH improves the absorption performance of the pure fluid – in our case DI-water – with respect to solar radiation. The doubly stabilised nanofluid NHSDSPVP shows lower absorption and extinction coefficients than the singularly stabilised nanofluid NHSDS. Thus, the absorption and extinction coefficients for samples after heating are lower than that for samples before heating.

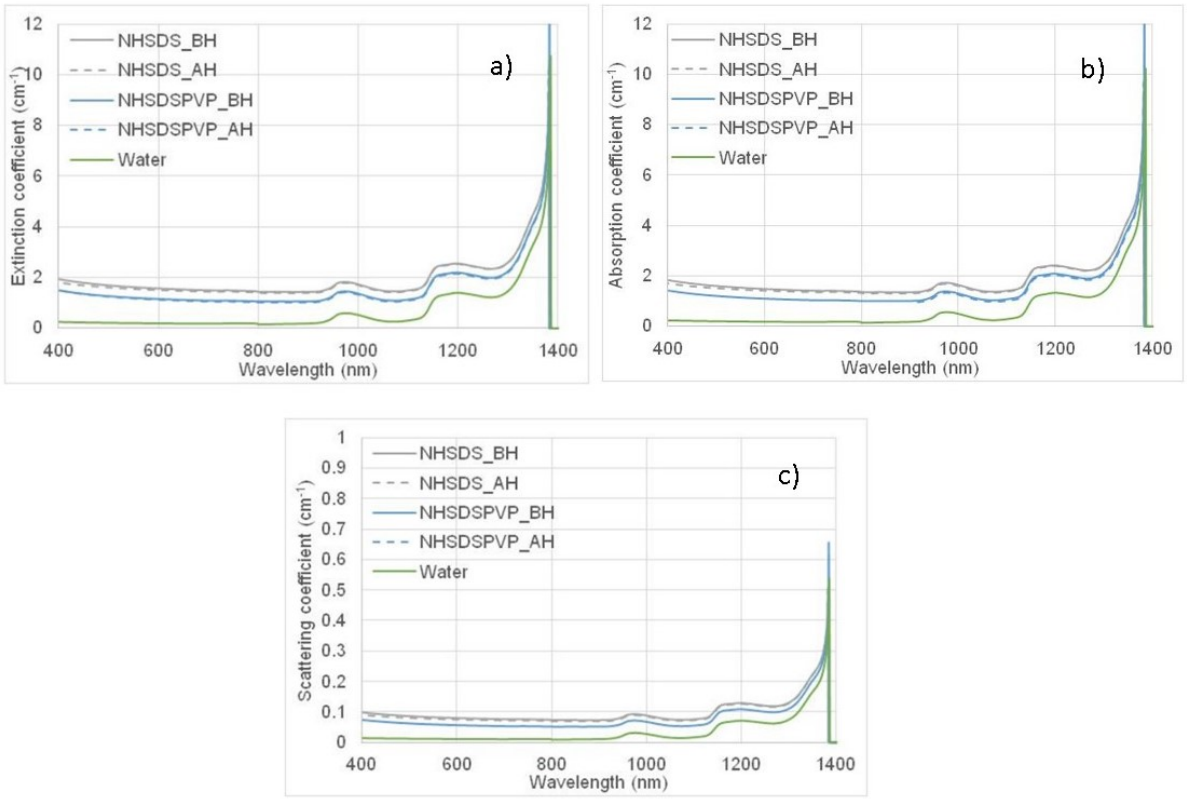

Figure 5.6. Optical coefficients of CNH nanofluids before (NHSDS_BH and NHSDSPVP_BH) and after heating (NHSDS_AH and NHSDSPVP_AH): a) the extinction coefficient; b)the absorption coefficients of the same nanofluids; c) the scattering coefficient

Upon analysing the scattering coefficient (Fig.5.6 c), it is found that the base fluid values are nearly zero around 900 nm. This is indeed an expected result, as the base fluid does not contain nanoparticles, which are usually responsible for the scattering phenomena. On the other hand, scattering coefficients for both black nanofluids are quite similar due to the same shape of nanoparticles employed and the same concentration, 0.002 g/L of CNH, utilised. However, due to the small size of the CNH, the scattering effects are very weak. Therefore, the extinction of the incident light by the CNH is mainly caused by absorption (95%) [18, 83, 121].

Transmittance values below 0.1% that give extinction coefficients higher than 6 cm^{-1} lead to intensity levels of transmittance below the resolution of the near-infrared detector and, as a result, some noise is seen above 1,400 nm. This is due to the strong absorption in the near-infrared range of the base fluid used and not due to absorption by the CNH.

5.3.2 Fraction of the incident power absorbed

In the following section, the incident power absorbed by the different working fluids is discussed. The light absorption capability of the different nanofluids is evaluated with the fraction F(x) of the incident power absorbed in the fluid after a path length x. Using the absorption coefficient from each of the nanofluids, the absorbed energy fraction is calculated following the expression:

$$F(x) = 1 - \frac{\int_{\lambda_{min}}^{\lambda_{max}} I(\lambda) \cdot \mathrm{e}^{-\mu_{abs} x} d\lambda}{\int_{\lambda_{min}}^{\lambda_{max}} I(\lambda) d\lambda} \tag{5.4}$$

where I(λ) is the spectral distribution of the incident light, keeping the solar radiation on the surface [38] in the wavelength range indicated by the American Society of Testing Materials (ASTM), while considering λ_{min} = 400 nm and λ_{max} = 2,000 nm as integration bounds. The approximated spectral absorption coefficient μ_{abs} is given by the equation 5.2, after the calculation of the respective spectral extinction coefficient.

The absorbed incident power fractions calculated using 5.4 are represented in Fig.5.7 for a range of fluid thicknesses that is representative for solar thermal collector geometries. It is clearly observable by comparing the blue (broken and full line) and grey (broken and full line) curves with the green curve that the addition of CNHs has a significant effect on the fraction of incident power absorbed by the nanofluid. Even though the utilised concentration, 0.02 g/L, in this work is low, at 10 cm of fluid thickness the nanofluids have an absorbed energy fraction of 100%.

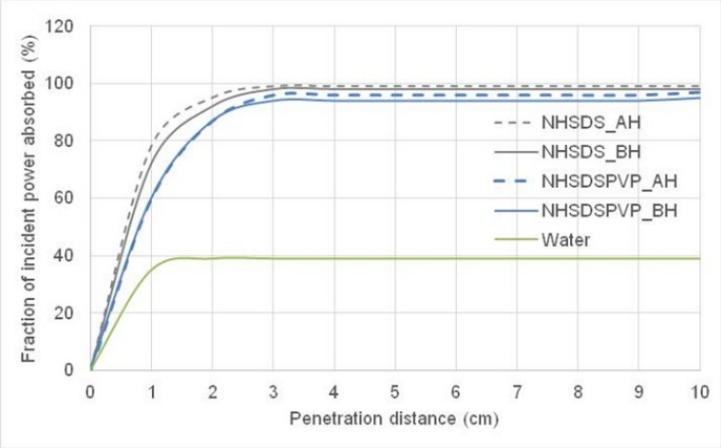

Figure 5.7. Comparison of the fraction of the incident power absorbed by ordinary stabilised before (NHSDS_BH) and after (NHSDS_AH) heating. Also, double stabilised before (NHSDSPVP_BH) and after (NHSDSPVP_AH) heating but with the same nanoparticle concentrations. The behaviour of the pure DI-water is also shown for comparison (green curve)

According to these results, it can be expected to optimise the size and the concentration of nanohorns to create a nanofluid where the absorption is close to 100% with as little penetration distance as possible. Moreover, these outcomes are in agreement with the results obtained with the absorption and the extinction coefficients where nanofluids indicate higher values after being

heated by the artificial sun during the thermal experiments than before being heated. One may hypothesise that this is due to the agglomeration produced by heating the samples. Because of that, samples stabilised just once produce higher values of absorption due to the presence of larger particles caused by the agglomeration.

5.3.3 Spatial distribution of the energy absorbed

To get a more detailed characterisation of both black nanofluids under exposure to the artificial sun, the spatial distribution S(x) of the energy absorbed is calculated using the equation 5.5 and compared to that of DI-water in order to analyse the enhancement provided by the CNHs.

$$S(x) = \frac{\int_{\lambda_{min}}^{\lambda_{max}} I(\lambda) \cdot \mu_{abs} \cdot \mathrm{e}^{-\mu_{abs} x} d\lambda}{\int_{\lambda_{min}}^{\lambda_{max}} I(\lambda) d\lambda} \tag{5.5}$$

As can be seen in Fig.5.8, the energy is mainly absorbed in the first layer of the samples. For black nanofluid samples, indistinctly before or after heating, the energy is stored near the surface and the deeper layers are heated by thermal conduction. On the other hand, the spatial distribution of the energy for pure DI-water is lower than that of the nanofluids. Once again, nanofluids after heating present higher values than those before heating, following the same trends as for the fraction of the incident power absorbed. Taking into account that the inner diameter of the cylinders employed in this work is 25 mm, it can be argued, based on Fig.5.8 that at this penetration distance about 90% of the energy is already absorbed for all the black nanofluids, while for the DI-water it would have been only absorbed around 80%.

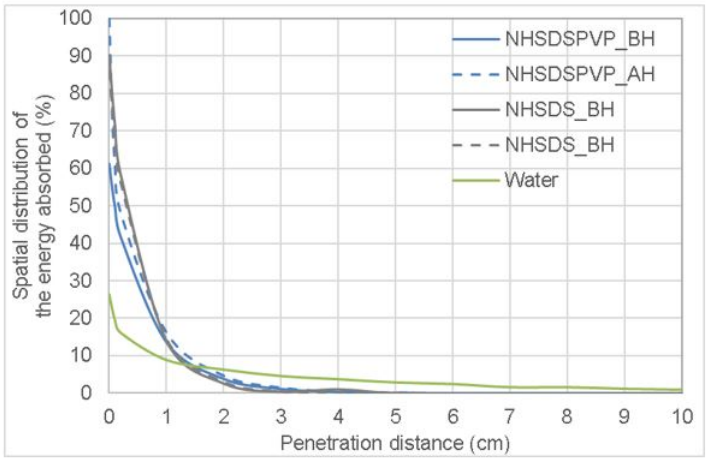

Figure 5.8. Spatial distribution of the energy absorbed as a function of the penetration distance in the nanofluid of NHSDS before heating (NHSDS_BH), NHSDS after heating (NHSDS_AH), NHSDSPVP before heating (NHSDSPVP_BH) and NHSDSPVP after heating (NHSDSPVP_AH)

5.3.4 Absorption spectra

The absorption spectra of the two CNH water-based nanofluids and the base fluid DI-water are evaluated before and after being exposed to the artificial sun. In this case, the same spectrophotometer than above is used (Spectrophotometer CARY 500. Varian Dev.) but with an integrating sphere. Then, the scattering phenomenon is taken out from the absorption spectra. These measurements are also carried out at room temperature and ranged from 400 nm to 2,000 nm, with a 1 nm spectral resolution. The absorption spectra are obtained as:

$$A(\%) = \frac{I_0 - I_{T+FS} - I_{R+BS}}{I_0} \cdot 100 \tag{5.6}$$

here, I_0 is proportional to the total incident light of the beam, I_{T+FS} is the light that has been either directly transmitted through the sample or forwardly scattered, and I_{R+BS} is the light that has been either reflected or backward scattered.

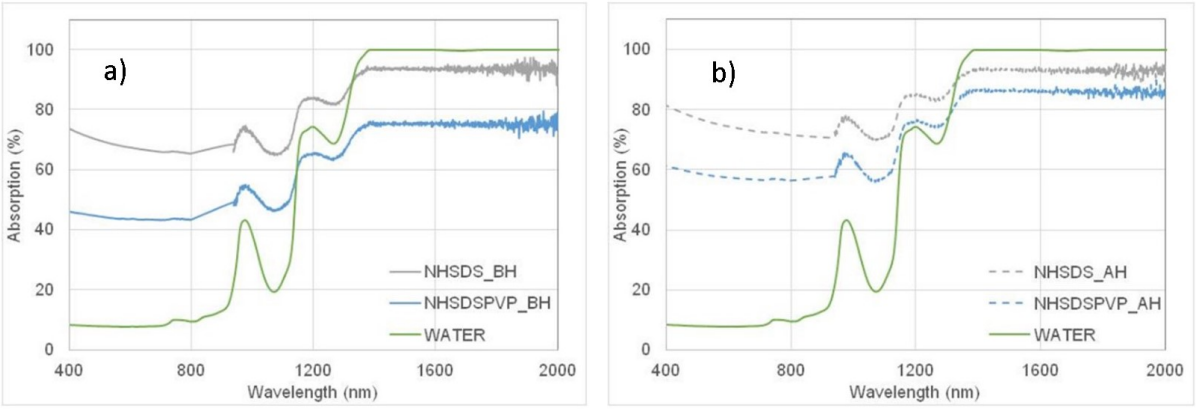

Figure 5.9. CNH water-based nanofluids absorption spectra. a) Shows samples before heating and b) presents samples after heating. The behaviour of the base fluid is also shown for comparison

Fig.5.9 a) presents the absorption spectra of the singularly stabilised black nanofluids (NHSDS) and the doubly stabilised black nanofluid (NHSDSPVP) before being exposed to the artificial sun; the same samples but after heating are presented in Fig.5.9 b). In both cases, the absorption of black nanofluids is higher than that of pure DI-water. An exception is found in the range between 1,380 nm and 2,000 nm. Especially the peak at about 980 nm is less pronounced in the black fluids. The addition of black nanohorns, even at the concentration of 0.02 g/L, makes the spectrum noticeably smoother. In addition, the absorption for both nanofluid samples is more homogeneous for different wavelengths. In general, higher absorptions for the NHSDS samples are found. It is evident, that the absorption spectrum values for NHSDS are in general higher than those of NHSDSPVP. This is true for the situation before and after heating.

From Mie scattering theory it is assumed that scattering is proportional to the averaged size of the nanoparticles suspended in the black nanofluid [127]. The larger the nanoparticles suspended in the nanofluid, the lower the scattering and, consequently, the higher the absorption efficiency. From that assumption and Fig.5.9 it is concluded that NHSDS should have the

larger effective particles both before and after heating during the thermal experiment. Or in other words, a stabilisation with SDS is not so effective in minimising agglomeration as double stabilisation employing both SDS and PVP. Consequently, there are larger particles suspended in NHSDS which lead to a higher absorption efficiency. This finding is seen as an indirect proof that double stabilisation with SDS and PVP is more efficient. Moreover, this double stabilisation also works under the heating imposed on the black nanofluid samples during the thermal experiments.

Fig.5.9b) clearly indicates that, despite the absorption spectra of both NHSDS and NHSDSPVP being raised, the NHSDS spectrum is still the higher of the two. The general increase of the absorption spectra values and therewith the effective particle size is explained with the more intense contact of the nanohorns due to enhanced Brownian and thermophoretic diffusion during heating. Additionally, free convection taking place inside the cylinders may play a role. Free convection has to be expected in any gaseous or liquid volume affected by heat transfer processes. It is driven by temperature gradients. In case of the glass cylinders investigated with this study such temperature gradients may occur between the front and the back side of the cylinder. Eventually these gradients generate convection rolls inside the cylinders which would transport warmer nanofluid into areas less heated. Therefrom, an homogeneisation of temperature gradients would follow. However, such processes could neither be monitored directly by observing any fluid motion inside the cylinder nor indirectly by identifying temperature gradients inside the cylinders. The latter is due to the fact that only one thermocouple is utilised.

Averaging the data over the measured wavelengths, NHSDS_BH and NHSDS_AH increase their absorption potential by 50% and by 52% with respect to the base fluid, respectively. For the cases of NHSDSPVP_BH and NHSDSPVP_AH, increments of 31% and 43% are found. In both black nanofluids, the absorption spectra after being exposed to the artificial sun increase: in the case of NHSDS, by 5%, and in the case of NHSDSPVP, by 28%. It is important to know that the base fluid DI-water is essentially transparent over the visible range (400 – 800 nm). The absorption in this wavelength range is therefore mostly attributed to the CNH [128].

In order to investigate the effect of heating on the black nanofluids in more detail, the ratio of absorption spectra is plotted in Fig.5.10. NHSDS is nearly unaffected by heating above a wavelength of about 1,300 nm. Below this threshold, a weak increase of maximum 10% takes place.

A much stronger effect is seen for NHSDSPVP. Here a significant enhancement of about 15% is detected for wavelengths larger than 1,100 nm. Once again, below this threshold the increase is stronger. The reason for this effect is that double stabilisation prevents nanohorns from agglomeration, meaning smaller particles are found in NHSDSPVP. Therefore, the potential of increasing the absorption spectrum by particle agglomeration is higher here. This is even true if the eventual spectrum of NHSDSPVP indicates lower values (Fig.5.9).

Finally, in order to study the PVP contribution with respect to the prevention of agglomeration and especially to split it from the SDS contribution, Fig.5.11 is presented. The curve shown is the difference between the two curves from Fig.5.10. By subtracting the increments of NHSDS and NHSDSPVP, the effect caused by the PVP is separated. Over a large range of wavelengths – 900 nm to 2,000 nm – this PVP contribution seems to be constant.

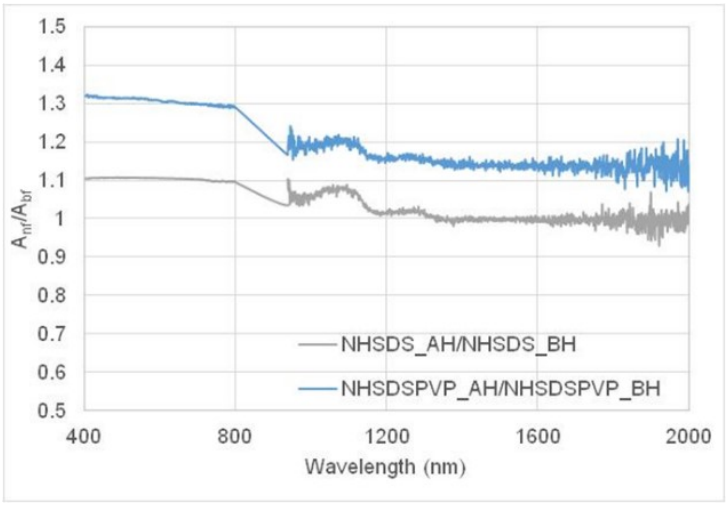

Figure 5.10. Ratio of absorption spectra of black nanofluids after exposure to artificial sun

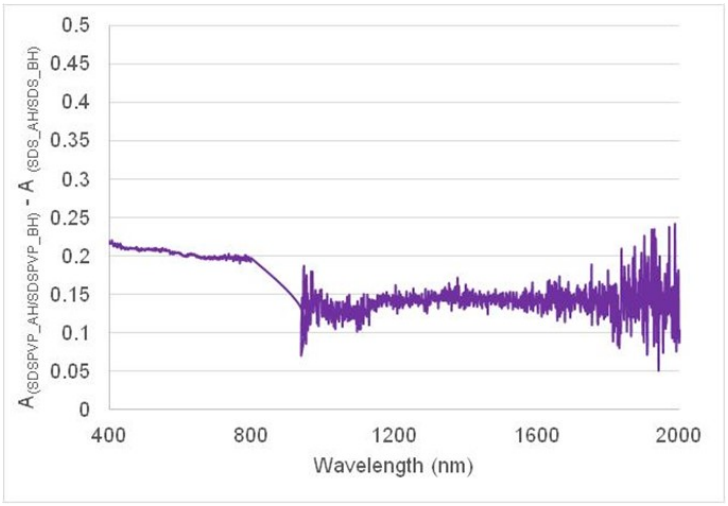

Figure 5.11. PVP-contribution to agglomeration after heating the samples by the artificial sun

5.4 Results and discussion of thermal experiments

Regarding the thermal experiments, DI-water based CNH nanofluids, where the appearance of solar thermal heat carriers is feasible, are tested under exposure to an artificial sun. In addition, DI-water is investigated with the same test rig to obtain reference values. The goals of the experiments are, on the one hand, to find out more about the thermal characteristics of nanohorn-based black nanofluids and, on the other hand, to investigate how the stabilisers SDS and SDS plus PVP influence the heat storage. In the following, a fitting of the obtained experimental data is carried out as part of the thermal analysis. The aim is to develop a model whit a reduced number of parameters which allows a comprehensive comparison of differently stabilised black nanofluids.

5.4.1 Instantaneous development of temperature

Fig.5.12 represents the normalised temperature development over time obtained in heating up the two black nanofluids and the reference fluid DI-water for tube A. The normalisation is undertaken with the starting temperature $t_0 = t$ ($\tau = 0$). Normalisation is a standard approach in fluid mechanics and heat transfer. It is carried out to reduce the number of variables and to make different test cases comparable.

In general, it is found that the black nanofluids heat up faster than the reference fluid DI-water. This is especially true for the time interval from 30 min to 90 min (1,800 sec to 5,400 sec). Here the black nanofluids show a steeper slope than DI-water. Moreover, the black nanofluids reach a final temperature of about 5 K higher, which transfers to an increase of τ/τ_{end} of about 0.17. Analysing the experimental data of tube A (Fig.5.12a)), it is found that the three different curves follow logarithmic trends in the time interval from about 30 min to 60 min (1,800 sec to 3,600 sec). A more sophisticated approach involves understanding the temperature development inside the cylinders as a step response to the incoming irradiation from the artificial sun. It is assumed that two main but independent physical phenomena have to be considered with respect to the temperature development. The first is storage of sensitive heat and the second compiles the heat losses. One may argue that the temperature increase inside the cylinders is accelerated by the free convection taking place due to local temperature gradients. For black nanofluids an additional acceleration follows after the enhanced absorption due to the nanohorns.

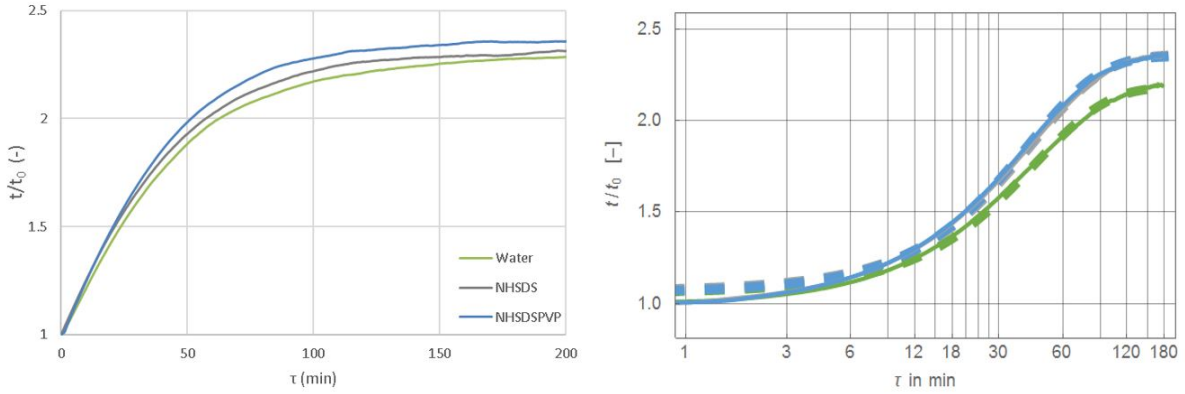

Figure 5.12. Normalised temperature development of carbon nanohorn nanofluids and reference fluid DI-water as a function of time for tube A. a) shows linear-linear and b) log-linear representation. Full curves indicate experimental data and bold broken curves fit according to 5.7 with parameters presented in Table 5.2

The above assumptions allow an understanding of the temperature development as the aperiodic limit case of a second order transfer element (PT2-element), which is described by the following equation:

$$t/t_0 = 1 + (t/t_0)_{end}(1 - [1 + \omega_0(\tau - \tau_0)e(-\omega_0(\tau - \tau_0))] \tag{5.7}$$

Note that the standard PT2 element is described by the second term of the right-hand side of equation 5.7 alone. The additional unity in front of this term is introduced to capture the

normalisation with the starting temperature t_0. An additional time offset τ_0 is introduced to capture the characteristic time delay of the different working fluids at the beginning of heating. Non-linear fitting employing the Levenberg-Marquardt algorithm (MATHEMATICA 10.0) for tube A delivers the following parameters for equation 5.7.

Table 5.1. Tube A parameters for equation 5.7

	t/t_0	ω_0	τ_0
DI-water	1.18	-6.97·10^{-4}1/sec	492 sec
NHSDS	1.36	-7.07·10^{-4}1/sec	502 sec
NHSDSPVP	1.35	-7.51·10^{-4}1/sec	436 sec

Fig.5.12 shows a reasonable agreement between the fitting functions with tube A parameters (Table5.1) and the experimental data found for tube A. The following three outcomes are of importance. First, the final normalised temperature (t/t_0)end increases from DI-water to the two black nanofluids by about 8%. Moreover, heating takes place faster in these two suspensions, which is specified by the increasing parameter ω_0. The parameter τ_0 is nearly the same for DI-water and NHSDS, but about 10% less for NHSDSPVP. The effects found for tube A disappear when the concentration of the black nanofluids is lowered to 10%, as it is the case in tube B. The parameters of equation 5.7 for this tube are:

Table 5.2. Tube B parameters for equation 5.7

	t/t_0	ω_0	τ_0
DI-water	1.25	-7.02·10^{-4}1/sec	491 sec
NHSDS	1.26	-6.66·10^{-4}1/sec	566 sec
NHSDSPVP	1.27	-7.06·10^{-4}1/sec	487 sec

Again, the fitting correlations and the experimental data are in reasonable agreement (Fig.5.13). However, it is striking that for tube B there is nearly no difference between the three working fluids. The parameters characterising the step response of the temperature development reflect this. There is not a clear tendency for any of the parameters.

As indicated by Fig.5.13, the behaviour found for tube B is not due to the dilution being so strong that a nearly water-like nanofluid is obtained. Tube B still shows a grey content, which points to a low but not negligible concentration of nanohorns. A clue comes from tube C, where the concentration amounts to one-hundredth of the original concentration in tube A. Fig.5.14 shows the experimental normalised temperature developments and its approximation according to equation 5.7 for tube C. The parameters found for the approximation are shown in Table 5.3:

It is noticeable that the black nanofluids perform a worse job than the reference fluid DI-water. The normalised end temperature $(t/t_0)_{end}$ decreases in comparison to DI-water by about 6% for NHSDS and by about 5% for NHSDSPVP. The values of ω_0 and τ_0 do not

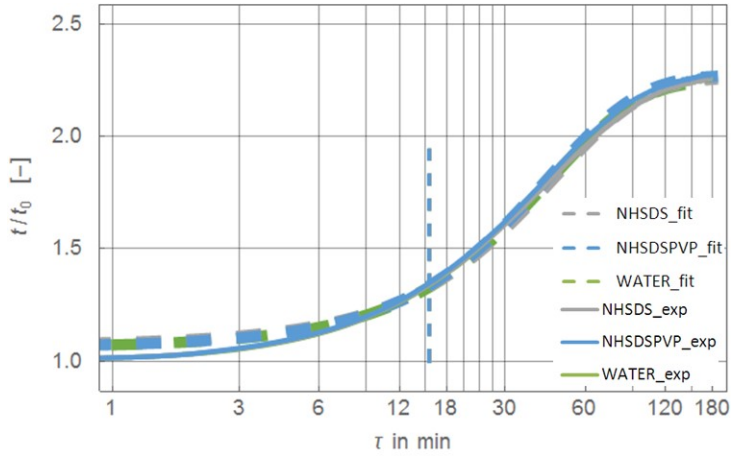

Figure 5.13. Normalised temperature development of carbon nanohorn nanofluids and reference fluid DI-water as a function of time for tube B

Table 5.3. Tube C parameters for equation 5.7

	t/t_0	ω_0	τ_0
DI-water	1.26	-7.17·10^{-4}1/sec	472 sec
NHSDS	1.14	-7.05·10^{-4}1/sec	496 sec
NHSDSPVP	1.16	-7.19·10^{-4}1/sec	464 sec

really show tendencies. Tube D with a concentration of merely one-thousandth of the original suspension indicates more or less the same results as tube C.

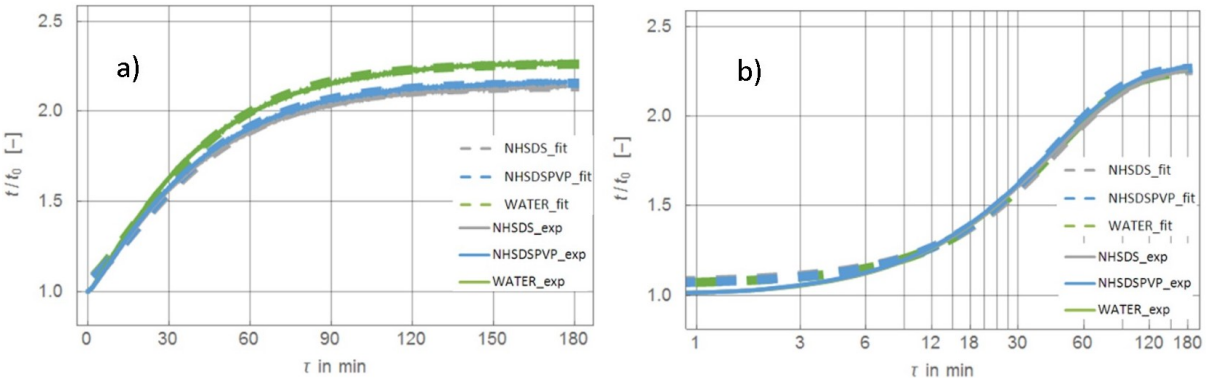

Figure 5.14. Normalised temperature development of carbon nanohorn nanofluids and reference fluid DI-water as a function of time for tube C

It is hypothesised that the mitigation of the temperature development is due to back scatter of the remaining nanohorns after dilution. So the question about the optimal concentration arises. To solve this issue, Fig.5.15 is plotted, which compiles the parameters of the step responses for the different tubes. Fig.5.15 a) shows the normalised end temperatures in dependency of the nanohorn concentration. While DI-water has – as expected – a nearly constant value, the two

black fluids indicate a significant increase with increasing concentration. However, both black fluids behave identically within the experimental error. The situation is different for ω_0. Here, neither a significant difference between DI-water and the black nanofluids nor any dependency on the concentration is seen. The time delay ω_0 shows once again as expected no change from tube to tube. However, the NHSDSPVP values are all, except for the lowest concentration, smaller than the respective values for NHSDS.

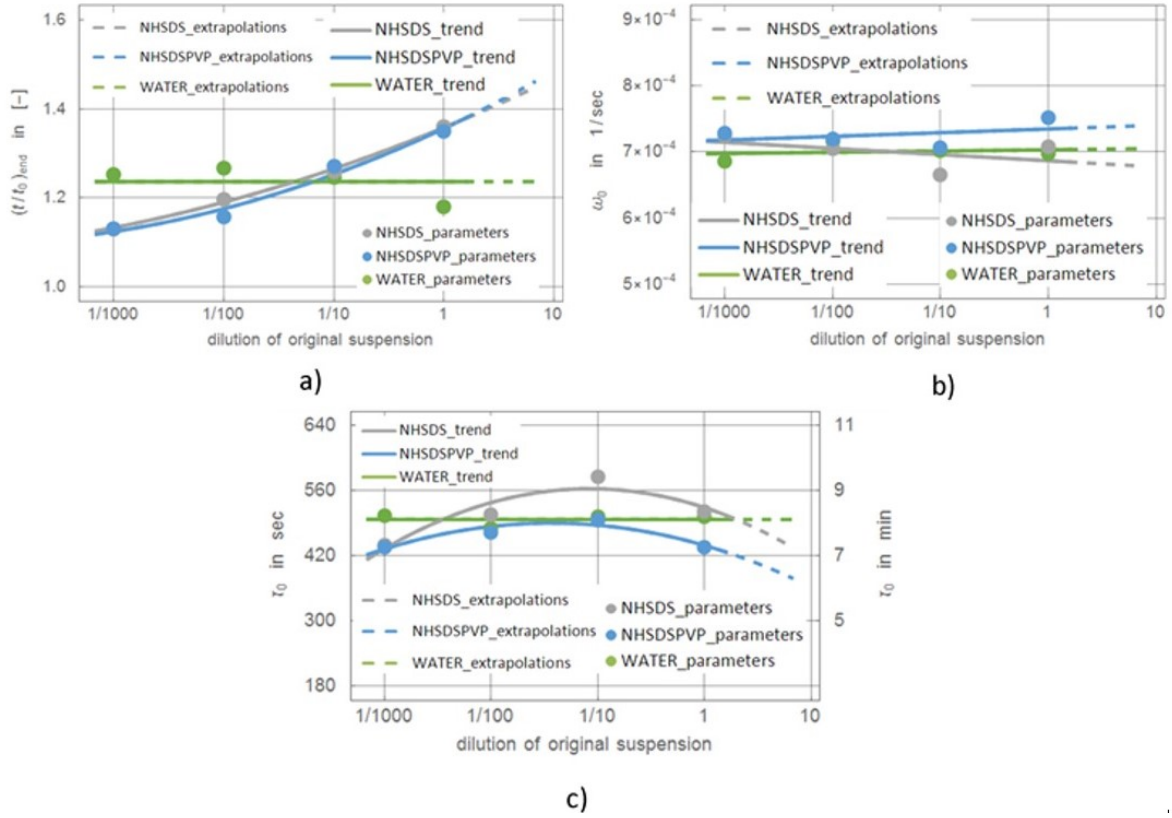

Figure 5.15. Parameters of approximation correlations according to equation 5.7 and parameters shown in Tables 5.1, 5.2 and 5.3. Symbols stand for parameters, full curves for trend lines and broken lines for extrapolations. Green shows DI-water, grey NHSDS and blue NHSDSPVP

To summarise, it seems to be possible that a black nanofluid with a higher nanohorn concentration than the one investigated here may absorb even more light. This follows especially from the steadily increasing parameter $(t/t_0)_{end}$ (Fig.5.15 a)). This parameter is basically related to the intensity of the transmittance spectra (Fig.5.9). The higher the absorption capability of a certain working fluid, the higher the end temperature. Moreover, heating up may occur faster for black nanofluids which have been double stabilised, as with NHSDSPVP.

To get a better understanding of the differences between DI-water and the black nanofluids already found with Figs.5.12 to 5.14, the ratios of the normalised temperatures of NHSDS to DI-water and of NHSDSPVP to DI-water are plotted in Fig.5.16 for tubes A to C.

Additionally, these diagrams show the ratio of NHSDSPVP to NHSDS. Both the experimental data and the curves following from equation 5.7 are plotted. For all tubes and

ratios a reasonably good agreement between experiment and approximation is found.

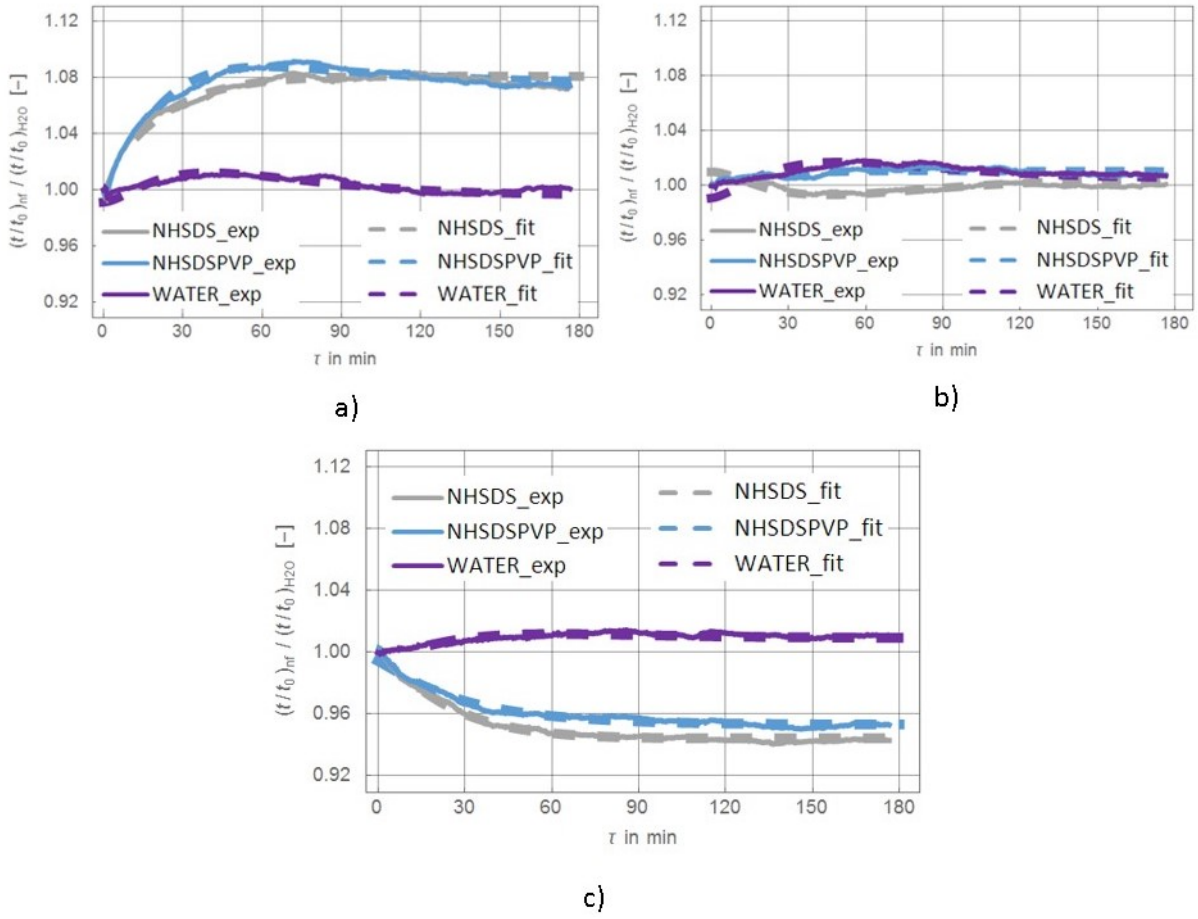

Figure 5.16. Ratios of normalised temperature developments for carbon nanohorn nanofluids and reference fluid DI-water as a function of time for a) pipe A, b) pipe B and c) tube C. Full curves indicate experimental data and broken curves fit according to equation 5.7 and parameters shown in Tables 5.1, 5.2 and 5.3

For tube A (Fig.5.16 a) it becomes immediately clear that a reasonable temperature increase is generated with the undiluted black nanofluids compared to DI-water. Starting with a ratio of unity, a significant increase follows in the first 40 min. After that the ratios for both black nanofluids are constant with an increase of about 8%. In the time interval from about 20 min to 65 min, the increase found for NHSDSPVP is slightly higher than that of NHSDS. This intensification is also visible in the ratio of NHSDSPVP to NHSDS. It is related to the time offset τ_0, which has the lowest value for NHSDSPVP.

The tube B shows nearly no differences between DI-water and the black nanofluids. However, it is of interest that in the same time interval as for tube A (20 min to 65 min) NHSDSPVP is slightly better than DI-water and NHSDS. The right plot of Fig.5.16 indicates the mitigation already discussed in relation to Fig.5.14. The lowering ranges between 5% for NHSDSPVP and 6% for NHSDS. However, even in this case NHSDSPVP shows a slightly better performance than NHSDS.

5.4.2 Quantity of heat stored

From a practical point of view, it is important to understand how much thermal energy is stored in a certain solar nanofluid. Here, based on the experiments with the artificial sun, a rough estimate of this storage ability is given for tube A. The other three tubes show either equal or lower temperatures than the reference fluid DI-water (Fig.5.17), which indicates that the nanohorn concentration is too low to improve the storage ability.

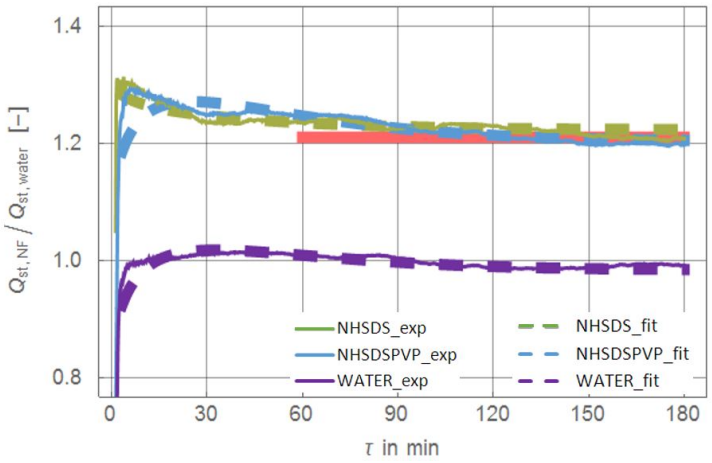

Figure 5.17. Ratio of normalised thermal energy stored for carbon nanohorn nanofluids and reference fluid DI-water as a function of time for pipe A. Full curves indicate experimental data and broken curves fit according to equation 5.7 and parameters presented in Tables 5.1, 5.2 and 5.3. The red lines indicates the asymptotic value reached by the black nanofluids. The purple curves indicate the ratio of the two black nanofluids

The radiation energy coming from the artificial sun increases the temperature inside the cylinder filled with DI-water or black nanofluid. The heat Q_{st} stored is approximately proportional to the temperature change ΔT and proportional to the mass of the fluid m_{fluid} inside the cylinder.

$$Q_{st} = c_p \cdot m_{fluid} \cdot \Delta T \tag{5.8}$$

The temperature difference is the instantaneous temperature minus the starting temperature. Fig.5.17 shows the ratios of Q_{st} of NHSDS to DI-water, NHSDSPVP to DI-water, and NHSDSPVP to NHSDS. Once again, the experimental data and results following from the equation 5.7 and values found in Table 5.1 are in reasonable agreement. Both black nanofluids show about 20% more heat being stored compared to DI-water. This value is reached at about 90 min after the start of the experiment. In these first 90 minutes, stored heat increases significantly in all fluids. However, the nanofluids generate a slightly higher ratio of stored thermal energy than the DI-water.

5.5 Conclusions

The capabilities of black nanofluids to harvest solar radiation have been investigated. Two black nanofluids, which are candidates to be direct solar absorbers, are studied. The nanoparticles employed are carbon nanohorns with dahlia-like structure with a diameter of about 60 nm. Both of them are water based. The only difference is that one is singularly stabilised with SDS alone and the other one is doubly stabilised using SDS and PVP. The experiments are carried out by putting the samples into transparent glass cylinders which are exposed to an artificial sun. The produced CNH nanofluids show potential as direct solar energy absorbers. The optical properties of nanofluid samples are measured before and after the experiment to analyse the influence of heating.

One of the main outcomes of this work is that the transmission spectra shows that the black nanoparticles are a key element in enhancing the optical properties of solar fluids. These nanoparticles cause a significant increase in the light extinction.

The optical measurements carried out allow the calculation of the extinction, the absorption, and the scattering coefficients as functions of the penetration distance within the nanofluids. The absorption spectra of both black nanofluids show higher absorption values than DI-water. Moreover, after being exposed to the artificial sun, the absorption values of both black nanofluids exhibit an increase, specifically of 5% for the nanofluid singularly stabilised (NHSDS) and of 28% for the nanofluids doubly stabilised (NHSDSPVP). For CNH samples, the absorbed energy fraction obtained over short light penetration distances is higher than for the base fluid. The spatial distribution of the energy absorbed within the penetration distance indicates that the energy is mainly stored near the surface of the fluid.

Although further tests should be carried out, these initial results are a promising indicator that water-based black nanofluids with carbon nanohorns are potential candidates for the production of direct solar energy absorbers.

Chapter 6

Conclusions

This thesis has contributed to the solar thermal energy field. In particular, the focus has been on the full study of different solar nanofluids, from their synthesis to the simulation of a real application. This type of nanofluids present a promising improvement for the current solar collectors, therefore, they provide a solution to take a step forward in the use of renewable energies, achieving, in addition, higher efficiencies to the current ones.

The thesis is a compendium of three journal papers and generally, it could be divided in three main points: synthesis, characterisation and energy conversion of solar nanofluids.

The first step in all of the works developed during the thesis was the synthesis, since it consists of producing the nanofluid that will be further characterised. Several synthesis methods exist but in this case, the two-step method has been chosen, in which the surfactant is first dissolved in the base fluid by ultrasonic probe for a determined time (it depends on the surfactant concentration). Then the nanoparticles are added and dispersed using again an ultrasound probe for some minutes, depending on the nanoparticles concentration again. Usually, as the concentration used for both nanoparticles and surfactant is very low, ultrasonic time is around 1 min. a high-pressure homogeniser operating at 1,000 bar was used for processing the addition of nanoparticles to the base fluid-surfactant suspension. It is important to mention that the surfactant used in each sample is selected on the basis of the chemical affinity with the base fluid. Moreover, it is needed a surfactant that presents stability under high temperature conditions because in real applications these solar nanofluids will be working at high temperature, then it is mandatory to ensure their stability at working temperatures.

Deepening in this thesis, several base fluids have been used with different carbon based nanoparticles, and, consequently, different surfactants. Below is a breakdown of the different materials used:

- In the first work, water Milipore was used as base fluid and SWCNH were the nanoparticles. Two different concentration were prepared 0.002%wt and 0.005%wt. These concentrations were determined in previous works as being suitable for solar nanofluids, and two samples of each concentration were synthesised, with and without surfactant. Samples without surfactant contained oxidised SWCNH and in the other samples. The surfactant-to-nanoparticle weight ratio was 10:1, based also on the literature.

- In the second work, TH66 and SO were the base fluids. As their chemical compositions are different, even if the nanoparticles used were the same CB, two different surfactants were employed. DS was used for the TH66 based nanofluid and BS for the SO sample. Both surfactants were chosen due to both their high chemical affinity with their corresponding base fluid and their high stability under high temperature conditions. The nanoparticle concentration was 0.0016%wt, being the surfactant-to-nanoparticle weight ratio 1:1.

- In the third work, two water based suspensions with a concentration of 0.02 g/L of SWCNH were synthesised. One of them was simply stabilised with 0.005 g/L of SDS while the other one was doubly stabilised with 0.005 g/L of SDS and 0.05g/L of PVP. The reason for using the two surfactants is that SDS is a saline compound that provides electrostatic stabilisation, giving a negative zeta potential to particles that repulse each other. It means that the thermal motion of particles is sufficient to overcome electrostatic barrier offered by the SDS. Since PVP is is composed by a long polymeric chain, it could avoid the particle to come into close contact acting as a spacer. Combining the two effects, colloidal stability of the samples is improved at high temperature.

Once the synthesis step has been generally concluded, compiling all the methods carried out, the next step is the characterisation of the synthesised nanofluids. Several properties of a nanofluid can be studied, but in this thesis, the main ones are particles' morphology, optical, particle size distribution and energy conversion.

SEM is the electronic microscope that were used in this work. Each of them allows the study of different characteristics of a sample. The SEM provides information on morphology and surface characteristics, while the TEM the internal structure and ultrastructural details are observed. It is also possible to study the particle size distribution of the nanoparticles by means of the software ImageJ.

As the optical characterisation is one of the most important since it determines the absorption of the samples, which is the parameter used to classify solar nanofluids as potential directly solar absorbers. The system used in this PhD thesis was CARY 500 Spectrophotometer (Varian Dev.). It allows incorporating an integrating sphere that will complete the optical characterisation including the absorption measurement.

When the equipment is used without the integrating sphere, the ballistic transmittance is obtained and from it, the extinction coefficient can be calculated. This parameter is widely used and most of the optical characterisation found in the literature are based on it. On the other hand, when the device is used with the integrating sphere mounted, the scattering spectra can be extracted as well as the reflectance. Using some optical laws (Mie, Kubelka-Munk, Beer Lambert), the absorption, scattering, extinction and albedo coefficients can be determined. This is a differentiating feature since, in most research works; the scattering is just neglected or estimated but not measured.

In all of the nanofluids studied with carbon nanoparticles, the scattering albedo coefficient value is around 5-15% of the total extinction coefficient, which is much lower than the absorption that represents the rest 95% of the extinction. It was also observed that in all the samples,

the absorbance increased considerably (more than 80%, approx.) just by adding a few load of nanoparticles. It is a positive result because the cost of nanoparticles and nanofluids is high, however, as only a very few loading of nanoparticles is enough to considerably enhance the absorption in direct absorption solar collectors systems, which avoids pushing up the cost. Moreover, the carbon nanoparticles are quite cheap. It was also extracted from the different works that the energy is mainly absorbed in the first layer of the sample and with a thickness sample of 5 cm will be enough to collect the 100% of the energy. This can help to optimise the design of the solar collector and it is a piece of advantage of these solar nanofluids that the system can have reduced dimensions.

Another important parameter that plays an important role when evaluating a solar nanofluid as promising direct solar absorber is the stability. As it was mentioned before, the stability of the nanofluids handled in these works, was reached by the use of surfactants. The stability of the nanofluids has been analysed using the DLS technique. This technique measures the light scattered by the particles due to their Brownian motion, and associates its intensity with their size. It is so important to know the stability at room temperature as well as at high temperature, since later; the solar nanofluids will be used at high temperature. During the thesis period, the DLS technique has been used to obtain the mean diameter of the samples and studying the size along the time, the stability over a period could be determined if changes in size where found or not.

Two different DLS systems have been used to measure the stability and the particle size distribution at room and high temperature. Both of them, Zetasizer Nano and VASCO FLEX, works by means of the same operating principle, the only difference between them is that the first one is an internal device and the latter one is external. The Zetaiszer is widely used in the literature because of that the VASCO FLEX was set-up at room temperature comparing the data obtained with the Zetasizer. Moreover, by comparing the mean diameters obtained at different temperatures it is also possible to establish if the nanofluid is stable with the temperature.

The stability of some nanofluids was measured before and after they were thermally treated. In this way, the effect of surfactants after being at high temperature during a period of time was observed. Similar size particle distributions were obtained for all of them before and after the thermal treatment, indicating that the nanofluid is stable at room and at high temperature. There were other nanofluids whose mean diameter were evaluated along three months, and the results were excellent since no changes were observed.

Finally, taking a step forward on the solar nanofluids characterisation, a solar simulator was set-up to estimate the solar energy absorbed that was converted into thermal energy. This experiment was carried out with just two water-based CNH nanofluids, simply and doubly stabilised. The solar simulator illuminated them and their temperature development was acquired. After that, the temperature-registered data was mathematically handled in order to know their thermal behaviour while trying to be closer to the real application. The response of both nanofluids was quite similar obtaining better results with the nanofluid stabilised with SDS and PVP, as it was expected. Moreover, as different concentrations were also tested, it was possible to notice that the higher concentration the higher temperature reached.

To conclude, the six solar nanofluids studied along the development of this PhD thesis showed excellent optical properties comparing with the base fluids with low nanoparticles concentrations, presenting averaged improvements around 900%. Their absorbance spectra is quite wide so they can absorb in the most of the solar spectrum. Their scattering is quite low, which results very interesting. In addition, the stability was checked and presenting positive outcomes at room and high temperature, before and after the thermal treatment. All of these characteristics obtained, encouraged us to think about plans with solar nanofluids since they are a promising alternative for the current solar thermal collectors, moreover, they boost the use of renewable energies in order to achieve a cleaner world.

Chapter 7

Gaps and future research works

Solar nanofluids are promising working fluids for enhancing the performance of solar thermal systems. There is still much to discover and this motivates to continue working in this field. Several aspects involved in the study of solar nanofluids have been addressed in the present thesis, however, there are still some gaps and suggestions that may be considered as future works. Some of suggestion can be listed as:

- Various nanoparticles with different sizes and shapes could be investigated in future works. The morphology (size, shape and nature) of nanoparticles plays the main role in the determination of optical properties of nanofluids.
- Hybrid or even triple solar nanofluids (which are made from two or three different types of nanoparticles) need to be investigated more deeply.
- Theoretical analysis of the nanoparticles' absorption depending on their size, shape and concentration.
- Developing a new set-up which is able to work under higher working temperatures.
- The effect of possible sedimentation of nanoparticles on the performance of direct absorption solar collectors could be investigated both numerically and experimentally.
- It is suggested that with the development of the present work, the ability of various solar nanofluids for power and steam generation is investigated under high temperatures.
- To add some theoretical analysis on the steam generation processes in a CSP, to optimise the design of the solar thermal collectors and deepen in the knowledge of the process.

Chapter 8

Scientific production

8.1 Journal contributions

- Gimeno-Furio, A., Julia, E., Barison, S., Agresti, F., Friebe, C., Buschmann, M.H. **2019** *Nanofluids as direct solar energy absorbers* Journal of Nanofluids 8, pp. 1-13.
- Gimeno-Furio A., Navarrete, N., Martinez-Cuenca, R., Julia, J.E., Hernandez, L **2018** *Influence of high temperature exposure on the thermal and optical properties of thermal oil-based solar nanofluids* Journal of Nanofluids 7, pp. 1-8.
- Navarrete, N., Gimeno-Furio, A., Mondragon, R., Hernandez, L., Cabedo, L., Cordoncillo, E., Julia, J.E. **2017** *Nanofluid based on self-nanoencapsulated metal/metal alloys phase change materials with tuneable crystallisation temperature* Scientific Reports 7, pp. 17580.
- Gimeno-Furio, A., Navarrete, N., Mondragon, R., Hernandez, L., Martinez-Cuenca, R., Cabedo, L., Julia, J.E. **2017** *Stabilization and characterization of a nanofluid based on a eutectic mixture of diphenyl and diphenyl oxide and carbon nanoparticles under high temperature conditions* International Journal of Heat and Mass Transfer, 113 pp. 908-913.

8.2 Recently submitted papers

- Gimeno-Furio, A.,, Barison, S., Agresti, F., Cabaleiro, D., Mancin, S. **2018** *Optical characterisation of oxidised carbon nanohorn nanofluids for direct solar energy applications* Solar Energy, Submitted paper.
- Navarrete, N., Gimeno-Furio A., Forner-Escrig, J., Julia, J.E., Mondragon, R. **2018** *Colloidal stability of molten salt-based nanofluids: dynamic light scattering tests at high temperature conditions* Powder Technology, Submitted paper.
- , Gimeno-Furio A., Hernandez, L., Navarrete, N., Mondragon, R. **2019** *Characterization study of a thermal oil-based carbon black solar nanofluid* Renewable energy, Submitted paper.

8.3 Contribution to international conferences

- Gimeno-Furio A., Hernandez, L., Navarrete, N., Mondragon, R. **2019** *Stability and optical analysis of carbon black thermal oil-based nanofluid as direct solar energy absorber* 1st International Conference on Nanofluids (ICNf 2019) (Castellón, Spain).

- Gimeno-Furio A., Navarrete, N., Hernandez, L., Mondragon, R., Barreneche C., Cabedo, L. **2019** *Thermal stability of the black-coloured sand for concentrated solar power applications* Eurotherm Seminar #112, Advances in Thermal Energy Storage (Lleida, Spain).

- Martinez-Cuenca, R., Gimeno-Furio, A., Navarrete, N., Torró, S., Chiva, S., Hernandez, L. **2018** *CFD modelling of volumetric vapour generation and its applications to the receiver design* 4th Working Group Mettings, Workshop on Nanofluids in Energy Systems (Napoli, Italy).

- Gimeno-Furio, A.,Hernandez, L., Barison, S., Agresti, F., Doretti, L., Mancin, S. **2018** *The effect of oxidized carbon nanohorn nanofluid pool boiling on an aluminium surface* 4th Working Group Mettings, Workshop on Nanofluids in Energy Systems (Napoli, Italy).

- Gimeno-Furio, A., Buschmann, M.H. **2018** *Experimental study on solar nanofluids* Topical problems of fluid mechanics (Prague, Czech Republic).

- Gimeno-Furio, A., Julia, E., Barison, S., Agresti, F., Friebe, C., Buschmann, M.H. **2017** *Nanofluids as direct solar energy absorbers* 1st European Symposium on Nanofluids (ESNf2017) (Lisbon, Portugal).

- Gimeno-Furio A., Navarrete, N., Martinez-Cuenca, R., Julia, J.E., Hernandez, L **2017** *Influence of high temperature exposure on the thermal and optical properties of thermal oil-based solar nanofluids* 1st European Symposium on Nanofluids (ESNf2017) (Lisbon, Portugal).

- Navarrete, N., Gimeno-Furio, A., Mondragon, R., Hernandez, L., Cabedo, L., Cordoncillo, E., Julia, J.E. **2017** *On the use of nano-encapsulated phase change materials for thermal-oil and molten salt-based nanofluids* 1st European Symposium on Nanofluids (ESNf2017) (Lisbon, Portugal).

- Gimeno-Furio A., Hernandez, L, Martinez-Cuenca, R., Cabedo, L., Barreneche, C., Julia, J.E., Cabeza, L.F. **2017** *On the use of colored sand for volumetric solar radiation absorption for concentrated solar power applications* 13th International Conference on Heat Transfer, Fluid Mechanics and Thermodynamics (Portoroz, Slovenia).

- Gimeno-Furio, A., Navarrete, N., Mondragon, R., Hernandez, L., Martinez-Cuenca, R., Cabedo, L., Julia, J.E. **2017** *Thermophysical properties of a nanofluid based on a eutectic mixture of diphenyl and diphenyl oxide and carbon black nanoparticles* 3th International Conference on Heat Transfer, Fluid Mechanics and Thermodynamics (Portoroz, Slovenia).

- Gimeno-Furio A., Navarrete, N., Martinez-Cuenca, R., Julia, J.E., Mondragon, R., Hernandez, L **2016** *Thermal and optical chatacterization of tetraethylene glycol-based solar nanofluid at high temperature conditions* 12th International Conference on Heat Transfer, Fluid Mechanics and Thermodynamics (Málaga, Spain).

8.4 Contribution to national conferences

- Gimeno-Furio A., Hernandez, L, Martinez-Cuenca, R., Cabedo, L., Barreneche, C., Julia, J.E., Cabeza, L.F. **2017** *Optical and thermal characterization of colored sand for Concentrated Solar Power applications* 10 Congreso Nacional de Ineniería Termodinámica (Lleida, Spain).

- Gimeno-Furio, A., Navarrete, N., Mondragon, R., Hernandez, L., Martinez-Cuenca, R., Cabedo, L., Julia, J.E. **2017***Stabilization and characterization of a nanofluid based on a eutectic mixture of diphenyl and diphenyl oxide and carbon nanoparticles under high temperature conditions*10 Congreso Nacional de Ineniería Termodinámica (Lleida, Spain).

Bibliography

[1] John A Duffie and William A Beckman. *Solar engineering of thermal processes*. John Wiley & Sons, 2013.

[2] Rafael Torres-Mendieta, Rosa Mondragón, Verónica Puerto-Belda, Omel Mendoza-Yero, Jesús Lancis, J Enrique Juliá, and Gladys Mínguez-Vega. Characterization of tin/ethylene glycol solar nanofluids synthesized by femtosecond laser radiation. *ChemPhysChem*, 18:1055–1060, 2017.

[3] Suhas Pandurang Sukhatme. Solar energy. 4th. *Tata McGram Hill Publishing Company Limited*, 1999.

[4] Zetasizer Nano Series User Manual. Malvern instruments ltd. *United Kingdom, Man0317*, 2:5–5, 2004.

[5] Varian devices. Uv-vis-nir cary 100/300/400/500 spectrophotometers. *United Kingdom, Man0317*, 2007.

[6] CIA. Central intelligence agency-the world factbook. *New Zealand*, 2016.

[7] Wolfgang Lutz, Warren C Sanderson, and Sergei Scherbov. *The end of world population growth in the 21st century: New challenges for human capital formation and sustainable development*. Earthscan, 2004.

[8] Sarah Royston, Jan Selby, and Elizabeth Shove. Invisible energy policies: A new agenda for energy demand reduction. *Energy Policy*, 123:127 – 135, 2018.

[9] Dim Coumou and Stefan Rahmstorf. A decade of weather extremes. *Nature climate change*, 2:491, 2012.

[10] James Hansen, Makiko Sato, and Reto Ruedy. Perception of climate change. *Proceedings of the National Academy of Sciences*, 109:E2415–E2423, 2012.

[11] Georgios A Florides and Soteris A Kalogirou. Measurements of ground temperature at various depths. *Proceedings of CLIMA 2005, Lausanne, Switzerland.*, 2004.

[12] Rana Adib, HE Murdock, F Appavou, A Brown, B Epp, A Leidreiter, C Lins, HE Murdock, E Musolino, K Petrichenko, et al. Renewables 2015 global status report. *Paris: REN21 Secretariat*, 2015.

[13] J Hernández-Moro and JM Martínez-Duart. Analytical model for solar pv and csp electricity costs: Present lcoe values and their future evolution. *Renewable and Sustainable Energy Reviews*, 20:119–132, 2013.

[14] Soteris Kalogirou. Thermal performance, economic and environmental life cycle analysis of thermosiphon solar water heaters. *Solar energy*, 83:39–48, 2009.

[15] Manuel Romero and Aldo Steinfeld. Concentrating solar thermal power and thermochemical fuels. *Energy & Environmental Science*, 5:9234–9245, 2012.

[16] Robert A Taylor, Patrick E Phelan, Todd P Otanicar, Ronald Adrian, and Ravi Prasher. Nanofluid optical property characterization: towards efficient direct absorption solar collectors. *Nanoscale research letters*, 6:225, 2011.

[17] Luca Mercatelli, Elisa Sani, Giovanni Zaccanti, Fabrizio Martelli, Paola Di Ninni, Simona Barison, Cesare Pagura, Filippo Agresti, and David Jafrancesco. Absorption and scattering properties of carbon nanohorn-based nanofluids for direct sunlight absorbers. *Nanoscale research letters*, 6:282, 2011.

[18] E Sani, L Mercatelli, S Barison, C Pagura, F Agresti, L Colla, and P Sansoni. Potential of carbon nanohorn-based suspensions for solar thermal collectors. *Solar Energy Materials and Solar Cells*, 95:2994–3000, 2011.

[19] Todd P Otanicar, Patrick E Phelan, and Jay S Golden. Optical properties of liquids for direct absorption solar thermal energy systems. *Solar Energy*, 83:969–977, 2009.

[20] John E Minardi and Henry N Chuang. Performance of a "black" liquid flat-plate solar collector. *Solar Energy*, 17:179–183, 1975.

[21] Y Caouris, R Rigopoulos, J Tripanagnostopoulos, and P Yianoulis. A novel solar collector. *Solar Energy*, 21:157–160, 1978.

[22] Rudi Bertocchi, Abraham Kribus, and Jacob Karni. Experimentally determined optical properties of a polydisperse carbon black cloud for a solar particle receiver. *Journal of Solar Energy Engineering*, 126:833–841, 2004.

[23] M Abdelrahman, P Fumeaux, and P Suter. Study of solid-gas-suspensions used for direct absorption of concentrated solar radiation. *Solar Energy*, 22:45–48, 1979.

[24] SUS Choi, ZG Zhang, WLockwoodFE Yu, FE Lockwood, and EA Grulke. Anomalous thermal conductivity enhancement in nanotube suspensions. *Applied physics letters*, 79:2252–2254, 2001.

[25] Xiang-Qi Wang and Arun S Mujumdar. Heat transfer characteristics of nanofluids: a review. *International journal of thermal sciences*, 46:1–19, 2007.

[26] Myung-Ki Lee, Tae Geun Kim, Woong Kim, and Yun-Mo Sung. Surface plasmon resonance (spr) electron and energy transfer in noble metal- zinc oxide composite nanocrystals. *The Journal of Physical Chemistry C*, 112(27):10079–10082, 2008.

[27] Yimin Xuan and Qiang Li. Heat transfer enhancement of nanofluids. *International Journal of heat and fluid flow*, 21:58–64, 2000.

[28] S Zeinali Heris, S Gh Etemad, and M Nasr Esfahany. Experimental investigation of oxide nanofluids laminar flow convective heat transfer. *International Communications in Heat and Mass Transfer*, 33:529–535, 2006.

[29] Huaqing Xie, Jinchang Wang, Tonggeng Xi, Yan Liu, Fei Ai, and Qingren Wu. Thermal conductivity enhancement of suspensions containing nanosized alumina particles. *Journal of applied physics*, 91:4568–4572, 2002.

[30] F Matino and A Maccari. Molten salt receivers operated on parabolic trough demo plant and in laboratory conditions. *Energy Procedia*, 69:481–486, 2015.

[31] Gao Lihong, Fabien Lemarchand, and Michel Lequime. Comparison of different dispersion models for single layer optical thin film index determination. 2011.

[32] Todd P Otanicar, Drew DeJarnette, Yasitha Hewakuruppu, and Robert A Taylor. Filtering light with nanoparticles: a review of optically selective particles and applications. *Advances in Optics and Photonics*, 8:541–585, 2016.

[33] Luis M Liz-Marzán. Tailoring surface plasmons through the morphology and assembly of metal nanoparticles. *Langmuir*, 22:32–41, 2006.

[34] Michael Quinten. *Optical properties of nanoparticle systems: Mie and beyond*. John Wiley & Sons, 2010.

[35] Craig F Bohren and Donald R Huffman. *Absorption and scattering of light by small particles*. John Wiley & Sons, 2008.

[36] Adnan Jaradat, M-Ali H Al-Akhras, G Makhadmeh, K Aljarrah, A Al-Omari, Z Ababneh, Majed M Masadeh, HM Al-Khateeb, BA Albiss, and M Alshorman. Artificial semi-rigid tissue sensitized with natural pigments: Effect of photon radiations. *Journal of Pharmacy and Bioallied Sciences*, 3:266, 2011.

[37] E Sani, S Barison, C Pagura, L Mercatelli, P Sansoni, D Fontani, D Jafrancesco, and F Francini. Carbon nanohorns-based nanofluids as direct sunlight absorbers. *Optics Express*, 18:5179–5187, 2010.

[38] G03 Committee et al. Tables for reference solar spectral irradiances: Direct normal and hemispherical on 37 tilted surface. *ASTM International*, 2012.

[39] Dongsheng Wen, Guiping Lin, Saeid Vafaei, and Kai Zhang. Review of nanofluids for heat transfer applications. *Particuology*, 7:141–150, 2009.

[40] Rosa Mondragón, J Enrique Juliá, Luis Cabedo, and Nuria Navarrete. On the relationship between the specific heat enhancement of salt-based nanofluids and the ionic exchange capacity of nanoparticles. *Scientific reports*, 8:7532, 2018.

[41] Robert A Taylor, Patrick E Phelan, Todd Otanicar, Ronald J Adrian, and Ravi S Prasher. Vapor generation in a nanoparticle liquid suspension using a focused, continuous laser. *Applied Physics Letters*, 95:161907, 2009.

[42] Todd Otanicar, Robert A Taylor, Patrick E Phelan, and Ravi Prasher. Impact of size and scattering mode on the optimal solar absorbing nanofluid. In *ASME 2009 3rd International Conference on Energy Sustainability collocated with the Heat Transfer and InterPACK09 Conferences*, pages 791–796. American Society of Mechanical Engineers, 2009.

[43] Todd P Otanicar, Patrick E Phelan, Ravi S Prasher, Gary Rosengarten, and Robert A Taylor. Nanofluid-based direct absorption solar collector. *Journal of renewable and sustainable energy*, 2:033102, 2010.

[44] R Saidur, TC Meng, Z Said, M Hasanuzzaman, and A Kamyar. Evaluation of the effect of nanofluid-based absorbers on direct solar collector. *International Journal of Heat and Mass Transfer*, 55:5899–5907, 2012.

[45] Diego Rativa and Luis A Gómez-Malagón. Solar radiation absorption of nanofluids containing metallic nanoellipsoids. *Solar Energy*, 118:419–425, 2015.

[46] Yuki Kameya and Katsunori Hanamura. Enhancement of solar radiation absorption using nanoparticle suspension. *Solar Energy*, 85:299–307, 2011.

[47] Yuan He, Shiva Vasiraju, and Long Que. Hybrid nanomaterial-based nanofluids for micropower generation. *RSC Advances*, 4:2433–2439, 2014.

[48] Qinbo He. Experimental investigation on photothermal properties of MWCNT-H_2O nanofluids for direct absorption solar collectors. *Applied Mechanics & Materials*, 521.

[49] Hui Zhang, Hui-Jiuan Chen, Xiaoze Du, and Dongsheng Wen. Photothermal conversion characteristics of gold nanoparticle dispersions. *Solar Energy*, 100:141–147, 2014.

[50] Z Said, R Saidur, and NA Rahim. Optical properties of metal oxides based nanofluids. *International Communications in Heat and Mass Transfer*, 59:46–54, 2014.

[51] M Karami, MA Akhavan-Behabadi, M Raisee Dehkordi, and S Delfani. Thermo-optical properties of copper oxide nanofluids for direct absorption of solar radiation. *Solar Energy Materials and Solar Cells*, 144:136–142, 2016.

[52] Sanjay Vijayaraghavan, S Ganapathisubbu, and C Santosh Kumar. Performance analysis of a spectrally selective concentrating direct absorption collector. *Solar Energy*, 97:418–425, 2013.

[53] E Natarajan and R Sathish. Role of nanofluids in solar water heater. *The International Journal of Advanced Manufacturing Technology*, pages 1–5, 2009.

[54] Seung-Hyun Lee and Seok Pil Jang. Extinction coefficient of aqueous nanofluids containing multi-walled carbon nanotubes. *International Journal of Heat and Mass Transfer*, 67:930–935, 2013.

[55] Debbie Stokes. *Principles and practice of variable pressure/environmental scanning electron microscopy (VP-ESEM)*. John Wiley & Sons, 2008.

[56] David J Smith. Fundamentals of high resolution transmission electron microscopy. In *Surface and Interface Characterization by Electron Optical Methods*, pages 31–42. Springer, 1988.

[57] Hidetoshi Masuda, Akira Ebata, and Kazumari Teramae. Alteration of thermal conductivity and viscosity of liquid by dispersing ultra-fine particles. dispersion of Al_2O_3, SiO_2 and TiO_2 ultra-fine particles. 1993.

[58] PK Nagarajan, J Subramani, S Suyambazhahan, and Ravishankar Sathyamurthy. Nanofluids for solar collector applications: a review. *Energy Procedia*, 61:2416–2434, 2014.

[59] Alibakhsh Kasaeian, Amin Toghi Eshghi, and Mohammad Sameti. A review on the applications of nanofluids in solar energy systems. *Renewable and Sustainable Energy Reviews*, 43:584–598, 2015.

[60] Mohammad Hossein Ahmadi, Amin Mirlohi, Mohammad Alhuyi Nazari, and Roghayeh Ghasempour. A review of thermal conductivity of various nanofluids. *Journal of Molecular Liquids*, 2018.

[61] Muhammad Usman Sajid and Hafiz Muhammad Ali. Thermal conductivity of hybrid nanofluids: A critical review. *International Journal of Heat and Mass Transfer*, 126:211–234, 2018.

[62] Suhaib Umer Ilyas, Rajashekhar Pendyala, and Marneni Narahari. Stability and thermal analysis of MWCNT-thermal oil-based nanofluids. *Colloids and Surfaces A: Physicochemical and Engineering Aspects*, 527:11–22, 2017.

[63] A Gimeno-Furio, N Navarrete, R Martinez-Cuenca, JE Julia, and L Hernandez. Influence of high temperature exposure on the thermal and optical properties of thermal oil-based solar nanofluids. *Journal of Nanofluids*, 7:1045–1052, 2018.

[64] Alexandra Gimeno-Furio, Nuria Navarrete, Rosa Mondragon, Leonor Hernandez, Raul Martinez-Cuenca, Luis Cabedo, and J Enrique Julia. Stabilization and characterization of a nanofluid based on a eutectic mixture of diphenyl and diphenyl oxide and carbon nanoparticles under high temperature conditions. *International Journal of Heat and Mass Transfer*, 113:908–913, 2017.

[65] Mirunalini Thirugnanasambandam, Selvarasan Iniyan, and Ranko Goic. A review of solar thermal technologies. *Renewable and sustainable energy reviews*, 14:312–322, 2010.

[66] Robert A Taylor, Patrick E Phelan, Ronald J Adrian, Andrey Gunawan, and Todd P Otanicar. Characterization of light-induced, volumetric steam generation in nanofluids. *International Journal of Thermal Sciences*, 56:1–11, 2012.

[67] Jürgen Birnbaum, Markus Eck, Markus Fichtner, Tobias Hirsch, Dorothea Lehmann, and Gerhard Zimmermann. A direct steam generation solar power plant with integrated thermal storage. *Journal of Solar Energy Engineering*, 132:031014, 2010.

[68] Jan Fabian Feldhoff, Daniel Benitez, Markus Eck, and Klaus-Jürgen Riffelmann. Economic potential of solar thermal power plants with direct steam generation compared with htf plants. *Journal of Solar Energy Engineering*, 132:041001, 2010.

[69] MJ Montes, A Rovira, M Muñoz, and JM Martínez-Val. Performance analysis of an integrated solar combined cycle using direct steam generation in parabolic trough collectors. *Applied energy*, 88:3228–3238, 2011.

[70] Andrej Lenert, Yoshio S Perez Zuniga, and Evelyn N Wang. Nanofluid-based absorbers for high temperature direct solar collectors. In *2010 14th International Heat Transfer Conference*, pages 499–508. American Society of Mechanical Engineers, 2010.

[71] Robert A Taylor, Patrick E Phelan, Todd P Otanicar, Chad A Walker, Monica Nguyen, Steven Trimble, and Ravi Prasher. Applicability of nanofluids in high flux solar collectors. *Journal of Renewable and Sustainable Energy*, 3:023104, 2011.

[72] JA Eastman, US Choi, Shaoping Li, LJ Thompson, and Shinpyo Lee. Enhanced thermal conductivity through the development of nanofluids. *MRS Online Proceedings Library Archive*, 457, 1996.

[73] Yuan-Xian Zeng, Xiu-Wen Zhong, Zhao-Qing Liu, Shuang Chen, and Nan Li. Preparation and enhancement of thermal conductivity of heat transfer oil-based MoS_2 nanofluids. *Journal of Nanomaterials*, 2013:3, 2013.

[74] Robert Taylor, Sylvain Coulombe, Todd Otanicar, Patrick Phelan, Andrey Gunawan, Wei Lv, Gary Rosengarten, Ravi Prasher, and Himanshu Tyagi. Small particles, big impacts: a review of the diverse applications of nanofluids. *Journal of Applied Physics*, 113:1, 2013.

[75] Wenhua Yu, David M France, Jules L Routbort, and Stephen US Choi. Review and comparison of nanofluid thermal conductivity and heat transfer enhancements. *Heat transfer engineering*, 29:432–460, 2008.

[76] Pankaj Raj and Sudhakar Subudhi. A review of studies using nanofluids in flat-plate and direct absorption solar collectors. *Renewable and Sustainable Energy Reviews*, 84:54–74, 2018.

[77] Sumio Iijima, M Yudasaka, R Yamada, S Bandow, K Suenaga, F Kokai, and K Takahashi. Nano-aggregates of single-walled graphitic carbon nano-horns. *Chemical physics letters*, 309:165–170, 1999.

[78] Vaiva Krungleviciute, Aldo D Migone, and Michael Pepka. Characterization of single-walled carbon nanohorns using neon adsorption isotherms. *Carbon*, 47:769–774, 2009.

[79] K Murata, K Kaneko, F Kokai, K Takahashi, M Yudasaka, and S Iijima. Pore structure of single-wall carbon nanohorn aggregates. *Chemical physics letters*, 331:14–20, 2000.

[80] Masako Yudasaka, Sumio Iijima, and Vincent H Crespi. Single-wall carbon nanohorns and nanocones. In *Carbon nanotubes*, pages 605–629. Springer, 2007.

[81] E Sani, P Di Ninni, L Colla, S Barison, and F Agresti. Optical properties of mixed nanofluids containing carbon nanohorns and silver nanoparticles for solar energy applications. *Journal of nanoscience and nanotechnology*, 15:3568–3573, 2015.

[82] Matteo Bortolato, Simone Dugaria, Filippo Agresti, Simona Barison, Laura Fedele, Elisa Sani, and Davide Del Col. Investigation of a single wall carbon nanohorn-based nanofluid in a full-scale direct absorption parabolic trough solar collector. *Energy Conversion and Management*, 150:693–703, 2017.

[83] L Mercatelli, E Sani, D Fontani, G Zaccanti, F Martelli, and P Di Ninni. Scattering and absorption properties of carbon nanohorn-based nanofluids for solar energy applications. *Journal of the European Optical Society-Rapid Publications*, 6, 2011.

[84] Erick R Bandala, Miguel A Pelaez, Maria J Salgado, and Luis Torres. Degradation of sodium dodecyl sulphate in water using solar driven fenton-like advanced oxidation processes. *Journal of Hazardous Materials*, 151:578–584, 2008.

[85] Hisao Hidaka, Shinya Yamada, Shinichi Suenaga, Hayashi Kubota, Nick Serpone, Ezio Pelizzetti, and Michael Grätzel. Photodegradation of surfactants. v. photocatalytic degradation of surfactants in the presence of semiconductor particles by solar exposure. *Journal of Photochemistry and Photobiology A: Chemistry*, 47:103–112, 1989.

[86] Jimmy Lea and Adesoji A Adesina. The photo-oxidative degradation of sodium dodecyl sulphate in aerated aqueous tio2 suspension. *Journal of Photochemistry and Photobiology A: Chemistry*, 118:111–122, 1998.

[87] Filippo Agresti, Simona Barison, Alessia Famengo, Cesare Pagura, Laura Fedele, Stefano Rossi, Sergio Bobbo, Marzio Rancan, and Monica Fabrizio. Surface oxidation of single wall carbon nanohorns for the production of surfactant free water-based colloids. *Journal of colloid and interface science*, 514:528–533, 2018.

[88] A Gimeno-Furió, E Juliá, S Barison, F Agresti, C Friebe, and MH Buschmann. Nanofluids as direct solar energy absorbers. *Journal of Nanofluids*, 8:17–29, 2019.

[89] Schiavon Mauro. Device and method for production of carbon nanotubes, fullerene and their derivatives, October 24 2006. US Patent 7,125,525.

[90] Instruments Malvern. Inform white paper dynamic light scattering. *Malvern: Malvern Instruments Ltd*, pages 1–6, 2011.

[91] TR Wagner, WG Houf, and FP Incropera. Radiative property measurements for india ink suspensions of varying concentration. *Solar Energy*, 25:549–554, 1980.

[92] Luca Mercatelli, Elisa Sani, Annalisa Giannini, Paola Di Ninni, Fabrizio Martelli, and Giovanni Zaccanti. Carbon nanohorn-based nanofluids: characterization of the spectral scattering albedo. *Nanoscale research letters*, 7:96, 2012.

[93] Wenshi Ma, Fang Yang, Jingjing Shi, Fuxian Wang, Zhengguo Zhang, and Shuangfeng Wang. Silicone based nanofluids containing functionalized graphene nanosheets. *Colloids and Surfaces A: Physicochemical and Engineering Aspects*, 431:120–126, 2013.

[94] M Chiesa and Sarit K Das. Experimental investigation of the dielectric and cooling performance of colloidal suspensions in insulating media. *Colloids and Surfaces A: Physicochemical and Engineering Aspects*, 335:88–97, 2009.

[95] V Sridhara and LN Satapathy. Effect of nanoparticles on thermal properties enhancement in different oils–a review. *Critical Reviews in Solid State and Materials Sciences*, 40:399–424, 2015.

[96] Suleiman Akilu, KV Sharma, Aklilu Tesfamichael Baheta, and Rizalman Mamat. A review of thermophysical properties of water based composite nanofluids. *Renewable and Sustainable Energy Reviews*, 66:654–678, 2016.

[97] Babita, S.K. Sharma, and Shipra Mital Gupta. Preparation and evaluation of stable nanofluids for heat transfer application: a review. *Experimental Thermal and Fluid Science*, 79:202–212, 2016.

[98] SUS Chol and JA Estman. Enhancing thermal conductivity of fluids with nanoparticles. *ASME-Publications-Fed*, 231:99–106, 1995.

[99] Prasad Gurav, S Srinu Naik, Komel Ansari, S Srinath, K Anand Kishore, Y Pydi Setty, and Shirish Sonawane. Stable colloidal copper nanoparticles for a nanofluid: Production and application. *Colloids and Surfaces A: Physicochemical and Engineering Aspects*, 441:589–597, 2014.

[100] Kwangho Lee, Yujin Hwang, Seongir Cheong, Laeun Kwon, Sungchoon Kim, and Jaekeun Lee. Performance evaluation of nano-lubricants of fullerene nanoparticles in refrigeration mineral oil. *Current Applied Physics*, 9:e128–e131, 2009.

[101] Elena V Timofeeva, Michael R Moravek, and Dileep Singh. Improving the heat transfer efficiency of synthetic oil with silica nanoparticles. *Journal of colloid and interface science*, 364:71–79, 2011.

[102] MinSheng Liu, Mark ChingCheng Lin, and ChiChuan Wang. Enhancements of thermal conductivities with Cu, CuO, and carbon nanotube nanofluids and application of MWNT/water nanofluid on a water chiller system. *Nanoscale research letters*, 6:297, 2011.

[103] Xiaohao Wei, Haitao Zhu, Tiantian Kong, and Liqiu Wang. Synthesis and thermal conductivity of Cu_2O nanofluids. *International Journal of Heat and Mass Transfer*, 52:4371–4374, 2009.

[104] A Ghadimi, R Saidur, and HSC Metselaar. A review of nanofluid stability properties and characterization in stationary conditions. *International journal of heat and mass transfer*, 54:4051–4068, 2011.

[105] Wenjing Li, Changjun Zou, and Xiaoke Li. Thermo-physical properties of waste cooking oil-based nanofluids. *Applied Thermal Engineering*, 112:784–792, 2017.

[106] Wei Yu, Huaqing Xie, Lifei Chen, and Yang Li. Enhancement of thermal conductivity of kerosene-based Fe_3O_4 nanofluids prepared via phase-transfer method. *Colloids and surfaces A: Physicochemical and engineering aspects*, 355:109–113, 2010.

[107] Rudi Bertocchi, Jacob Karni, and Abraham Kribus. Experimental evaluation of a non-isothermal high temperature solar particle receiver. *Energy*, 29:687–700, 2004.

[108] Meiriane CF Soares, Marcelo M Viana, Zachary L Schaefer, Varun S Gangoli, Yinhong Cheng, Vinicius Caliman, Michael S Wong, and Glaura G Silva. Surface modification of carbon black nanoparticles by dodecylamine: thermal stability and phase transfer in brine medium. *Carbon*, 72:287–295, 2014.

[109] Dileep Singh, Elena V Timofeeva, Michael R Moravek, Sreeram Cingarapu, Wenhua Yu, Thomas Fischer, and Sanjay Mathur. Use of metallic nanoparticles to improve the thermophysical properties of organic heat transfer fluids used in concentrated solar power. *Solar Energy*, 105:468–478, 2014.

[110] Baojie Wei, Changjun Zou, Xihang Yuan, and Xiaoke Li. Thermo-physical property evaluation of diathermic oil based hybrid nanofluids for heat transfer applications. *International Journal of Heat and Mass Transfer*, 107:281–287, 2017.

[111] Caixia Wang, Jun Yang, and Yulong Ding. Phase transfer based synthesis and thermophysical properties of Au/Therminol VP-1 nanofluids. *Progress in Natural Science: Materials International*, 23:338–342, 2013.

[112] Rosa Mondragón, Rafael Torres-Mendieta, Marco Meucci, Gladys Mínguez-Vega, J Enrique Juliá, and Elisa Sani. Synthesis and characterization of gold/water nanofluids suitable for thermal applications produced by femtosecond laser radiation. *Journal of Photonics for Energy*, 6:034001, 2016.

[113] Wenhua Yu, Elena V Timofeeva, Dileep Singh, David M France, and Roger K Smith. Investigations of heat transfer of copper-in-Therminol 59 nanofluids. *International Journal of Heat and Mass Transfer*, 64:1196–1204, 2013.

[114] Thomas R Henderson, Charles R Clark, Thomas C Marshall, Ray L Hanson, and Charles H Hobbs. Heat degradation studies of solar heat transfer fluids. *Solar Energy*, 27:121–128, 1981.

[115] Ning Wang, Guoying Xu, Shuhong Li, and Xiaosong Zhang. Thermal properties and solar collection characteristics of oil-based nanofluids with low graphene concentration. *Energy Procedia*, 105:194–199, 2017.

[116] JM Vandenbelt. A collaborative study of cary spectrophotometers. *JOSA*, 44(8):641–643, 1954.

[117] Dongxiao Han, Zhaoguo Meng, Daxiong Wu, Canying Zhang, and Haitao Zhu. Thermal properties of carbon black aqueous nanofluids for solar absorption. *Nanoscale research letters*, 6:457, 2011.

[118] Haitao Zhu, Dongxiao Han, Zhaoguo Meng, Daxiong Wu, and Canying Zhang. Preparation and thermal conductivity of CuO nanofluid via a wet chemical method. *Nanoscale research letters*, 6:181, 2011.

[119] John Philip, Shima P Damodaran, and Baldev Raj. Influence of aggregation on thermal conductivity in stable and unstable nanofluids. *Applied Physics Letters*, 97:153113, 2010.

[120] John Philip, Shima P Damodaran, and Baldev Raj. Evidence for enhanced thermal conduction through percolating structures in nanofluids. *Nanotechnology*, 19:305706, 2008.

[121] Yanan Gan and Li Qiao. Optical properties and radiation-enhanced evaporation of nanofluid fuels containing carbon-based nanostructures. *Energy & Fuels*, 26:4224–4230, 2012.

[122] Antoni Gil, Marc Medrano, Ingrid Martorell, Ana Lázaro, Pablo Dolado, Belén Zalba, and Luisa F Cabeza. State of the art on high temperature thermal energy storage for power generation. Part 1—Concepts, materials and modellization. *Renewable and Sustainable Energy Reviews*, 14:31–55, 2010.

[123] Gang Xiao, Kaikai Guo, Zhongyang Luo, Mingjiang Ni, Yanmei Zhang, and Cheng Wang. Simulation and experimental study on a spiral solid particle solar receiver. *Applied Energy*, 113:178–188, 2014.

[124] Christopher J Gippel. The use of turbidimeters in suspended sediment research. *Hydrobiologia*, 176:465–480, 1989.

[125] Aranzazu Fernández-García, Eduardo Zarza, Loreto Valenzuela, and Manuel Pérez. Parabolic-trough solar collectors and their applications. *Renewable and Sustainable Energy Reviews*, 14:1695–1721, 2010.

[126] Marc J. Assael, C-F Chen, Ifigeneia Metaxa, and William A. Wakeham. Thermal conductivity of suspensions of carbon nanotubes in water. *International Journal of Thermophysics*, 25:971–985, 2004.

[127] Rasha M Elnoby, M Hussein Mourad, Salah L Hassab Elnaby, and Maram TH Abou Kana. Monocrystalline solar cells performance coated by silver nanoparticles: Effect of nps sizes from point of view mie theory. *Optics & Laser Technology*, 101:208–215, 2018.

[128] Nathan Hordy, Delphine Rabilloud, Jean-Luc Meunier, and Sylvain Coulombe. High temperature and long-term stability of carbon nanotube nanofluids for direct absorption solar thermal collectors. *Solar Energy*, 105:82–90, 2014.